Enhancing Vehicle Stability and Rollover Prevention through Model Predictive Control

By

Mohd Fitri Bin Mohd Yakub

Tokyo Metropolitan University

Japan

2015

Enhancing Vehicle Stability and Rollover Prevention through Model Predictive Control

By

Mohd Fitri Bin Mohd Yakub

A dissertation submitted in fulfilment of requirement for the Degree Doctor of Engineering in Human Mechatronic Systems

Graduate School of System Design
Tokyo Metropolitan University

Japan

September 2015

Abstract

Let start with a scenario where we are sitting behind the wheel of car, staring at mobile phone, reading a new e-mails message, texting a friend or others activities instead of looking at the road or the car in front. Suddenly, the driver in the car ahead slams on the brakes or we might crash with some avoidance. Rather than becoming a victim of distracted driving, we might feel a gentle deceleration as ours car comes to a stop on its own, easily avoiding a collision, the car starts itself up again as soon as the road is clear. While this is not a realistic portrayal yet, but this future is coming and some of the technology that will make it possible is already present in today's cars. The more advanced models and control technologies can warn of obstacles, adjust the distance to a car ahead, and activate the brakes when a distracted driver does not. However, while technology will ultimately protect us from accidents on the road, sometimes it does the opposite. That is because so many people make phone calls, text, manipulate global positioning system units, and fiddle with infotainment systems when they should be concentrating on their driving. Even the most diligent drivers can choose the wrong moment to glance at a navigation screen or distracted by a minor things during the journey. According to the national highway traffic safety administration, driver distraction contributed to almost 20 percent of crashes which injuries to vehicle passenger.

As safety continues to take an increasingly important place in the automobile industry, there has been significant research and development in the area of closed loop control of vehicle dynamics. Avoidance control strategy first started with anti-lock braking system (ABS) that prevented loss of steering control due to wheels locking up with hard braking or low friction. Vehicle dynamics control further developed to include traction control: a system that optimally distributes tractive forces and prevents excessive wheel slip. The most recent developments have been in the area of electronic stability control (ESC). As vehicle technology has evolved over the years, ABS and ESC are now becoming standard on most vehicles, not only automobile manufacturers but even governments and regulation bodies have programs dedicated to ensure standards and understand limitations of these systems. For every driver, active-safety systems and automated-driving technologies will provide not only assistance and support but also the valuable gift of time to reach for something in the glove compartment, to turn around and fix a child's jacket. As a result, efforts have been made to develop intelligent control strategies and enhancing vehicle control dynamics with test maneuvers to quantify dynamic properties.

The first stage of this thesis is focuses on studying standard with emergency maneuvers and developing new strategies to control, evaluate, and rate the performance of modern vehicles equipped with advanced vehicle dynamic control systems. Recent studies have focused on the lateral and yaw dynamics models, neglecting the roll dynamic model. By including the roll dynamics in the system, we can evaluate the effectiveness of controllers, especially under high-speed conditions. For this study, we limit the path-following control of an unmanned ground vehicle and emphasizes that we assume a known trajectory for the lateral position and yaw angle.

During evasive maneuvers the tire forces are no longer a linear function of slip angles and the vehicle response is nonlinear and potentially unstable, a condition which the active stability systems are designed to mitigate. Thus, we have proposed

model predictive control (MPC) with a feedforward (FF) or proportional integral (PI) controllers to minimize tracking errors in the lateral position and yaw angle. To evaluate the effectiveness of the proposed control method, we compare it with linear quadratic control with a FF/PI controller. The method can be used to benchmark a vehicle regardless of passive or active control. We utilize ABS which focuses on direct yaw control (DYC) which produces the corrective yaw moment by using the rear braking forces between the left and the right side of the rear tire vehicle in order to avoid the interferences between active front steering and DYC.

On the other hand, heavy vehicle stability safety systems are currently available from a number of manufacturers of heavy road transport equipment. Advisory systems to warn the driver of impending rollover were developed over a decade ago and have been superseded by technology development. Stability safety technology is claimed to be highly effective in potentially dangerous situations like overestimating curve speed limit (e.g. narrowing curves, highway exits); obstacle avoidance maneuvers with sudden steering input (e.g. steering from the shoulder back onto the road and skidding); and laden semi-trailer in narrow curves on slippery surface (jackknifing on turns).

However, when making an emergency or abrupt lane change, especially in the strong wind condition, drivers have not enough time to make the compensation for adjusting the handle and it will be initiate a vehicle to spin, instability, and rollover. Therefore, it is required and urgently to establish a rapid and safety with secure control techniques systems to discover and prevent the yaw motion instability, in doing so will enhance vehicle stability. Therefore, the second stage of this thesis is to take the advantages of the MPC control method that can be used effectively for the constraint and multivariable systems particularly focuses on the directional yaw stability control and rollover prevention of heavy vehicles under the inclement scenario on emergency threat avoidance maneuver.

Generally, this thesis contains of two main parts which are: The first study is conducted in order to improve the ground vehicle performance of the autonomous sport utility vehicles with emphasis on path-following control and yaw stability control through proposed integrated control maneuver. The second study of this thesis is improvement of the ground heavy vehicle performance of the single lorry with emphasis on rollover prevention, yaw stability control, and fast safe lane change trajectory control through proposed integrated control maneuver. The enhancement of the MPC control is design through switching technique in order to stabilize the vehicle while preventing the rollover in the emergency threat avoidance scenario.

Page Approval

I certify that I have supervised and read this study and that in my opinion it conforms to acceptable standards of scholarly presentation and is fully adequate, in scope and quality, as a thesis for the Degree Doctor of Engineering in Human Mechatronic Systems.

_____
Yasuchika Mori
Supervisor

I certify that I have read this study and that in my opinion it conforms to acceptable standards of scholarly presentation and is fully adequate, in scope and quality, as a thesis for the Degree Doctor of Engineering in Human Mechatronic Systems.

_____
Akira Kojima
Internal Examiner

_____
Masuda Shiro
Internal Examiner

_____
Yoshihiko Miyasato
External Examiner

This dissertation was submitted to the Department of Human Mechatronic Systems and is accepted as fulfilment of the requirement for the Degree Doctor of Engineering in Human Mechatronic Systems.

_____
Head, HMS

This dissertation was submitted to the Graduate School of System Design and is accepted as fulfilment of the requirement for Degree Doctor of Engineering in Human Mechatronic Systems.

_____
Dean, Graduate School of
System Design

Declaration

I hereby declare that this dissertation is the result of my own investigations, except where otherwise stated. I also declare that it has not been previously or concurrently submitted as a whole for any other degrees at TMU or other institutions.

Mohd Fitri Mohd Yakub

Signature …… Date ……..

Tokyo Metropolitan University

Declaration of Copyright and Affirmation of Fair Use of Unpublished Research

Enhancing Vehicle Stability and Rollover Prevention through Model Predictive Control

I hereby affirm that the Tokyo Metropolitan University (TMU) hold all rights in the copyright of this work and henceforth any reproduction or use in any form or by means whatsoever is prohibited without the written consent of TMU. No part of this unpublished research may be reproduced, stored in a retrieval system, or transmitted, in any form or by means, electronic, mechanical, photocopying, recording or otherwise without prior written permission of the copyright holder.

Affirmed by Mohd Fitri Mohd Yakub

…… ……

Signature Date

To:

My beloved parents, brothers, sisters, wife and daughters

Acknowledgements

Alhamdulillah. All thanks and prayers to Allah the Almighty for His endless blessing and granting me patience to complete my thesis and Doctor Engineering Degree. A large means of gratitude is owed to my great supervisor Prof. Dr. Yasuchika Mori for being my supervisor. Effective and successful research writing would be next to impossible without his constant encouragement, support, and invaluable suggestions. A large debt is owed to him, for his imperative supervision, knowledge, constructive criticism, advice and sincere guidance throughout the course of this research. Special thanks are extended to Prof. Dr. Kitajima with the strong recommendation and support that had played the primarily important role in the selection procedure of doctoral course in Tokyo Metropolitan University.

I would like to thank also to my external and internal examines: Prof. Dr. Yoshihiko Miyasato, Prof. Dr. Akira Kojima, and Prof. Dr. Shiro Masuda for examining my dissertation and giving comments, criticisms, corrections and suggestions in improving my work. Special thanks are also extended to Dr. A. Zahran M. Khudzari for his help in preparing this thesis particularly in improving English language.

Many thanks to my friends and fellow researchers from the Mori's Laboratory or Automatic Control Laboratory: Yusuke Shiota, Takahiro Nakamura, Toshibu Nakamura, Lee Shihao, Tostuka, Yastusuka, Koizumi, Ebisawa, Kazuki Enari, Taichi Mizoshiri, Chin, Goto, Watanabe, and others whom presented somehow perpetually refreshed, helpful, and memorable.

I shall take this opportunity to express my appreciation to the Tokyo Metropolitan Government for providing the research funding through 'Asian Human Resource Fund', and Graduate School of System Design for making the invaluable resources available in enhancing my human mechatronics systems engineering knowledge.

I especially wish to extend my sincere thanks to all of my family especially to my beloved mother, father and my siblings for giving me moral support and prayers. Special thanks to my lovely wife, Siti Hasriah and my cute daughters Ameera Qaysha, Ameera Sofiyyah, and Ameera Izzah. Your love, support, and patience make me stronger to facing any challenges and difficulties. You always stand by my side.

Finally, I would like to thank everybody who was important to the successful realization of this thesis, as well as expressing my apology that I could not mention the names personally one by one.

Table of Contents

List of Tables

List of Figures

List of Abbreviations

ABS	Anti-lock Braking System
AFS	Active Front Steering
AMPC	Adaptive MPC
ARS	Active Rear Steering
AS	Active Steering
ATD	Automated Test Drive
CoG	Center of Gravity
DARPA	*Defense Advanced Research Projects Agency*
DOB	Disturbance Observer
DoF	Degree of Freedom
DBC	Differential Braking Control
DRC	Disturbance Rejection Control
DYC	Direct Yaw Moment Control
ECR	Equal Concern for the Relaxation
EMPC	Explicit MPC
ESC	Electronic Stability Control
FASM	Force-Angle Stability Metric
FF	Feedforward
FMPC	Fast MPC
GPS	Global Positioning System
HMPC	Hybrid MPC
HVSST	*Heavy Vehicle* Stability Safety Technologies
IMU	I*nertial Measurement Unit*
ITARDA	International Road *Traffic* and *Accident Database*
J-TAD	Japan Traffic Accidents Databases
LCQP	Linearly-Constrained Quadratic Programming
LPF	Low Pass Filter
LQ	Linear Quadratic
LQC	Linear Quadratic Control
LQR	Linear Quadratic Regulator
LTR	Load Transfer Ratio
LTV MPC	Linear Time Varying MPC
MPC	Model Predictive Control
NHTSA	National Highway Traffic Safety Administration
NMPC	Nonlinear Model Predictive Control
PD	Proportional Derivative
PI	Proportional Integral
PID	Proportional Integral Derivative
PWA	Piecewise Affine

QP	Quadratic Program
RED	Roll Energy Diagram
SMPC	Switching Model Predictive Control
SSF	Static Stability Factor
SUV	Sport Utility Vehicle
TCS	Traction Control System
TTR	Time to Rollover
TWLO	Two-Wheel Lift Off
VDC	Vehicle Dynamics Control
2WS	Two-Wheel Steering
4WS	Four-Wheel Steering

List of Symbols

A	Frontal vehicle area [m^2]
C_F	Yaw moment dimensional coefficients parameter [Nm]
C_f, C_r	Linear approximations of tire stiffness for front and rear tires [N/rad]
F_b	Force from the road bank angle [N]
F_{wy}	Force exerted by a side wind [N]
F_x, F_y	Longitudinal and lateral tire forces [N]
F_z	Normal tire load forces [N]
H_p, H_c	Prediction and control horizons
I_{xx}	Inertia around the roll, x-axis [kgm^2]
I_{xz}	Inertia product around the roll and yaw [kgm^2]
I_{zz}	Inertia around the yaw, z-axis [kgm^2]
J	Cost function of MPC and LQC
J_b	Tire wheel inertia [kgm^2]
M_f, M_r	Reaction moments at front and rear wheels [Nm]
M_{wx}, M_{wz}	Roll and yaw moments around the CoG of vehicle affected by the wind [Nm]
M_z	Total reaction moment [Nm]
M_z^*	Total corrective reaction moment from the DYC [Nm]
R_w	Radius of circular road [m]
Q, R	Weighting matrices of MPC and LQC
S	The frontal area of the vehicle
T	Simulation time [s]
T_b	Braking/wheel torque [Nm/s]
T_s	Sampling time [s]
Y	Lateral position [m]
a_y	Vehicle lateral acceleration, [m/s^2]
$b_ø$	Equivalent suspension roll damping coefficient [Nms]
$b_{\phi f}$, $b_{\phi r}$	Damping coefficient of the front and rear suspension, [Nm/radian/ s]
b_w	Driveline damping coefficient [Nms]
e_t	Tracking error
e_ψ	Vehicle yaw angle error with respect to road [radian]
e_x	Longitudinal position error of the vehicle [m]
e_y	Lateral position error of vehicle CoG with respect to center line of lane [m]
g	Acceleration due to gravity [m/s^2]
h	Distance between vehicle CoG and assumed roll axis [m]
$h_{uf,}$ h_{ur}	Front and rear roll center distances below sprung mass CoG [m]
h_w	Distance between the vehicle's aerodynamic center and CoG of the vehicle on the Y-axis [m]

l	Vehicle wheelbase length [m]
l_f, l_r	Distances of front and rear wheels from CoG [m]
l_w	Distance between the vehicle's aerodynamic center and CoG of the vehicle on the *X*-axis [m]
k_{ff}	Feedforward gain term
k_p	Proportional gain term
k_i	Integral gain term
k_{ss}	Steady-state steering angle [radian]
$k_{ø}$	Equivalent suspension roll stiffness coefficient [Nm]
$k_{\phi f}$, $k_{\phi r}$	Stiffness coefficient of the front and rear suspension, [Nm/radian]
n	Number of time periods of root-mean-square error
m	Vehicle mass [kg]
m_s	Total vehicle mass and sprung mass [kg]
m_{uf},, m_{ur}	Front and rear unsprung mass [kg]
r_w	Wheel radius [m]
r_i	Reference input
s	Tire slip ratio
t_w	Vehicle track width [m]
u	Control input signal of prediction model
Δu	Control rate input signal of prediction model
ΔM_z	Change in total reaction moment [Nm]
$\Delta\delta_f$, $\Delta\delta_r$	Changes in steering angles of front and rear wheels [radian /s]
v_x, v_y	Longitudinal and lateral vehicle velocities [m/s]
v_w, v_r	Crosswind speed and it relative wind speed [m/s]
x, y, z	Coordinates of vehicle position in body frame
α_f, α_r	Front and rear slip angles [radian]
δ_f, δ_r	Steering angles of front and rear wheels [radian]
δ_f^*	Steering angle of the front wheel generated by the AFS [radian]
ω_w	Angular velocity of tires [m/s]
ρ	Density of air [kg/m^3]
κ	Path curvature
μ	Track friction coefficient
ψ, ϕ	Yaw and roll angles [radian]
$\dot{\psi}$, $\dot{\phi}$	Yaw and roll rates [radian /s]
β	Vehicle side slip angle [radian]
β_w	Wind attack angle [radian]
θ	Road bank angle [radian]
$(\cdot)_f$, $(\cdot)_r$	Variables at front and rear wheels

Chapter 1
Introduction

1.1 Background

Autonomous vehicles are a major technological advancement in automobile technology. Numerous research programs have been undertaken by various governments, research organizations and institutes towards development of unmanned ground vehicles. These include automated highway research where autonomy is applied to passenger cars to drive on paved roads and unmanned off road driving such as the DARPA grand challenge. Another very important application of autonomy in vehicles is automated test drivers systems that are replacing human drivers in vehicle dynamic testing. This increases the reliability and repeatability of test maneuvers which is imperative for dependable results. Figure 1.1 shows a white Google self-driving SUV car under testing in California [1].

The above example just emphasizes one of the reasons why autonomous cars are so important: they are better drivers than we are. They are always paying attention, and never get tired or distracted or bored. However, like any robotic system that depends on a lot of complicated hardware and software working together synchronously, autonomous cars are vulnerable to errors, and even if an accident has not happened yet, it is definitely going to.

Other vehicle systems that have been given the automated or semi-automated treatment include the transmis1sion, accelerator (cruise control), brakes (ABS and traction control), and suspension (stability control), to name just a few; all are essential or near essential driver aids designed to lessen drivers' burdens without intruding on the driving experience.

Figure 1.1: A white Google self-driving car [1].

The fantastic thing about autonomous cars is that everything that is happening around the car is recorded, as well as what they are thinking all the time. After an accident, it would be possible for engineers to replay what happened in detail, and follow the chain of logic that the car followed to reach the decision that led to the accident. The specific cause of the accident could then be identified, and then, more than likely, engineers could develop a way of making sure that the car would never, ever have that accident again. Furthermore, the update could be instantly propagated to every other autonomous car, making them all that much safer.

The more advanced models and control technologies can warn of obstacles, adjust the distance to a car ahead, and activate the brakes when a distracted driver does not, and this is just the beginning of the autonomous vehicle. However, while technology will ultimately protect us from accidents on the road, sometimes it does the opposite. That is because so many people make phone calls, text, manipulate GPS units, and fiddle with infotainment systems when they should be concentrating on their driving. And even the most diligent drivers can choose the wrong moment to glance at a navigation screen. According to the NHTSA, driver distraction is a factor in almost 20 % of crashes in which someone is injured [2].

Therefore, the first stage of this thesis is focused on development and enhancement of the path-following control of autonomous SUV through integrated steering and braking control as well as extending the applicability of the proposed method under simulation environments as explained in detail in Chapter 4. An alternative approach to minimizing the tracking error of path follower based on MPC with FF or PI controllers is presented.

Second stage of the study in this thesis is mainly focus on rollover prevention control of heavy vehicle system. Rollovers occur in one of two ways, namely tripped or un-tripped. There are two types of rollovers as shown in Figure 1.2 [3]. A tripped rollover happens due to tripping from external inputs. An example of this rollover happens when a vehicle leaves the roadway and slides sideways, digging its tires into soft soil or striking an object such as a curb or guardrail. On the other hand, an un-tripped rollover happens due to high lateral acceleration from a sharp turn and without tripping. An example of un-tripped rollover is when a vehicle makes a collision avoidance maneuver or a cornering maneuver with high speed. However, in bad

environmental conditions such as in the strong wind or on the bumpy road, both tripped rollover and un-tripped rollover are easy to happen.

Vehicle rollover accidents have been extremely hazardous to the occupants of the vehicle and identified as the most fatal vehicle crashes. According to JTAD [4], rollover accounted for nearly 20% of all the single-vehicle accidents. Research by the NHTSA in the United States also shows that rollover accidents contributed nearly 35% of all deaths from passenger vehicle crashes [5]. In 2010, more than 7,600 people were killed in the US in rollover accidents involving light vehicles. While the majority of these accidents involved tripped rollovers, it is clear that an active safety system capable of preventing un-tripped rollover accidents will save lives, and as such is worthy of investigation. Moreover, the expansion of functionality of active safety systems is in keeping with the trend towards greater integration of control design in automotive vehicles.

Because of the high CoG, SUVs and heavy trucks have a proclivity to rollover accidents. While vehicle type does play a significant role, other factors such as driver behavior and road and environmental conditions can also cause a vehicle to roll over. Most rollover occurs under the following conditions:

i. Traveling at high speed on a curved road: When a vehicle travels on a curved road, lateral centrifugal force will pull it in an outboard motion. Some 40% of fatal rollover crashes involved excessive speeding. Additionally, nearly 75% of fatal rollovers took place where the posted speed limit was 88.5 kilometer per hour or higher.

ii. Severe cornering maneuver: This case is similar to the preceding case where the centrifugal force pulls the vehicle to rollover. For example, a driver avoiding an accident and steering rapidly can cause a yaw disturbance.

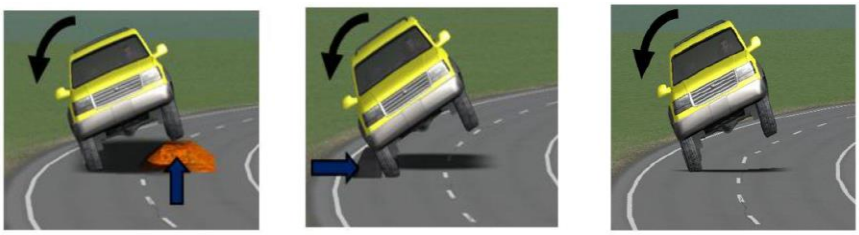

Figure 1.2: Types of rollover [139].

iii. Traveling on a collapsing road and suddenly providing steering input for a vehicle with a low level of roll stability: This kind of rollover also is caused by a yaw disturbance.

iv. Losing control due to a rapid decrease of friction, such as driving on an icy road: Steering can cause yaw motion because forces on the tires in the lateral direction are strong enough to roll the vehicle. The forces also produce lateral acceleration on the vehicle CoG. The forces are produced by the friction between the tires and the road; therefore, these rollover scenarios are called friction rollovers.

v. Bad environmental conditions are also considered to be an important factor in fatal rollover: Particularly, the strong lateral wind or significant road bank may harass the behavior of the heavy vehicle and can even initiate rollover accidents, because the lateral and roll motion are easily affected by these disturbances.

The most effective way to keep the vehicle from rolling over is to make the CoG of the vehicle as low as possible or increase the track width of the vehicle. However, the suitable control methods for rollover prevention are still few and less demonstrated.

Therefore, second stage of this thesis focuses on yaw stability control and rollover prevention control of heavy vehicle system through integrated steering and braking control based on MPC. It presents an alternative approach to providing stabilization assistance to the driver which level rages additional information about the road and environmental conditions of vehicle behavior and disturbances. This study is well elaborated and explained in Chapter 5 through threat avoidance scenario with emergency steering maneuver.

1.2 Problem Statement and its Significance

Lane departure warning employs a simple camera that needs costs. It could save thousands lives in crash repairs. The camera plus processing software watch how close the vehicle to road surface markings. It alerts driver when driver are about to drift across, but only if driver turn signal is not on.

Lane departure warning has emerged as a key tool for driver safety. The technology has evolved over the last few years to lane keep assist where the car

automatically corrects course if it reaches the lane markings, and now a higher level of lane keep assist that automatically keeps the car centered on the road. The corrections are subtle and the driver can always override the car and turn the wheel manually.

The first study in this thesis is an attempt to address the advantages of integrated control allocation to improve the path-following by minimizing the tracking error of autonomous vehicle system.

On the other hand, rollover prevention and detection such as active suspension and active stabilizer has been studied extensively [6-7]. However, the installation of dedicated actuators to control active parts and it also problem due to their high costs prevented their widespread use. There are many maneuver control approaches such as AFS [8-9], 4WS [10-11], and ARS [12-13] which has been used for degrading the roll rate and lateral acceleration while going around a bend that exhibit stability and maneuverability in high-speed situations during a lane change. Active differential braking control shows good effect on limit roll angle during an urgent situation [14-15].

Thus, this research also addresses the advantages of integrated control allocation to track the driver's desired path as closely as possible while preventing the vehicle from rollover at the same time which can also prevent collision avoidances.

1.3 Research Objectives

The objectives can be described as follows:

1. To enhance the vehicle model with most represented real vehicle and enhancing the load transfer ratio as indicator for the rollover.
2. To enhance an autonomous ground vehicle of path-following control under consideration of disturbances through MPC and LQR. FF/PI controller has been proposed with combination of MPC to minimizing the trajectory tracking error, enhance vehicle stability and maneuverability.
3. To enhance the braking control method through direct yaw moment and differential braking control by using the torque distribution of the left and right wheel instead of using the front and rear wheel.
4. To enhance the heavy duty vehicle of rollover prevention control under consideration of disturbances through MPC. Switching technique of MPC has been proposed in order to minimize the trade-off between the

emergency lane change maneuver, vehicle stability, and rollover due to threat avoidance scenario.

5. To enhance a disturbance rejection control for improvement of vehicle performance. A DOB and MPC based on DRC are proposed for rollover prevention control, particularly for heavy duty vehicle systems. The autonomous steering control of a heavy vehicle that is travelling in a straight line is simulated in two different environmental conditions: step wind of typhoon, and the combination of the sinusoidal wind of a typhoon with a random road bank angle.

1.4 Research Methodology

The following works were conducted in order to achieve the objectives of this research:

1. The research started with literature review by exploring the MPC control concept and its control design, vehicle dynamics model, and vehicle dynamic control system i.e. yaw stability control, roll stability control, and suspension control. MPC control fundamental concepts, principles, developments, scientific, technical and problems are studied and analyzed.
2. The mathematical model of the vehicle dynamics system with the improvement of the rollover indicator model were studied and enhanced. Vehicle model validation was made for the simulation process through the standard maneuver test such as Fishhook, double lane change, roll feedback, etc.
3. The path-following maneuver control problem particularly for autonomous vehicles was studied. The integrated control through steering and braking control maneuver with emphasis on minimizing tracking error was improved. Braking control method via direct yaw moment control between left and right wheel instead of front and rear wheel were enhanced. The proposed method is implemented in the double lane change maneuver control compared to LQC control under the disturbances effect through simulation process.
4. The heavy vehicle dynamic system problem particularly for rollover prevention and yaw stability control was studied. The integrated control

through steering and braking control maneuver with emphasis on lane tracking, yaw stability, and rollover prevention was improved. MPC control method via switching technique to reduce the trade-off of the main objectives was enhanced. The proposed method is implemented in the emergency threat avoidance scenario in single lane change maneuver control compared to conventional MPC control under the disturbances effect through simulation process.

5. Conclusion of the overall simulation process is evaluated and discussed. The advantages and disadvantages proposed method is mentioned and evaluated. Future work with the recommendation for the drawback is highlighted and discussed with case studies.

1.5 Scope of Research

The scope of this research covers the advantages of the MPC control method that can be used effectively for the constraint and multivariable systems particularly focuses on vehicle dynamics systems. The first stage is conducted in order to improve the ground vehicle performance of the autonomous SUVs with emphasis on path-following control and yaw stability control through proposed integrated control maneuver. The enhancement of the MPC control is added with the FF/PI control in order to minimizing the path tracking error. The disturbances such as crosswind, bank angle, and split friction are considered to evaluate the effectiveness and robustness of the proposed method on a double lane change scenario. Our general idea of this study is depicted as shown in Figure 1.3.

The second contribution of this thesis is improvement of the ground heavy vehicle performance of the single lorry with emphasis on rollover prevention, yaw stability control, and fast safe lane change trajectory control through proposed integrated control maneuver. The enhancement of the MPC control is designed through switching technique in order to stabilize the vehicle while preventing the rollover in the emergency threat avoidance scenario. The disturbances such as crosswind, bank angle, and split friction are considered to evaluate the effectiveness and robustness of the proposed method on a fast single lane change scenario. Our general idea of this study is also illustrated in Figure 1.3.

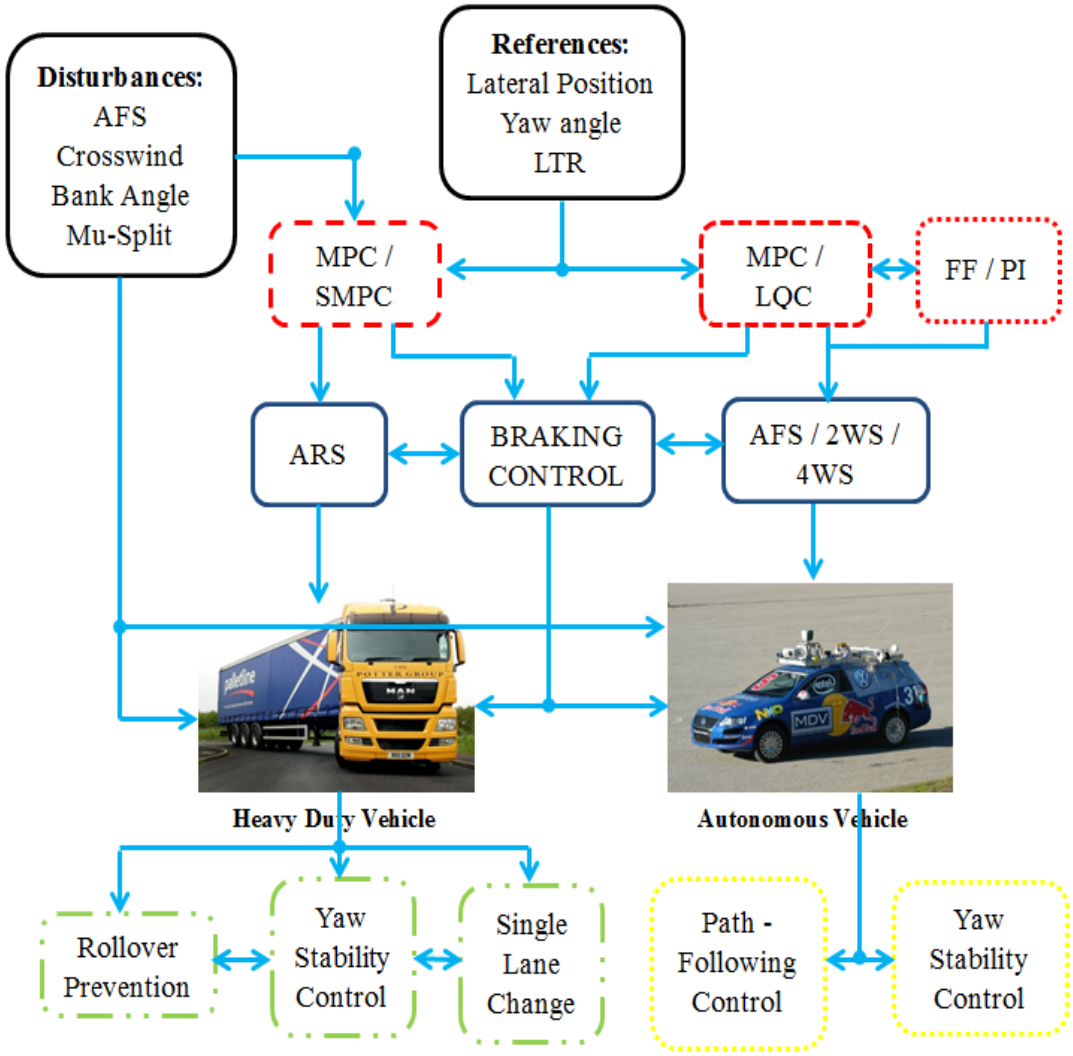

Figure 1.3: Overall flow chart of the research study.

1.6 Dissertation Outline

This thesis can be summarized as follows:

1. **Chapter 1:** This chapter describes the overall system that covers in the thesis. It consists of background, problem statement, research objectives, research methodology, scope of research, and the thesis outline.
2. **Chapter 2:** This chapter discusses the literature review generally on research and development of vehicle dynamic control systems and with the focus on path-following control, yaw stability control, and roll stability control of autonomous ground vehicle and heavy duty vehicle. The basic concept of MPC control theory is also described and its design is explained. The design covers the MPC rule, cost function, and the optimization problem. Related literature reviews regarding implementation of MPC to the vehicle dynamics control are studied.

3. **Chapter 3:** This chapter explains the modeling of complete nonlinear vehicle model, nonlinear tire model, disturbances model i.e. crosswind and bank angle for simulation purpose. A little modification of the vertical forces particularly related to roll motion and lateral acceleration are taken into account. The rollover indicator called LTR is explained with a few enhancement of the indicator by considering the lateral acceleration. The development of the vehicle model is validated through standard maneuvers test. Based on the vehicle responses in yaw rate, roll rate and lateral acceleration, it is proven and shown that the vehicle model is validated and corrected, thus, can be implemented for controller design.
4. **Chapter 4:** The improved MPC controller with proposed PI and FF controller for autonomous SUV systems is discussed in this chapter. Thorough discussion of MPC structure, PI/FF control design, control allocation between the AFS and ABS maneuver are also presented in this chapter. The simulation results showed that, by including roll dynamics in the linear vehicle model leads to considerable improvements in the stability and trajectory performance of the vehicle. It is also highlighted that the MPC structure capable of keeping the actuators within the limited boundaries during a lane change is the important component of the control system. Furthermore, the results showed that by adding the PI/FF controller with MPC, it proved that the vehicle stability, handling, and maneuverability can be enhanced and the lateral position tracking can be improved. The simulations also proved that MPC is more useful than LQC for multivariable systems and systems with constraints. The results also proved that the right and left wheels' brake distribution in DYC are more effective and successfully implemented with the combination of AFS for vehicle steering maneuver.
5. **Chapter 5:** Chapter five discusses the improvement of yaw stability and rollover prevention control of heavy duty vehicle through SMPC. Switching technique of the MPC controller and the trade-off between the path tracking, yaw stability, and rollover are discussed. The controller design process using the linear vehicle into the nonlinear heavy system is presented. The simulation result showed that the vehicle stability, driver handling, and maneuverability can be improved through switching MPC instead of nominal MPC. Emergency braking of the front vehicle or obstacle appeared suddenly without warning can be avoided and collision can be prevented through proposed method by minimizing the lateral position tracking

error for a heavy vehicle. The results also demonstrated that the brake pressure distribution between the difference braking torque at the right and the left rear axles that providing the DBC are more sufficient and adequately applied with combination of ARS rather than mixture of ARS with DYC.

6. **Chapter 6:** In this chapter, results obtained in the previous chapters are summarized and discussed. Moreover, a DOB and MPC based on DRC are proposed for rollover prevention control, particularly for heavy duty vehicle systems. The results demonstrated that MPC leads to a better and faster optimal operation of front steering than LQC, which can reduce LTR predictively by the prediction time.

Chapter 2
Literature Review

2.1 Introduction

Mathematical models of the real systems are required for the design, analyzing, and development of a new approaches and techniques in most engineering disciplines. In modern times, rapid development of technology in control software offers the opportunity and chances to implement more advanced control theory or algorithm towards it applications. Most of the optimal control design approaches rely on dynamic model of the process to be controlled. In spite of that, the PID controller remains industries most preferred strategy and implemented controller because of easy to design, simple, and understandable control structures [16-17].

However, the PID controller has a drawback, where lacks of coordinator within the hierarchy for a good and systematic process control design and it performance objectives. Another limitation is the omission of a facility to accommodate and handle process operational with constraints easily and handle with multivariable system.

Contrary to PID controller method, the MPC method can easily be used in different levels of the process control structure, and capable to handle a wide variety of process control constraints systematically. These are two of the reasons why MPC is often cited as one of the more popular advanced techniques for industrial process applications [18-20].

This chapter presents the literature review, which is divided into four main parts. The first one is focused on the vehicle dynamics control system particularly focuses on yaw and roll stability control. This is presented in Section 2.2. Next, we also discussed about path-following maneuver control especially for autonomous vehicle in Section 2.3. Many control methods have been proposed for ground vehicle control systems with difference aims and approaches.

The basic concept of the MPC controller theory are explained and reviewed in Section 2.4, in which the structure of MPC controller and its strategy are discussed. Section 2.4 also discusses the design process of MPC controller, which covers the cost function and optimization problem determination. Section 2.5 is dedicated to the

literatures for car vehicle dynamics system for active safety and stability that related to author's work, focused on steering and braking control, yaw and roll control, and suspension control.. Lastly, all the discussions are summarized in Section 2.6.

2.2 Vehicle Dynamics Control System

Recent trends in the automotive industry are such that there is an increased use of on-board computers controlling various functions, performance, efficiency and overall system robustness. There has been emphasis on stability and particular interest in active safety. ESC [21-22], which has been available for a few years, is a safety feature that could prevent catastrophic injuries and save lives. Some claim that ESC is as important as seatbelts in terms of protecting drivers and passengers. ESC is the evolution of ABS and TCS [23-24].

ABS brakes are systems that prevent wheel lock-up by automatically modulating the brake pressure during hard braking or an emergency stop. TCS are designed to address primarily side-to-side loss of friction between the vehicle's tires and the road surface while the vehicle is accelerating. ESC systems are technological developments evolving from and incorporating these two technologies.

ESC combines a third yaw control stability system, which compares the direction the driver is intending to steer the vehicle to the direction the car is actually traveling. It assists drivers in maintaining control of their vehicles during extreme steering maneuvers by keeping the vehicle headed in the driver's intended direction, even when the vehicle nears or exceeds the limits of road traction.

This is accomplished by selected braking and by reducing excess engine power. If a vehicle begins to oversteer in a turn and the rear end starts losing its lateral force capacity and it starts to come around (which would cause the car to spin out), the speed difference between the left and right front wheels increases. If the vehicle understeers (loses front traction and goes wider in a turn), the speed difference between the left and right front wheels decreases.

If the stability control software in the ABS control module detects a difference in the normal rotational speeds between the left and right wheels when turning, it immediately reduces engine power and applies counter braking at individual wheels as needed until steering control and vehicle stability are regained. In addition to braking and traction systems, active front steering has been used to improve lateral stability.

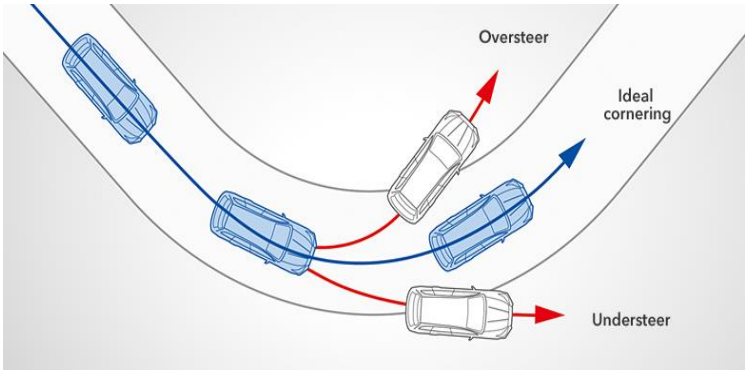

Figure 2.1: Vehicle dynamics control system [172].

The driver's driving habits are detected from the steering angle, engine speed, selected gear and braking conditions. VDC [25-26] monitors and analyses whether or not the vehicle is following the driver's intended course via these sensors as shown in Figure 2.1. If the vehicle approaches the limits of stability whilst cornering or avoiding an obstacle, the AWD torque distribution, engine output and brakes at each wheel are adjusted to assist in keeping the vehicle on course. All this happens in an instant, without hindering the sporty driving required by the driver, so as to maintain a safe level of driving.

2.2.1 Vehicle Yaw Stability

The prevention of excessive deviations between the intended and actual lateral response of the vehicle is important in the vehicle's stability control systems. The lateral response mainly includes the yaw rate, side slip angle, side slip gradient, and path radius of curvature. The individual wheel torque distribution control of an in-wheel driving motor to control the yaw moment and improve vehicle stability has been studied in [27-28].

The 2DoF vehicle dynamics model is suggested as follows:

$$mv_x(\dot{\beta}+\dot{\psi}) = 2C_f(\delta_f - \frac{l_f}{v_x}\dot{\psi} - \beta) + 2C_r(\frac{l_r}{v_x}\dot{\psi} - \beta) \tag{2.1}$$

$$I_{zz}\ddot{\psi} = 2l_fC_f(\delta_f - \frac{l_f}{v_x}\dot{\psi} - \beta) - 2l_rC_r(\frac{l_r}{v_x}\dot{\psi} - \beta) + M \tag{2.2}$$

Where M denotes the yaw moment to implement the direct yaw moment control which is generated by the difference of the driving force of left and right wheel:

$$M = \frac{t_w}{2}(-F_{x,rl} + F_{x,rr}) \tag{2.3}$$

The DYC system is usually implemented by the active braking or driving system to generate braking or driving torque and additional yaw moment. Ackermann et al. develop an alternative AS system to generate additional yaw moment [29]. It was found that an AS system has an added advantage over the emergency braking system, particularly regarding safety and ride comfort. The active steering control is implemented by adding an additional steering angle. Abe suggested ARS in this vehicle dynamics equation [30]:

$$mv_x\dot{\beta} + 2(C_f + C_r)\beta + (mv_x + \frac{2}{v_x}(l_f C_f - l_r C_r))\dot{\psi} = 2C_f\delta_f + 2C_r\delta_r \tag{2.4}$$

$$I_{zz}\ddot{\psi} + 2(l_f C_f - l_r C_r)\beta + (\frac{2}{v_x}(l_f^2 C_f + l_r^2 C_r))\dot{\psi} = 2C_f l_f \delta_f - 2C_r l_r \delta_r \tag{2.5}$$

In this equation, the rear wheel steering angle is used to provide additional yaw moment. The rear wheel steering angle is calculated to ensure that the vehicle has a zero side slip angle response.

In the literatures, lots of researcher focused on analyzing the stability of the vehicle. Horiuchi et al. proposed constrained bifurcation and continuation methods to analysis the stability of accelerating and braking [31]. Zboinki and Dusza develop a method to analysis the nonlinear laterals stability of a railway vehicle [32]. Marghitu et al. suggested an analytical methodology based on Poincad maps and Floquet theory to analysis the dynamic stability of a vehicle system [33]. The stability moment which is a new stability metric was developed to measure the stability of high speed vehicles [34]. A novel non-holonomic equation of motion to analysis vehicle stability has been presented in [35]. Shen performed a nonlinear stability analysis of the phase plane motion of a vehicle while a velocity stability indicator for a passenger car has been designed in [36-37].

Anwar presents a method for enhancing yaw stability based on a generalized predictive control method [38]. The method uses a full-car handling model to predict yaw rate error. Differential braking is applied according to a control law to stabilize the vehicle around the desired yaw rate. The method was shown to enhance the stability of a vehicle on a snow covered surface [38].

Karbalaei et al. use fuzzy logic to implement a direct yaw rate controller using active front steering and differential braking [39]. The fuzzy controller uses a set of rules to determine the corrective steering angle and braking moment to apply in order to stabilize the vehicle about the desired yaw rate. Simulations show the effectiveness of this method [39].

Zhao et al. implement sliding mode control for yaw stabilization using differential braking [40]. A 4DoF vehicle model is used to estimate state variables and a sliding mode controller takes yaw rate error and side slip into account. The controller estimates the proper sliding trajectory and generates differential braking commands. Simulation results have shown the applicability of the method, but the authors did not conduct real vehicle testing [40].

Nishio et al. describe an estimation and control architecture for stability control [41]. In order to make the system robust to uncertain terrain environments, a nonlinear tire model is combined with a switching friction state estimator and road bank estimator. The friction estimator performs a similarity analysis on the phase lag in the lateral acceleration wave form and chooses one of three friction states. Vehicle spin-out is detected by detecting the saturation of measured acceleration with respect to modeled acceleration. The side slip is then estimated using a pseudo-integral technique. The controller is designed to restrict extreme understeer and oversteer behavior by tracking side slip versus its derivative. The controller intervenes with differential braking to stabilize the vehicle when the controller criteria are met. The efficacy of the control architecture was validated in full-scale testing [41].

Liebemann et al. outline the concepts behind the Bosch electronic stability control system [42]. The Bosch system uses measurements of lateral acceleration, forward velocity, and steering angle to recognize potentially dangerous situations. In yawing situations, the system applies controls to the center differential and wheel brakes to balance the drive torque and reduce the likelihood of loss of directional control. Additionally, the system detects potential rollover states and applies similar inputs to mitigate the rollover propensity [42].

2.2.2 Vehicle Roll Stability

Rollover can be defined as an overturning of a vehicle about its longitudinal axis. Rollover tends to be a highly dynamic event and a variety of models and metrics have been proposed to predict its occurrence.

Putney applied a simplified rigid body model to the problem of rollover prevention in an autonomous vehicle [43]. The model consists of a rigid block on a banked surface. Rollover was predicted when the moments due to the centripetal acceleration exceeds the moment due to the vehicles weight about the outside tire. A safe maneuvering range for the current vehicle state is calculated and actuation commands are limited to prevent violation of these limits [43].

Odenthal et al. use steering and braking control to prevent rollover of human controlled road vehicles [44]. The vehicle is modeled using a bicycle model extended with roll dynamics. A rollover metric is derived by calculating the relative lateral load transfer between the left and right wheels. This metric is used to predict the proximity of the vehicle to rollover and a controller is developed that uses active steering and braking control to reduce the value of the metric [44].

Whitehead et al. implemented an electronic stability controller to detect and intervene to prevent rollover [45]. The controller was implemented on a scaled testbed equipped with an IMU and GPS. The testbed was then run through a series of fishhook maneuvers with differing CoG locations to reveal the effectiveness of the controller [45].

Lambert analyzes the effects of vehicle parameters on the rollover propensities of passenger vehicles [46]. Rollover propensity is judged using a measure known as the static stability factor that is largely dependent on the ratio of the track width to the CoG height. The effects of CoG height, track width, understeer gradient, suspension stiffness, and friction coefficients are analyzed using CarSim models of vehicles. CoG height, understeer gradient, and friction coefficients were found to have the strongest relationships with rollover propensity [46].

A rollover metric known as the FASM is presented by Papadopoulos et al. [47] and Peters et al. [48]. Papadopoulos proposes the FASM based on the principle that the angle of the vector representing the resultant force on the CoG must not exceed the angle between the CoG and the nearest ground support. It is shown that the metric can be used to successfully predict and prevent rollover of mobile manipulators [47].

Peters extends the FASM for use with four-wheeled vehicles by calculating the moments about the axes connecting the tire contact points of each of the wheels. Additionally, the moments and support polygon are modified to account for the mass of the wheels and movements of the suspension. Simulation and empirical testing using a dynamic fishhook maneuver shows that the metric can provide an accurate measure of rollover and parameter sensitivity studies indicate that knowledge of both the un-sprung mass and CoG location are significant factors in the calculation [48].

Chen and Peng propose a method known as TTR for rollover prediction [49]. The TTR approach calculates the time until wheel lift off by simulating a very fast model forward in time. As future control states are not known for human driven vehicles, the assumption is made that the control inputs will remain constant. In order to be able to rapidly simulate the rollover conditions, a simple model that trades accuracy for speed is used. To compensate for the low-order model, a neural network is implemented to compensate. The neural network compensated TTR improved performance, but as is often the case with neural networks, the gains were maximized in the vicinity of the training data set [49]. This work is expanded by Yu et al. who use the TTR paradigm to develop an active roll-stabilizing controller [50].

Dahlberg addresses the issue of rollover from an energy perspective [51]. The dynamic rollover threshold is contrasted with the steady-state rollover threshold. It is analytically demonstrated using energy metric that a rollover event can occur at a lower lateral acceleration in a dynamic event than in a steady-state situation. Rollover in both dynamic and static situations can be predicted by plotting a RED with static energy mapped to potential energy and dynamic to kinetic energy. Testing with an articulated semi-trailer with a variable CoG validated the results and also indicated that rollover for articulated vehicles is dependent on longitudinal velocity as well as lateral dynamics [51].

2.3 Path-Following Maneuvers Control

This section is dedicated to test maneuvers involving path-following. The main difference between such maneuvers and the ones performed by steering machines is that the latter are open-loop in a sense that the test specifies a hand wheel angle profile to be executed whereas path following maneuvers specify a path or course that a vehicle is made to negotiate. The main purpose of these tests is to validate vehicle's

dynamic response with respect to handling. Modern vehicles are being equipped with electronic stability control systems and the tests are designed to evaluate them.

Lateral control refers to steering control of a vehicle. Modeling and control of lateral dynamics is a complex subject. A vehicle's lateral response to steering inputs depends on a number of parameters such as vehicle inertia, tire properties, road surface, speed, etc. Researchers have developed various models to study lateral vehicle dynamics and control [52-55]. One simplified model known as "the bicycle model" is commonly used. In this model the front and rear axles of the vehicle are represented by a single wheel in the front and rear respectively, like a bicycle. It is also referred to as "single track model".

For higher accuracy, four wheel models that include lateral load transfer effects are also used. Various other complex effects like suspension compliances, tire relaxation lengths and steering compliances have been included in high fidelity models. The bicycle model as simple as it is, captures the lateral dynamics in the linear range fairly well and is considered appropriate for many control applications.

A path-following algorithm along with the knowledge of lateral dynamics of the vehicle forms the complete steering controller of the automated test drive (ATD). A number of path following algorithms have been discussed in the literature [56-57]. Pure pursuit and vector pursuit are two of many geometric algorithms applied to the path following problem. Other complex control strategies such as sliding mode control and neural networks have been developed. Most researchers in the autonomous vehicles field consider sensitivity to parameter variation and adaptability of any algorithm to different vehicles to be sufficient challenges.

The algorithm implemented by Sidhu et al. [58] is briefly discussed here. The controller determines the goal point which is a certain fixed look ahead distance on the path ahead as shown in Figure 2.2.

Once the goal point is known, the angle between the goal point direction and vehicle heading, called heading error is computed. PD control applied to this heading error results in the steering command:

$$\delta = K_p\theta + K_d \frac{d\theta}{dt} \tag{2.6}$$

The proportional gain, K_p in the above equation is adapted from Tseng et al. [59]. This method offers a way to determine K_p based on four key vehicle parameters:

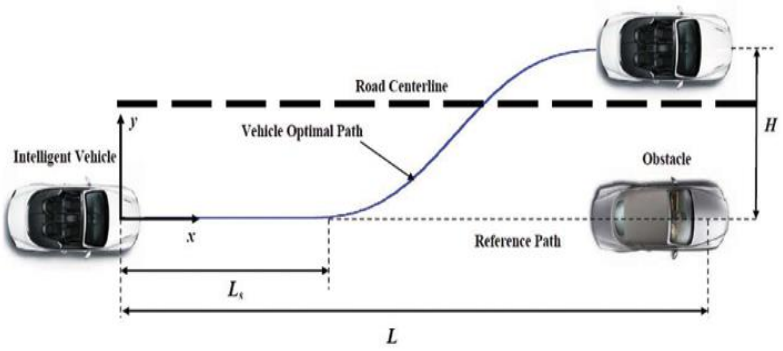

Figure 2.2: Look ahead in lane change maneuver [143].

$$K_p = \frac{2(L + kv_x^{\,2})}{(LA + L_b)} K_{sr} \tag{2.7}$$

where L_b is the distance of CoG from the rear axle, L is the wheelbase, K_{sr} is the steering ratio (hand wheel angle to road wheel angle), and k is the understeer gradient.

2.4 Model Predictive Control

Fast development of technology in control software offers the opportunity and chances to implement more advanced control theory or algorithms towards applications. Most of the optimal control design approaches rely on dynamic model of the process to be controlled. In spite of that, MPC, also known as receding horizon control, is an optimal control based algorithm has intensely investigated by the academia and industry since its commercialization in early 1980s [60-61].

MPC is the one of the most popular optimal control techniques, widely employed for controlling constrained linear or nonlinear systems. MPC uses a mathematical dynamic process model to predict a future value and to optimize process control performance over a prediction horizon [62-63]. MPC is a model based control structure and widely employed for the control of constrained linear or nonlinear systems including multi variable systems where a mathematical dynamics process model is used to predict the future behavior of the system and optimizing the process control performance over a prediction horizon.

The MPC model is easy to use at different levels of the process control structure such as multiple input and multiple output dynamics systems that offers attractive solutions for regulation and tracking problems [64] while guaranteeing stability [65]. Since the end of the 1980s, robust MPCs which explicitly take account

of model uncertainties, plant-model mismatch, and disturbances or noise have been studied for more practical applications. These have been applied mainly to impulse response models and state-space approaches by solving a finite horizon open-loop control optimization problem [66]. An overview of robust MPC has been presented in [67-68].

On the other hand, linear quadratic control (LQC), which is also based on a quadratic cost function, is widely implemented for process control [69] and motion control [70]. LQC's main advantage is that the optimal input signal can be obtained from the full state feedback, whereas the optimization of MPC is implemented in closed-loop systems. However, LQC has limitations in systems where it is necessary to consider actuator limitations; for example, it is difficult to restrict the manipulated variable or the controlled variable [71].

2.4.1 Principle of MPC

Figure 2.3 and Figure 2.4 shows the basic idea of MPC with receding horizon control concept and a block diagram of MPC respectively. It can be characterized by the following strategy method [18-20]:

(1) A dynamics process model is used to predict the behavior of the plant and future plant outputs, $y(k+i|k)$ for $i = 1,2,...,H_p$, for a determined prediction horizon, H_p, at each instant k based on past and current inputs and outputs measurements up to instant k, and on the future control signal, $u(k+i|k)$, $i = 0,1,\ldots,H_c-1$, where H_c is called control horizon.

(2) These control signals, $u(k+i|k)$ are calculated by optimizing the error between the predicted output signal and reference or target trajectory to keep the process as close as possible follow the reference trajectory, $r(k+i|k)$. The objective function and all constraints are considered in many cases.

(3) Only one control signal, $u(k|k)$ is implemented on the plant whilst others are rejected, due to the next sampling instant, $y(k+1)$ is known.

(4) Step 1 is repeated with the updated value and all sequences are brought up to date.

Generally, there are two types of MPC which is linear; they are used linear model to predict the system behaviors/dynamics and consider linear constraints, while nonlinear; based on nonlinear models and consider nonlinear constraints.

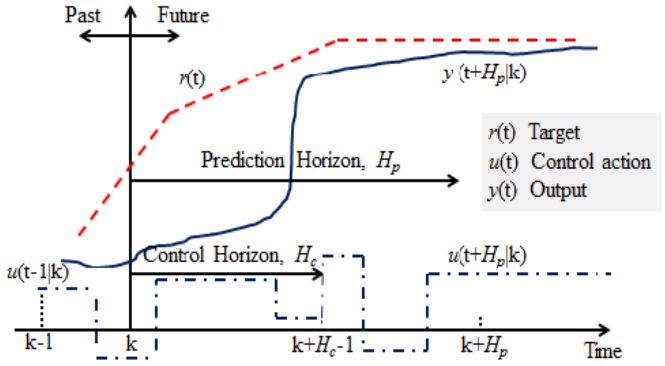

Figure 2.3: Basic idea of predictive control.

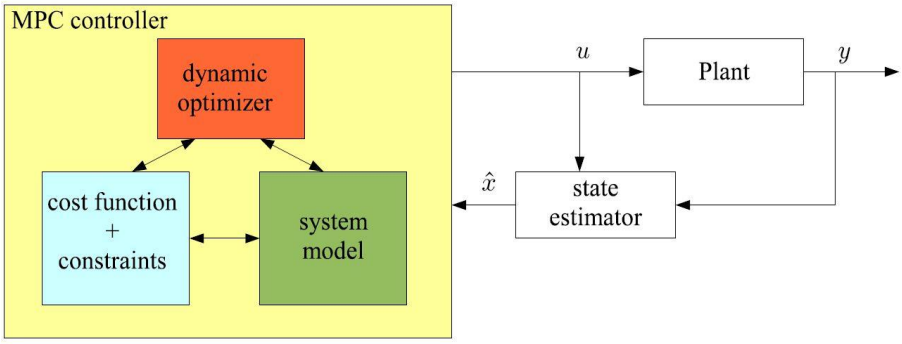

Figure 2.4: Block diagram of MPC [173].

Here, we assume a discrete-time setting and the current time is labelled as time step k, $k > 0$, and the state variable vector denoted as $x(k)$ available through measurement. The future control trajectory and future state variables are denoted by:

$$\begin{aligned} &u(k),\ u(k+1),\ ...,\ u(K+H_c-1) \\ &x(k+1|k),\ x(k+2|k),\ ...,\ x(k+H_p|k) \end{aligned} \tag{2.8}$$

where, H_c is used to dictate the number of parameters used to capture the future control trajectory.

2.4.2 Cost Function

Assume that estimates of $x(k)$, $x_d(k)$ are available at time k. The model predictive control action at time k is obtained by solving the optimization problem:

$$\min_{\Delta u(k|k),\ldots,\Delta u(m-1+k|k),\varepsilon} \left\{ \sum_{i=0}^{p-1} \left(\begin{array}{c} \sum_{j=1}^{n_y} \left| w_{i+1,j}^{y} \left(y_j(k+i+1|k) - r_j(k+i+1) \right) \right|^2 + \sum_{j=1}^{n_u} \left| w_{i,j}^{\Delta u} \Delta u_j(k+i|k) \right|^2 \\ \sum_{j=1}^{n_u} \left| w_{i,j}^{u} \left(u_j(k+i|k) - u_{jref}(k+i) \right) \right|^2 + \rho_\varepsilon \varepsilon^2 \end{array} \right) \right\} \tag{2.9}$$

In this equation, the subscript $(\ )_j$ denotes the j component of a vector, $(k+i|k)$ denotes the value predicted for time $k+i$. This predictive value is based on the information available at time k. $r(k)$ is the current sample of the output reference, subject to:

$$\begin{aligned}
&u_{j,\min}(i) - \varepsilon V^{u}_{j\min}(i) \le u_j(k+i\,|\,k) \le u_{j,\max}(i) + \varepsilon V^{u}_{j\max}(i)\\
&\Delta u_{j,\min}(i) - \varepsilon V^{\Delta u}_{j\min}(i) \le \Delta u_j(k+i\,|\,k) \le \Delta u_{j,\max}(i) + \varepsilon V^{\Delta u}_{j\max}(i)\\
&y_{j,\min}(i) - \varepsilon V^{y}_{j\min}(i) \le y_j(k+i+1\,|\,h) \le y_{j,\max}(i) + \varepsilon V^{y}_{j\max}(i)\\
&\Delta u(k+h\,|\,k) = 0\\
&\varepsilon \ge 0\ ,\ i = 0,\ldots,p-1, \qquad h = m,\ldots,p-1
\end{aligned} \tag{2.10}$$

with respect to the sequence of input increments $\{\Delta u(k|k),...,\Delta u(m\text{-}1+k|k)\}$ and to the slack variable ε. The control action sent to the plant is $u(k) = u(k–1)+\Delta u(k|k)^*$. In this case, $\Delta u(k|k)^*$ is the first element of the optimal sequence. Only the measured output vector $y_m(k)$ is feedback to the model predictive controller. However, $r(k)$ is a reference for all the outputs (measured and unmeasured).

When the reference r is not known in advance, the current reference $r(k)$ is used over the whole prediction horizon, so $r(k+i+1) = r(k)$ in Equation 2.9. In MPC, the exploitation of future references is referred to as anticipative action (or look-ahead or preview). $w^{\Delta u}_{i,j}$, $w^{u}_{i,j}$, $w^{y}_{i,j}$ are nonnegative weights for the corresponding variable. The smaller the value of w, the less important the behavior of the corresponding variable is to the overall performance.

$u_{j,min}$ $u_{j,max}$, $\Delta u_{j,min}$, $\Delta u_{j,max}$, $y_{j,min}$, $y_{j,max}$ are lower and upper bounds on the corresponding variables. In Equation 2.9, the constraints on u, Δu, and y are relaxed or softened by introducing the slack variable $\varepsilon \ge 0$. In Equation 2.10, the weight ρ_ε on the slack variable ε penalizes the violation of the constraints. As ρ_ε increases relative to the input and output weights, the controller gives minimization of constraint violations higher priority.

The ECR vectors V^{u}_{min}, V^{u}_{max}, $V^{\Delta u}_{min}$, $V^{\Delta u}_{max}$, V^{y}_{min}, V^{y}_{max} have nonnegative entries that quantify the concern for relaxing the corresponding constraint; the larger V, the softer the constraint. $V = 0$ means the constraint is hard and cannot be violated. By default, all input constraints are hard ($V^{u}_{min} = V^{u}_{max} = V^{\Delta u}_{min} = V^{\Delta u}_{max} = 0$) and all output constraints are soft ($V^{y}_{min} = V^{y}_{max} = 1$).

The MPC penalizes the worst case soft constraint violation the one for which the inclusion of the non-zero slack variable (and the associated ECR value) allows the

constraint to be satisfied at equality. As the MPC attempts to minimize the cost function, it might increase violations of other soft constraints. We can use the ECR values to adjust the priority. Doing so allows us to determine which constraint is selected as the worst case violation.

Vector $u_{target}(k+i)$ is a set point for the input vector. We typically use u_{target} when the number of inputs is greater than the number of outputs. Doing so specifies a preferred value for the inputs when all other objectives have been achieved. As mentioned earlier, only $\Delta u(k|k)$ is actually used to compute $u(k)$. The remaining samples $\Delta u(k+i|k)$ are discarded, and a new optimization problem based on $y_m(k+1)$ is solved at the next sampling step $k+1$.

The algorithm implemented in the MPC Toolbox software uses different procedures depending on the presence of constraints. If there are no constraints, the controller uses a fast analytical solution to obtain its optimal moves at each sampling instant. Otherwise, a QP solver is used. The matrices associated with the quadratic optimization problem are described in QP Matrices.

If, for numerical reasons, the QP problem becomes infeasible, the second sample from the previous optimal sequence is applied, i.e. $u(k) = u(k-1)+\Delta^* u(k|k-1)$.

2.4.3 Convex Optimization

In order to use optimization for control allocation, it is natural to construct convex optimization problems. Such problems possess many attractive properties, and efficient solvers exist for a wide range of problem formulations. Additionally, a very large number of problems can be posed as convex optimization problems. In this section, a number of different problem formulations will be outlined. In the following section, methods for solving these types of problems will be reviewed.

The general form of a convex optimization problem is:

$$\min \ : f_o(x) \tag{2.11}$$

$$subject\ \ to: \ \ f_i(x) \le b_i, \quad (i=1,\cdots n) \tag{2.12}$$

in which the objective function $f_0(x)$ and the constraints $f_i(x) \le b_i$ are convex functions. The feasible set P of the optimization problem is the region in which the constraints are satisfied. The optimum x^* is the point in the feasible set where the objective function which is also called cost function is minimized. In QP problem, the objective function is convex quadratic.

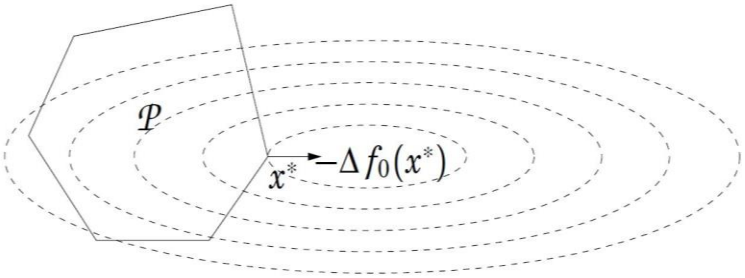

Figure 2.5: Interpretation of the solution of a LCQP problem [72].

When linear constraints are present, the QP problem has the form:

$$\min imize : \frac{1}{2}x^T Px + q^T x + r \tag{2.13}$$

$$\begin{aligned} subject\ \ to : Gx &\leq h \\ Ax &= b \end{aligned} \tag{2.14}$$

Figure 2.5 gives a graphical interpretation of a LCQP problem which happens in the controller design. Posing control allocation problems as convex optimization problems is attractive since there is a wide variety of an efficient solver for different types of problems. Two classes of methods are of particular interest to the optimization problems considered, interior point [72] and active set methods [73]. Interior point methods can be used for convex problems that include inequality constraints, such as LCQP problems.

Active set methods are based on finding the active constraints and solving simpler equality-constrained problems. These methods are particularly suitable for control allocation, for several reasons. Primarily, active set algorithms have the appealing property that a feasible solution is available after each iteration process. For applications in a real-time environment this is particularly useful, since it means that if the algorithm must be interrupted, a feasible solution will always be available. In addition, active set methods become much more efficient when a good estimate of the active set is available. For control allocation purposes, a good estimate of the active set is usually given by the active set from the previous sample.

2.5 Literature of MPC on Vehicle Application

New trends in automotive industry process applications with an increased content of computers, electronics, and controls stress on the improved capability and functionality for overall system robustness. This tendency affects the entire vehicle

areas such as aerial vehicle, underwater vehicle, and especially in particular interest for ground vehicle applications.

Today, MPC is one of the more popular optimal control techniques widely employed for the control of constrained linear or nonlinear systems where a mathematical dynamics process model is used to predict a future value and optimizing the process control performance.

Because of its advantages, MPC has been implemented in automotive applications covering a wide range of advanced control systems, such as various active safety and driver assistance systems [74-75], vehicle dynamics systems [76-77], driver modeling systems [78-79], autonomous driving and collision avoidance systems, path-following control, integrated chassis control systems [80-81], and other related topics in vehicle control.

At present, the most important topics for researchers and automotive manufacturers are those related to the use of active safety systems such as active steering [82], active traction [83], active braking [84], and active differentials [85] or suspension [86] to coordinate and improve vehicle handling, stability, ride comfort while avoiding collisions, and to prevent traffic accidents. A passive safety approach essentially focused on the body or structural stability of vehicle, while active safety are mainly used to prevent collisions before it happened and to facilitate better vehicle stability and controllability especially in unexpected or hazardous situations [87].

In this sub-chapter, we limit the vehicle to a ground vehicle which related to the authors work. These vehicles are increasingly studied by several researchers either from academia, industry, and the military, by using several control methods such as 2WS, which uses either front or rear steering [88-89], 4WS, which uses front and rear steering [90-91], and DYC, which uses driving or braking forces [92-93] with different control purposes.

In MPC approaches, the nonlinear MPC imposes challenges in computational optimization problems requiring instant solving at each sampling for real-time implementation algorithm; thus, the complexity become the reason why most researchers have moved to linear MPC.

Figure 2.6 shows a vehicle with coordinate systems to define the basic dynamics that are relevant for maintaining control of the vehicle. There are several aspects need to be considered for active safety and stability control. Here, we focused

MPC applications for car vehicle dynamics system at three main aspects; steering and braking control, yaw and roll control, and active and semi-active suspension control.

2.5.1 Steering and Braking Control

Initially, the work that related to active safety was focusing on longitudinal dynamics part of motion, under consideration on existed ABS and TCS due to main issue on braking performances. This work was followed by different types of VSC systems such as ESC or dynamic stability control that use brakes through controlling the yaw motion of the vehicles by stabilizing the vehicle in utmost limit handling situations. Later, there was an effort that related to enhance vehicle's handling performance by 4WS control. Unfortunately, the early efforts and development by this existed control systems were initially focused on handling improvement without clearly express on stability control for vehicle active safety.

A nonlinear MPC based on bicycle model for AS control design was firstly presented for autonomous vehicle systems in [94] as shown in Figure 2.7. The objective of designed controller for a given desired path is to stabilize a vehicle along the trajectory and rejecting winds gusts disturbance while satisfy its physical constraints. Simulation results showed the advantages of the systematic control methodology for a double lane change maneuver scenario with side wind rejection on slippery surfaces. Further research continued from [94], controller design was implemented in real time by using advanced sensors, actuators, and nonlinear optimization solvers to control a front wheel steering in order to stabilize a vehicle in the same scenarios [95].

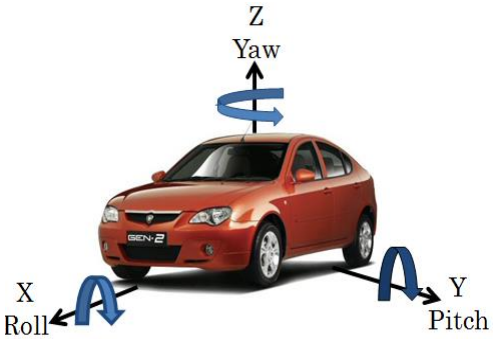

Figure 2.6: Vehicle dynamics axes coordinates .

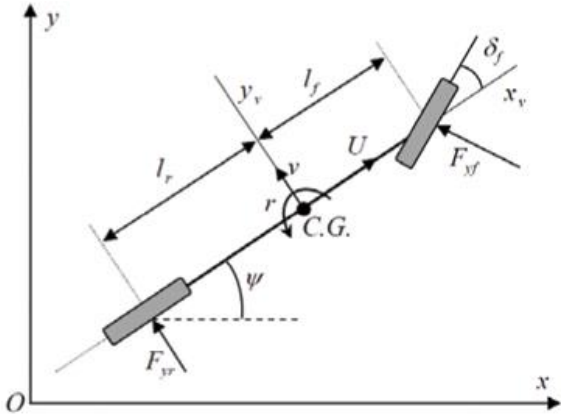

Figure 2.7: Simplified for bicycle and model [94].

Based on author's knowledge, it is the first time a NMPC has been successfully applied experimentally in fast automotive for autonomous vehicle application. However, the experimental results obtained only at a low vehicle speeds on icy roads with a passenger car due to computational complexity and limitation of the nonlinear programming solver. In [96], a LTV MPC has been designed, implemented and compared with NMPC through simulations and experiments. The results illustrated that both approaches compute worst computational time and have the difficulty in verifying the optimization code.

To overcome these issues, a modification of LTV MPC controller with a low order vehicle model can be easily implemented and shows better stability performance. With a finite dimensional optimal control problem, the nonlinear vehicle dynamics is discretized with a fixed sampling time can be rewritten in following compact form:

$$\begin{aligned} \xi(k+1) &= f_{s(k),\mu(k)}\ (\xi(k), \Delta u(k)) \\ u(k) &= u(k-1) + \Delta u(k) \end{aligned} \tag{2.15}$$

where, *u(k)* is control signal and $\xi(k)$ represent state vectors.

Moreover, issue in interaction between the vehicle interface and driver knowledge requires a demand an improved control and model of driver skill for steering and braking control task. The derivation of a nonlinear driver model based on steering control with multiple vehicle dynamics linearized models has been presented in [97-98]. A predictive control for driver steering skill and knowledge includes of multiple internal models which represents the actual vehicle dynamics system was explained. The simulation results indicated that there are continued and strong relationship for substantial improvement in understanding and modeling driver skill based on the internal model concepts.

Instead of only employed steering approach, a LTV MPC approach in autonomous car vehicle for combined braking and steering has been presented in [99] and compared with [96]. The comparison performance of the stability approach has been evaluated in simulation and experimental on a snow and icy road for a double lane change maneuver at high speed. The results showed that the LTV MPC with combination braking and steering control is capable to slowing down and stabilize the vehicle in order to completely follow the desired trajectory. It also enables the use of constraints for obstacle avoidance scenario.

In [100], MPC was used to investigate the problem of roadway departure prevention through steering and braking by considering a two layer architecture which are a threat assessment; within a future time horizon, detects the vehicle instability and the risk of roadway departure, and an intervention layer; this layer is enabled if a vehicle instability or risk of roadway departure is detected. Simulation and experimental results are elaborated and presenting the proposed approach which take into account road preview capabilities effectively in order to issue earlier and less intrusive interventions compared to standard ESC systems.

Previous worked in [96-100] is assumed for known trajectories while in [101], a HMPC design for coordinated control of AFS and ESC was applied to vehicle trajectory stabilization for unknown trajectories. Based on bicycle model as an appropriate model vehicle dynamics in high speed, the vehicle model is formulated as a linear hybrid dynamical system in PWA form by respect to the front and rear tire slip angles and with approximating the tire-force characteristics. Simulations of the controller for the dynamics system of longitudinal, lateral, and yaw rate with steering control showed the stability of the system response and a fast tracking response.

In [102], they investigated the coordination of AFS and DBC in a driver assist steering system by implemented a SMPC as a control approach to stabilize the vehicle and achieve the desired yaw rate based on PWA. Since the alternative to HMPC in [101], even in explicit form was shown to be too complex, a SMPC which is easier to implement has developed. The predictive control response in single and double lane change maneuvers was evaluated in simulations, also experimentally on a low friction test track by way of a rapid prototyping unit.

Recently in [103-104], there are research on designing of a controller that is capable of smoothly and progressively augmenting the driver steering input to enforce the boundaries of the trajectory. The MPC formulation provides a method for making trade-offs between enforcing the boundaries of the envelope, minimizing disruptive interventions, and tracking the driver's intended trajectory. It has been demonstrated that the MPC yields good performance in conjunction with the human driver and also stabilizes the vehicle.

2.5.2 Yaw and Roll Dynamics Control

Yaw stability is one of the most important to the overall safety and stability of an automotive vehicle in a steering maneuver condition. Basically, yaw is a rotation about the vertical or *z*-axis such as the vehicle is skidding or drifting, or in extreme circumstances or lateral wind force and a yaw angle usually considered being a difference between the direction of travel and the longitudinal axis of the vehicle body. On the other hand, roll is a rotation about the longitudinal axis, commonly referred to as the *x*-axis which the motion can be noticed for under heavy cornering where the body leans towards the outside of the bend.

Technology advances in software, vehicle and control design can provide an increased number of possible interference to influence the vehicle behavior. In recent years, existing control system which have potential of reducing vehicle accidents such as ESC and AFS are driver assist systems that can improve longitudinal, lateral and yaw vehicle stability have been introduced and implemented to industrial vehicle applications. However, in steering maneuver scenario, yaw and lateral stability of a car vehicle is difficult to stabilize and it handling performance become more challenging.

In [105], by using nonlinear computation multi-parametric programming, the problem of control allocation in yaw dynamics stabilization has been solved where an approximate solution obtained in online implementation throughout the piecewise linear function. Simulation result showed that, in case the vehicle lost steer ability under manual steering wheel control, the maneuver remained stable with controller applied.

However, due to the sampling time needed by control law application that gave too low response in real time optimization became a limitation in the practical use of NMPC. NMPC efficiency regarding it implementation has been solved using an approximated control function presented in [106]. With approximated control gave less computational time, FMPC methodology was determined and formulated with the nearest point approach that was based on offline computation. The simulation result showed that a highly damped behavior in reversal steer maneuvers was obtained and stability is guaranteed.

Moreover, in [107], a vehicle yaw stability controller based on MPC approach was designed to solve problem with brake torque constraints of electronic mechanical

brake mechanism and over actuated in vehicle yaw control. MPC was implemented to calculate control input online and it was implemented on simple 6DoF linear vehicle model that takes into account tire nonlinear characteristics as shown in Figure 2.8. Simulation results demonstrated the effectiveness of the proposed controller which forced the vehicle yaw rate to follow reference yaw rate which keep vehicle slip angle in small range.

In late 2011, MPC technique based on an integrated control algorithm for vehicle in active steering and dynamics yaw control was proposed in [108]. By adjusting the weight of control and inputs variables, the algorithm for yaw rate and slip angle is consider in order to achieve online computational real-time with future operation of optimization and prediction. Based on 2DoF vehicle model, the hierarchical integrated control structures was adopted in the algorithm by using of two line tire model for vehicle stability control. The tires limitations and force allocation problem was solved by designing the MPC and takes into account the quadratic programming. Based on simulation results, the predictive control algorithm is verified, tested and it proved the algorithm can enhanced the body vehicle stability.

On the other hand, in [109], instead of considering yaw and lateral stability through AFS control with friction roads in ranging scenarios from snow to dry asphalt, roll motion effects in lateral load transfer are sententious and take into account for stability control. With NMPC as a control approach, simulation results based on more complex twelfth-order full vehicle nonlinear model demonstrated that the involvement of the roll dynamics vehicle motions in the controller design for prediction model, consequentially improved the dynamics vehicle behaviour at high speed on high friction surfaces, thus improving the path following, and also steering control become much smoother.

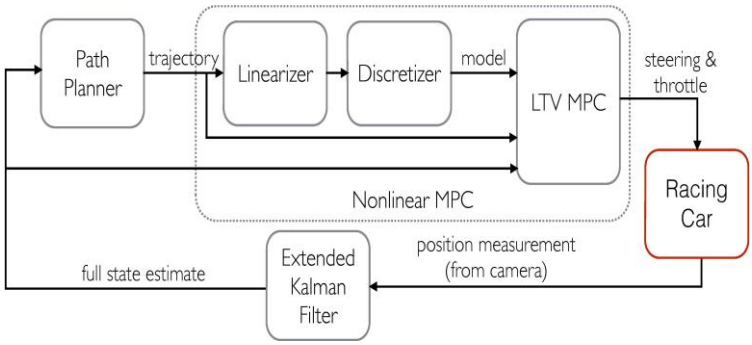

Figure 2.8: Diagram for vehicle yaw dynamics control system [107].

Roll dynamics vehicle motions is indicated through the nonlinear differential equation as follow:

$$(I_x + msh_{rc}^2)\ddot{\phi} + I_{xz}\ddot{\psi} = m_s g h_{rc}\phi - 2k_\phi\phi - 2b_\phi\dot{\phi} + m_s h_{rc}(\ddot{y} + \dot{\psi}\dot{x}) \quad (2.16)$$

Work in [110], presented simulation results for a MPC scheme that utilized front steer-by-wire and rear wheel drive/brake torque to modify the vehicle roll behavior while minimizing the error between the planar vehicle dynamics and those predicted by the unmodified driver input. This formulation of the rollover control problem provides a mechanism for the system to coordinate the control inputs to prevent the rollover event and simultaneously maintain the validity of the driver's internal model of the vehicle behavior.

Experimental results by using a custom-written convex optimization solver demonstrated that real time solutions to the MPC problem are feasible. There was a primary performance limitation to the MPC scheme due to actuator saturation of the drive/brake torque when attempting to compensate for changes to the front steering angle.

In concurrent work by [111], they presented a new controller, generated with the same MPC framework that uses front and rear wheel steering as the actuators. A roll stability controller was presented based on an 8DoF dynamic vehicle model. The controller was designed for and tested on a scaled vehicle performing obstacle avoidance maneuvers on a populated test track with the load transfer effects were neglected because of the consideration for low friction surfaces.

Simulation results were presented, they succeeded in demonstrating that the steering controller required significantly lower actuator effort than the drive/brake controller that was previously introduced. This lower actuator effort results in improved tracking of the nominal planar behavior of the vehicle and thus is interpreted as having better properties for interaction with the human driver.

2.5.3 Active and Semi-Active Suspension Control

Car vehicle suspensions control system serves several purposes; the main purposes are to maximize the passenger ride comfort, isolate the passenger compartment from road irregularities, and vehicle road handling quality especially from acceleration, braking, cornering, and changes in payload due to counteracting the body forces. Another issue

of suspension system is a permanent contact between the tires and the road should be assured for driving safety.

Two types of suspension systems; a passive suspension that have serious limitations is built from springs and dampers where the movement is being determined entirely by the road surface, while the active suspension or semi-active suspension on the other hand control the vertical movement of the wheels with an onboard system. Actuators active suspension systems which can exert an independent force are integrated between the wheels and the vehicle body, which can influence the vertical dynamics of the vehicle to improve the riding characteristics. Figure 2.9(a) shows example of active suspension systems for quarter-car model.

MPC was first designed for suspensions system to control an active suspension system for 2DoF quarter-car model by utilizing previewed road information in [112]. MPC was designed clearly expressed and incorporating all hard constraints on control signal, state, and output variables. Based on single step control to multiple step control over a receding prediction horizon, it used feedback linearization and dynamic inversion for generalizes approaches. Based on simulation results, it showed better improvement in the ride comfort and road handling quality.

In [113], MPC was applied and it is assumed that the preview information of the oncoming road disturbance is available based on a half-car model by considering the physical limits of the suspension travel for the vehicle running over a rough road. Thus, the limits of suspension travel are accounted with a high bandwidth actuator integrated between vehicle body and wheel mass.

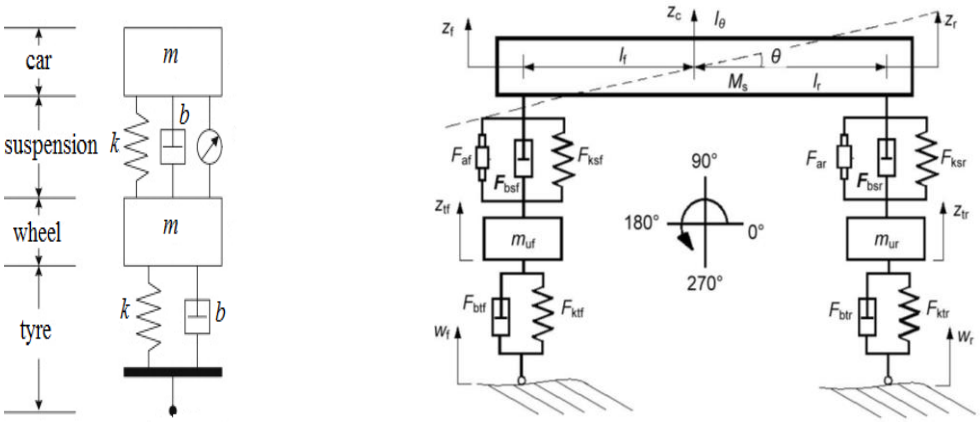

(a) Quarter-car [112]. (b) Half-car [113].

Figure 2.9: Active suspension model.

Furthermore in [114-115], a neural network with MPC has been designed for a nonlinear quarter-car servo-hydraulic active suspension system. The designed controller showed that neural network predictive controller can be successfully applied in the vehicle suspension system. The results in the presence of deterministic disturbance input shows better tracking performance of the desired output compared to constant gain PID controller.

Recently, a model predictive approach as controller design for a vehicle with active suspension and available preview information about the oncoming road height profile has been presented in [116]. In that chapter, by considering the roll mode of the vehicle body respectively different road profiles in front of the left and the right wheels, a full-car nonlinear model of the vertical dynamics was used as model for the controller designed. Power saving low bandwidth active suspension systems was regarded with an actuator in series to the primary spring. The controller was designed to reduce vehicle body accelerations in order to improve ride comfort in consideration of constraints on the control variable. Simulation results showed a huge reduction of vehicle body accelerations and hence improvement of ride comfort was possible.

Full active suspension of automotive systems has the ability to save, store, and dissipate energy to the system. Consequence of the advantages, the trade-offs among conflicting design goals can be better resolved. Unfortunately, active suspension systems require high levels of energy consumption and more suitable actuator devices leading to highest system costs. The complication of the mechanism, difficulties to diagnose, and the need for frequent maintenance on some implementations, also become one of its drawbacks. To reduce its drawbacks, semi-active suspensions were proposed that can vary the damping coefficient by making use of a damper. Semi-active suspensions include devices such as air springs and switchable shock absorbers, and various self-levelling solutions.

FMPC strategy for control, design and analysis has been introduced for semi-active suspensions in car vehicles [117]. The effectiveness and performances of the proposed procedure was explained and shown based on comparison with well-established semi-active suspension control strategies i.e. Sky-Hook and linear quadratic optimal or clipped control.

Based on accurate information of the car vehicle dynamic behavior equipped with continuous damping control, the extensive tests have been performed on the half-

car nonlinear model. The test is an adequately compared to actual measurements test performed on a four-posters bench. Based on simulation results that take into account the inclusion of prediction in control computation design have shown improving the handling characteristics in almost all the considered road classes and significantly enhances comfort driving performances.

2.6 Summary

This chapter has discussed the basic ideas about MPC based on the receding horizon control principle, with its strategy approach. The main objective of this chapter is to review MPC schemes that are applied to car vehicle dynamics system for active safety and stability. We classify the literatures based on the three main criteria, i.e. steering and braking control, yaw and roll control, and suspension control. Although MPC approaches of car vehicle dynamics system have been particularly well studied, however, there are a few key areas in which this work may be extended and improved as mentioned in Chapter 6.

This chapter also has discussed about the path-following maneuver control, rollover prevention control, and vehicle dynamics control system: vehicle yaw stability and vehicle roll stability control. The literature regarding related topic has been reviewed and discussed.

Chapter 3
Modeling and Validation of Vehicle Dynamics System

3.1 Introduction

Modeling is the construction of physical or mathematical simulation of the real system. It is a process of representing the behavior of the real systems by a collection of mathematical equations. A model of a system is developed for several reasons, such as to solve a problem in short period of time economically, to ease the manipulation of variables plant or system and finally to enable to test the model for the best solution for the particular problem. Most of the controllers need a model in design process. These descriptions have to be relatively simple, yet accurate enough to serve the purpose of the modeler [118]. There are many approaches in obtaining a model of a system such as derivation directly from some physical laws, invoking the physical laws, and collecting experimental data and using them to obtain input(s) and output(s).

In this chapter, the mathematical model of a ground nonlinear vehicle dynamic system is developed by introducing tire model and bicycle models, which have been commonly adopted for vehicle dynamics control. The introduced models help to get a basic idea of what states and parameters of a vehicle those are important to implement vehicle dynamics control systems. This chapter also introduces disturbances model such as wind force model, road bank model, and friction split. Moreover, the rollover indicator called LTR also explained. Several important vehicle parameters and key words such as tire lateral force, steer characteristic and inertial trajectory of the vehicle are highlighted. The controller is implemented in the computer and drives the system through simulation process. At the end, the obtained vehicle dynamics system model and its parameters are validated through standard maneuver testing i.e. fishhook, double lane change, roll feedback, and etc. to stronger the validation of the vehicle model. Later in Chapter 4, the proposed controller are compared with the well-known controller particularly LQR control to strengthen the credibility of the thesis.

3.2 Vehicle Model

Figure 3.1 shows the well-known vehicle model, which is a single-track model based on the simplification that the right and left wheels are lumped together as a single

wheel at the front and rear axles. The simplified vehicle model used in this chapter illustrates the motion and dynamics of the vehicle subject to the longitudinal, lateral, yaw, and roll motions representing the 4DoF in the model.

The longitudinal, lateral, and yaw dynamics effects are shown from the top view of the vehicle in Figure 3.1(a) and 3.1(b) for different control maneuvers. While, the roll angle and road bank angle motions are demonstrated in Figure 3.1(c) and Figure 3.1(d), with the nomenclature for front and lateral view of the car vehicle.

In this study, we assume that the complexity of the actual vehicle can be reduced; the steering angles at the right and left wheels of each axle to be the same, i.e. $\delta_{f,l} = \delta_{f,r} = \delta_f$ and $\delta_{r,l} = \delta_{r,r} = \delta_r$. Second assumption that took into account is the slip angles at front and rear axles are both zero (free rolling wheels) at low speed vehicle motion where the radius of the vehicle path changes slowly. Through the small angles approximation, the vehicle side slip, steering, and roll motions are well approximated by a linear function i.e. $\cos\theta = 1$ and $\sin\theta = \theta$.

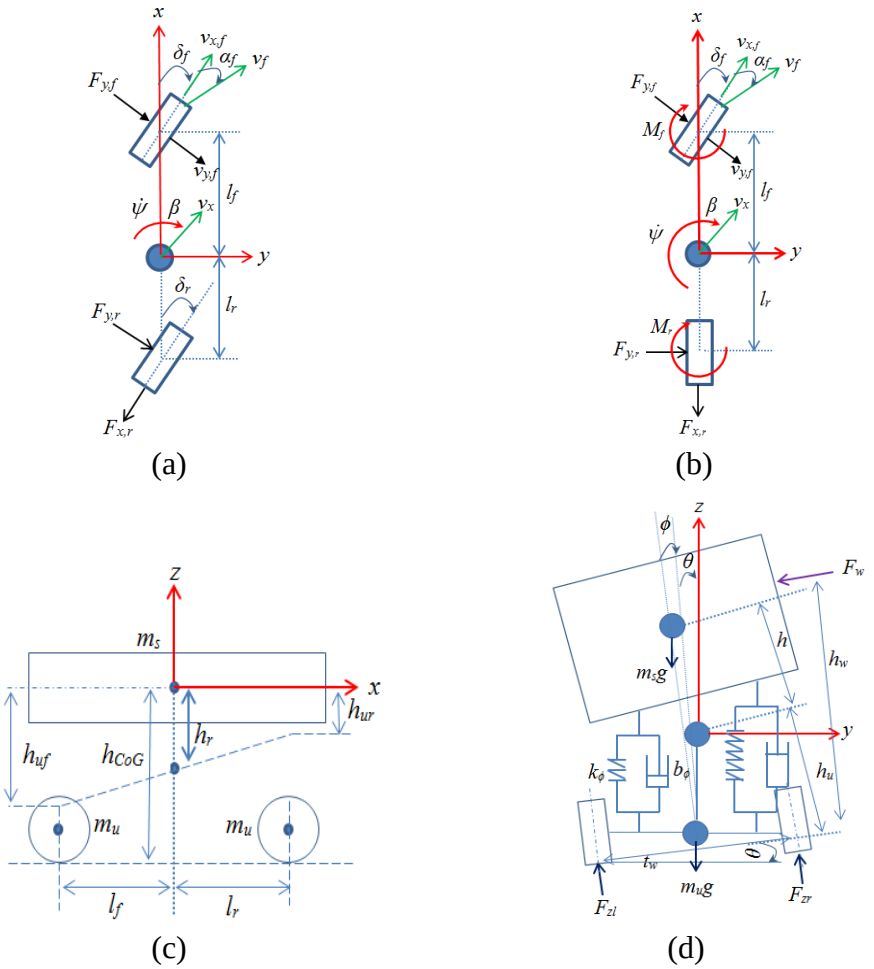

Figure 3.1: Simplified bicycle model: (a) 4WS, (b) 2WS with DYC, (c) Side view, (d) Front view.

The sprung vehicle mass and the suspension and wheel weight for un-sprung mass rotates in the yaw direction is considered in this chapter. Here, the pitch motion and bridge acceleration are neglected. The details of the mathematical calculations for the vehicle model are presented in [119-120].

Throughout this manuscript, we acquire the nomenclature which is denoted in the list of symbols. The first lower subscript $(\cdot)_f$ and $(\cdot)_r$ represent the variable associated with the front and rear axles, while the second lower subscript $(\cdot)_l$ and $(\cdot)_r$ denote left and right of front and rear axles respectively.

As described through assumption above; the vehicle lateral, longitudinal, roll, yaw, and each tire rotational dynamics motion of 8DoF for the nonlinear vehicle model, the dynamics motion incorporate with the disturbances impact are expressed in planar characteristics equations:

$$\sum F_y : m(\ddot{y}+\dot{x}\dot{\psi}) = 2F_{yf} + 2F_{yr} - m_s h\ddot{\phi} - m_s h\phi\dot{\psi}^2 - m_s h\phi\dot{\phi}^2 + (l_r - l_f)m_u\ddot{\psi} + F_b + F_{wy} \tag{3.1}$$

$$\sum F_x : m(\ddot{x}-\dot{y}\dot{\psi}) = 2F_{xf} + 2F_{xr} - m_s h\ddot{\psi}\phi - 2m_s h\dot{\psi}\dot{\phi} + (l_f - l_r)m_u\dot{\psi}^2 + F_{wx} \tag{3.2}$$

$$\sum M_x : (I_{xx} + m_s h^2)\ddot{\phi} + m_s h(\ddot{y}+\dot{x}\dot{\psi}) - I_{xz}\ddot{\psi} = m_s gh(\phi+\theta) - (k_{\phi f} + k_{\phi r})\phi - (b_{\phi f} + b_{\phi r})\dot{\phi} + M_{wx} \tag{3.3}$$

$$\sum M_z : I_{zz}\ddot{\psi} - I_{xz}\ddot{\phi} = {t_w}/{2}\,(-F_{xf,l} + F_{xf,r} - F_{xr,l} + F_{xr,r}) + 2l_f F_{yf} - 2l_r F_{yr} + (l_r - l_f)m_u(\ddot{y}+\dot{x}\dot{\psi}) + M_{wz} \tag{3.4}$$

$$J_b\,\dot{\omega}_{wi} = -r_w F_{xi} - T_{bi} - b_w\omega_i,\ \ i=(f,r) \tag{3.5}$$

Here, we need to consider that the desired yaw rate and desired side slip angle must be limited due to capability vehicle in maximum acceleration and as for body side slip angle under small angle assumptions. There are given in the following equation:

$$\dot{\psi}_{des} \le \frac{\mu g}{v_x}, \qquad \beta_{des} < \tan^{-1}(0.02\,\mu g) \tag{3.6}$$

$$\beta \approx \frac{\dot{y}}{v_x} \tag{3.7}$$

where the desired yaw rate and side slip responses cannot always be obtained when tire force goes beyond the adhesion limit of tire, thus, it has an upper bound limit [121]. The equations of motion for the vehicle in an inertial frame described by *Y-X* coordinates under the assumption of a small yaw angle may be written as:

$$\dot{X} = \dot{x}\cos\psi - \dot{y}\sin\psi \approx v_x - \dot{y}\psi \tag{3.8}$$

$$\dot{Y} = \dot{x}\sin\psi + \dot{y}\cos\psi \approx v_x\psi + \dot{y} \tag{3.9}$$

3.3 Tire Model

Tires exhibit highly nonlinear behavior during the cornering on different surfaces. There are mainly two kinds of tire models; a physical tire model and an empirical tire model. The physical tire model (brush model, LuGre tire model, Dugoff tire model, UniTire model) are able theoretically to describe the tire characteristics, but it lacks of accuracy, while an empirical tire model (Pacejka tire model, Unified semi-empirical) is the curve fitting results of the actual tire data which is quite accurate.

The brush model utilizes the concepts of force demand and force availability to determine the total force developed in the portion of the tire in contact with the road, typically referred to as the contact patch. Since the stress in the brushes is proportional to the displacement of the wheel over the time period from first contact, the distribution of stress throughout the contact patches increases at the angle between the lateral and longitudinal wheel velocities [122].

The LuGre tire model is more complicated tire model based on a dynamic visco-elastoplastic friction model for point contact that were initially derived as distributed models described by a set of partial differential equations [123]. The Dugoff tire model describes the decreasing effect in the sliding region and clearly divides the curve of the tire lateral force into the linear and nonlinear region of the adhesive region and the sliding region [124].

On the other hand, Pacejka tire model is the curve fitting results of actual data that can accurately describes the behavior of a certain type of tire. However, if the type of tire has changed, the coefficient parameters of the Pacejka tire model should be changed [125].

Therefore, the forces acting on a tire must be studied and considered for the determination of the dynamic behavior of a vehicle model, due to the fact that the tires are the only point of contact between a vehicle and the friction of the road surface. In all cases, except for aerodynamic drag and gravitational forces, all of the forces which may affect vehicle chassis, stability behavior, and handling characteristic are produced by the tires. Thus, tire has to help the vehicle steer with precision and increase vehicle stability regardless of road and weather conditions.

Due to the highly complexity and nonlinear of dynamic behavior of tires, thus, it must also reflect the controller design operating condition over their entire region throughout varied maneuvering range in lateral, longitudinal, and roll. The most

usually employed of the existing and continuing nonlinear tire models structure and applications are determined based on the key variable and parameters with analytical considerations that still depend on tire data measurements. This complex tire model so called Pacejka tire model or semi-empirical tire model [126] and is used in this study.

The tire model is illustrated in Figure 3.2, where the terminologies used for illustrating the longitudinal and lateral tire forces and it orientation are presented. Figure 3.3(a) and Figure 3.3(b) describe the connection between the longitudinal tire force, the tire slip ratio, and the normal load forces for rear and front wheels because of the weight transfer induced by roll motion and lateral accelerations. Their relationships can be expressed by the following equations:

$$\sqrt{F_{xi}^2 + F_{yi}^2} \le \mu F_{zi}, \quad i=(f,r) \tag{3.10}$$

$$F_{zf,i} = \frac{l_r mg}{2l} - \frac{F_{yf}\phi}{2} \pm \frac{k_{\phi f}\phi}{t_w} \pm \frac{b_{\phi f}\dot{\phi}}{t_w} \pm \frac{h_{uf}F_{yf}}{t_w} \pm \frac{h_{uf}l_r mg\phi}{t_w l} \tag{3.11}$$

$$F_{zr,i} = \frac{l_f mg}{2l} - \frac{F_{yr}\phi}{2} \pm \frac{k_{\phi r}\phi}{t_w} \pm \frac{b_{\phi r}\dot{\phi}}{t_w} \pm \frac{h_{ur}F_{yr}}{t_w} \pm \frac{h_{ur}l_f mg\phi}{t_w l} \tag{3.12}$$

The nonlinear dynamics behavior of the longitudinal and lateral tire forces on the rear and front wheels with road friction are defined and designed by a Pacejka tire model as:

$$F_x(s) = \mu_x(s) D_x \sin\left[C_x \tan^{-1}\left\{B_x(1-E_x)s + E_x \tan^{-1}(B_x s)\right\}\right] \tag{3.13}$$

$$F_y(\alpha) = \mu_y(\alpha) D_y \sin\left[C_y \tan^{-1}\left\{B_y(1-E_y)\alpha + E_y \tan^{-1}(B_y \alpha)\right\}\right] \tag{3.14}$$

where variable parameter expressed in Equations (3.13) and (3.14) for *B*, *C*, *D*, and *E* representing the constant values of tire stiffness factor, shape factor, peak factor, and curvature factor that vary with the vertical load which is depend on road conditions and tire characteristics. Figure 3.3(c) and Figure 3.3(d) describe the combined corresponding tire forces at different longitudinal tire slip ratio and lateral slip angle. Through nonlinear function in the kinematic relationship; the lateral wheel slip angles for front and rear axles, and the longitudinal wheel slip ratio may be defined as:

$$\alpha_f = \delta_f - \tan^{-1}\left(\frac{\dot{y} + l_f\dot{\psi}}{\dot{x}}\right), \qquad \alpha_r = \delta_r - \tan^{-1}\left(\frac{\dot{y} - l_r\dot{\psi}}{\dot{x}}\right) \tag{3.15}$$

$$s = \frac{r_w \omega_w}{v_x} - 1, \quad \text{braking if } r_w\omega_w < v_x \tag{3.16}$$

$$s = 1 - \frac{v_x}{r_w \omega_w}, \quad \text{acceleration if } r_w \omega_w \geq v_x \tag{3.17}$$

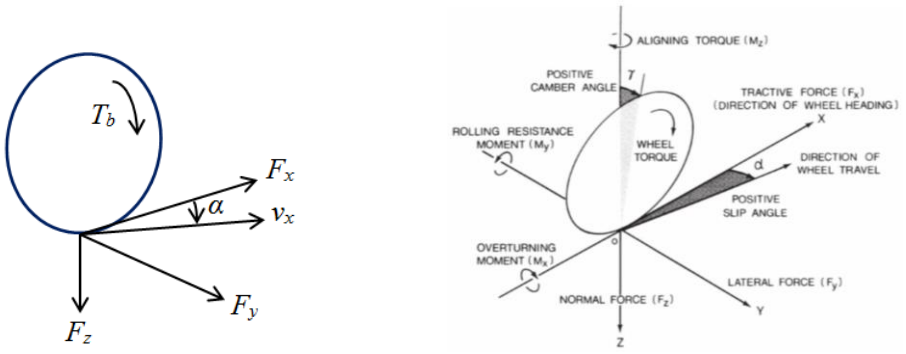

(a) (b) [122]

Figure 3.2: Tire force coordination and orientation.

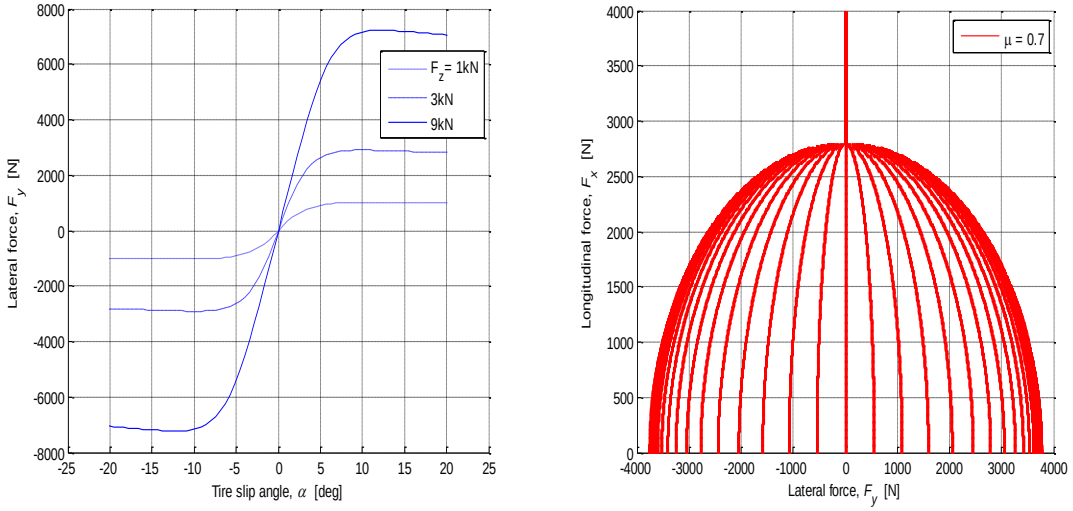

(a) (b)

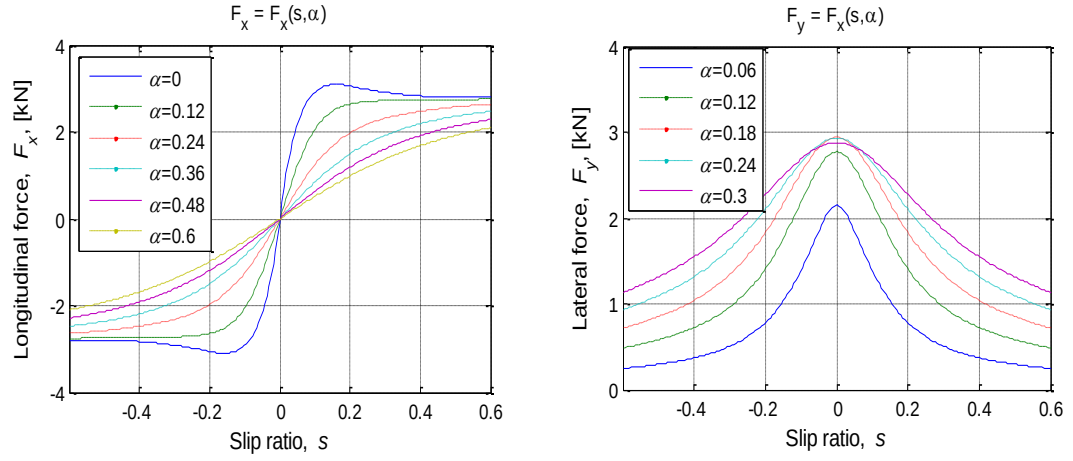

(c) (d)

Figure 3.3: Empirical Tire model: (a) Lateral forces with different vertical forces, (b) Tire forces under friction coefficient, (c) Combined longitudinal tire forces with different slip angle, (d) Combined lateral tire forces with different slip angle.

The lateral forces on the front and rear tires are characterized and modelled by a linear function with the front and rear tire slip angles α_f and α_r denoted by $F_{y,f}$ and $F_{y,r}$ respectively.

The linear tire model yields the following expression for the front and rear tire forces:

$$F_{y,f} = C_f \alpha_f, \qquad F_{y,r} = C_r \alpha_r \tag{3.18}$$

Assumptions and approximations presented in this chapter are representative of the nonlinear tire model at certain regional points; this provides a good balance between capturing the important features and regions of laterally unstable behavior [127].

3.4 Disturbances Model

The effect of the lateral wind especially on the stability and maneuverability of the vehicles is an important and primary safety consideration of this chapter. An extremely strong gust of wind either coming from the center or outside of the curve may yield the extra force and moment torque needed that helps and supports prevent the pull-out or overturning forces. The resulting forces and torques caused by the impact of wind pressure acting on the rigid body, in general, can be represented by three axes; longitudinal, lateral and vertical components. General expression of force and torque are given by the following equations:

$$F_{wy} = \frac{C_F \rho A v_r^2}{2}, \qquad M_{wz} = \frac{C_F l_w \rho A l v_r^2}{2}, \qquad M_{wx} = \frac{C_F h_w \rho A l v_r^2}{2} \tag{3.19}$$

The wind force and yaw moment coefficient are resolved with respect to the mass CoG of the vehicle [128]. Then, we define the distance between vehicle's aerodynamic center and CoG of the vehicle as l_w on X-axis and h_w on Y-axis respectively as shown in Figure 3.4(d). In general, crosswind can be at various angle, but for its simplicity, in this chapter we will assume that the crosswind at 90deg angle and we will focus the wind impact to the lateral forces and yaw torques [129]. Here, we neglect the wind effect on longitudinal motion. However, based on [130], we may neglect the wind effect on longitudinal and roll motion; thus, a side wind impacting the car at the wind velocity exerts a force and a moment, respectively given by:

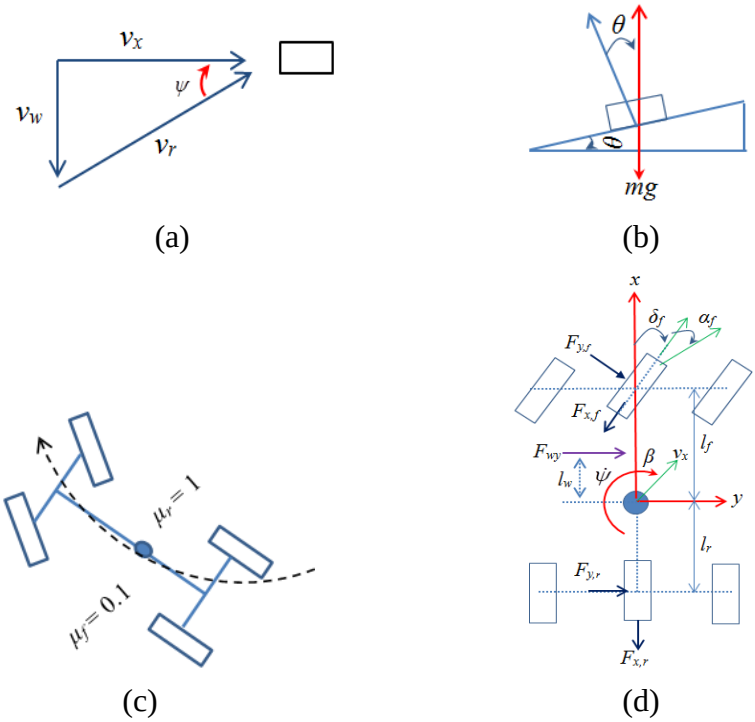

Figure 3.4: Vehicle under disturbances situation: (a) Gust of wind, (b) Bank angle, (c) Mu-split, (d) Vehicle's aerodynamic center.

$$F_{wy} = \frac{2.5\pi v_w^2}{2}, \qquad M_{wz} = \left(\frac{2.5\pi}{2} - 3.3\left(\frac{\pi}{2}\right)^3\right) v_w^2 + \frac{(l_f - l_r)F_{wy}}{2} \tag{3.20}$$

On the other hand, the road bank angle is defined as an angle between the vehicle frame and the intermediate coordinate [131-132]. In many cases, the road profile is not perfectly level in the lateral direction. This is also the case just outside the road boundaries, as the terrain typically slopes down as it moves away from the road. Therefore, it is necessary to take the road bank angle into consideration for these driving situations. Figure 3.4(b) illustrates the road bank angle effect. If we consider the road bank angles that might influence the vehicle, then, it can be written as:

$$\begin{aligned} \sum F_y &: F_b = m_s g\theta \\ \sum M_x &: m_s hg(\phi + \theta) \end{aligned} \tag{3.21}$$

Split friction is a rare road safety issue and problem that happens when the road friction certainly contrasts between the front and rear wheels or the right and the left wheel-path [133-134]. In the case of vehicle in the normal accelerating, turning, drifting or even braking softly, the split friction scenario then the road may not be anticipated as dangerous or hazardous. However, in a case of emergency braking, the heavy vehicle's tires lose their grip on the surface of the road, which will start to

spin/twist over the wheel-path contributing collision and flip over. Therefore, it is necessary to take the mu-split into consideration for these driving situations. Figure 3.4(c) illustrates the mu-split scenario. If we consider the mu-split on left and right of the wheels into Pacejka tire model, then, it can be defined as:

$$\begin{aligned} F_{xf,l}(s) &= \mu_{xf,l} D_{xf,l}\,, \quad F_{xf,r}(s) = \mu_{xf,r} D_{xf,r} \\ F_{yf,l}(\alpha) &= \mu_{yf,l} D_{yf,l}\,, \quad F_{yf,r}(\alpha) = \mu_{yf,r} D_{yf,r} \end{aligned} \tag{3.22}$$

The nonlinear vehicle motion in Equations (3.1) to (3.22) can be described by the following compact differential equation assuming a certain road friction coefficient and tire slip angle values:

$$\dot{\xi} = f_{\mu,\alpha}\,(\xi, u,\ w_d, r_{ref}) \tag{3.23}$$

$$\eta = h\,(\xi) \tag{3.24}$$

where the state, input, disturbance, reference, and output vectors are given as:

$$\xi = [v_y\ \beta\ \ Y\ \ X\ \ \psi\ \ \dot{\psi}\ \dot{\phi}\ \ \phi\ \ \omega_{fl}\ \omega_{fr}\ \omega_{rl}\ \omega_{rr}]^T \tag{3.25}$$

$$\begin{aligned} u &= [\delta_i\,], \qquad AFS / ARS \\ u &= [\delta_i\ M_z]^T, \quad AFS / ARS\ +\ DYC \\ u &= [\delta_i\ \rho_{r,r}\ \rho_{r,l}]^T, \quad AFS / ARS\ +\ DBC \end{aligned} \tag{3.26}$$

$$w_d = [\delta_f\ \ \mu_i\ \ F_b\ \ F_{wy}\ M_{wz}\, M_{wx}]^T \tag{3.27}$$

$$r_{ref} = [Y_{des}\, \psi_{des}]^T \tag{3.28}$$

$$h(\xi) = [Y\ \ \psi\ \dot{\psi}]^T \tag{3.29}$$

3.5 Rollover Indicator

The underlying cause of un-tripped vehicle rollover accidents is the rotational motion occurring when a vehicle makes a turn. Figure 3.5(a) illustrates a vehicle performing a turn with a radius of curvature [23]. In order to maintain the curved trajectory, a force directed towards the center of rotation must act upon the CoG of the vehicle.

Figure 3.5(b) shows the pseudo-force may act on the CoG of a vehicle performing a turn. Note that the pseudo-force acts in the opposite direction to the acceleration that it replaces, that is, it is directed radially outwards from the center of rotation. The external forces acting on the vehicle act at the road-tire contact point, not the CoG, meaning that a resulting moment acts on the vehicle. The magnitude of the resulting moment depends on the height of the CoG above the road. A higher CoG gives a larger moment.

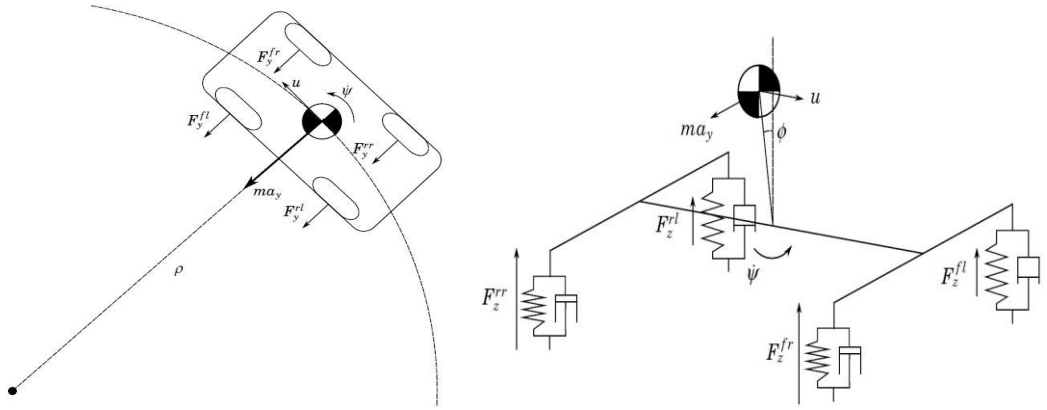

(a) (b)

Figure 3.5: Illustration roll motion: (a) Vehicle driving along a curved trajectory [23], (b) The pseudo-force acting on the vehicle's CoG [128].

This moment is counteracted by a moment due to the reaction (normal) forces acting on the tires. Accurate detection of the danger of a vehicle rollover is important. Initially, the concept of a static rollover threshold called the SSF [128], was studied to detect vehicle rollovers. However, the SSF by itself is not adequate for rollover prediction in dynamic situations.

After SSF, the concept of a rollover index has been introduced, LTR is considered as the most reliable rollover indicator regardless of vehicle configurations and operational conditions, is utilized to detect the onset of the rollover in this chapter. The details about LTR can be found in [130]. The LTR can simply be defined as the load difference between the right and left wheels of the vehicle, normalized by the total load:

$$LTR = \frac{F_{zr} - F_{zl}}{F_{zr} + F_{zl}} \tag{3.30}$$

where F_{zl} and F_{zr} are defined as the vertical tire forces acting on the left side and right side wheels. The TWLO of one side of the vehicle occurs if LTR becomes 1 or -1.

We consider TWLO is equally dangerous to the occupants and as the threshold of rollover, so LTR is not allowed be more than 1 or no less than -1. As the wind and road bank disturbance affect the roll motion directly, the roll rate and roll angle containing the disturbances can be calculated as a whole.

Most of the published paper assumed the un-sprung mass weight to be insignificant and the main body of the vehicle rolls about an axis along the centerline of the track at the ground level. However, we can make a torque balance about the

assumed horizontally roll axles in terms of the suspension torques, and the vertical wheel forces by considering un-sprung mass and lateral load transfer due to lateral acceleration:

$$-F_{zr}\frac{t_w}{2}+F_{zl}\frac{t_w}{2}+k\dot{\phi}+c\phi=0 \tag{3.31}$$

Then, if we consider un-sprung mass in the vertical forces in Equations (3.11) and (3.12) to the LTR equation in Equation (3.30), then, the Equation (3.30) can be transformed to the function below:

$$LTR=\frac{2\left[c\dot{\phi}+k\phi+m_s(\ddot{y}+v_x\dot{\psi}-h\ddot{\phi})+h_u(\frac{l_r m_s g}{l})(\phi+\theta)\right]}{mgt_w} \tag{3.32}$$

It is important to note that the longitudinal load transfer has the effect of decreasing the normal forces at the rear wheels during cornering. This effect implies that the rear wheel on the inside of the turn will be the first to lose contact with the road during a rollover. This type of rollover index is used for detecting un-tripped rollovers only. For the controller design, LTR can be represented in term of state equation as:

$$LTR=Cx=[0\ \ 0\ \ 0\ \ 0\ 0\ \frac{2c}{mg(l_r/t_w)}\ \ \frac{2[k+h_{uf}(l_r m_s g/t_w)]}{mg(l_r/t_w)}\ \ 0\ \ 0\ 0\ 0]^T \tag{3.33}$$

3.6 Maneuver Testing

Vehicle maneuvers testing are applied in order to validate and verify the complex nonlinear vehicle model. As most vehicle engineers know, the most common handling maneuvers used for a vehicle test are J-turn, Fishhook, and double lane change [137] which are representative of on-road maneuvers where the vehicle is not tripped (caused by forces from an external object, such as a curb or a collision with another vehicle). For a basic knowledge, the J-turn test is a single steer maneuver, where, following a sudden turn, the steering wheel is then held fixed for the remainder of the test.

A Fishhook test is a steering reversal maneuver, where the vehicle turns with the steering angle changing from 0deg to -270deg and then from -270deg to 600deg. The last test is the double lane change for the avoidance test which represents a changing vehicle path based on pre-determined cone placement in the road. In this thesis, we performed the NHTSA J-turn, roll rate feedback fishhook, single lane change, and

double lane change test, for vehicle validation purposes in the open-loop simulation, as shown in Figures 3.6 to 3.9. For these scenarios, Table 3.1, Table 3.2, and Table 3.3 shows the model parameters for a Ford Taurus SUV, SUV based on [138], and single lorry based on [139] respectively.

In the first scenarios, we make the J-turn and roll rate feedback fishhook tests, where we set the vehicle speed at 20m/s with a road surface coefficient of 1 under the vehicle parameters in Table 3.1. The maneuver tests responses are shown in Figures 3.6 and 3.7.

Table 3.1
Parameters of Ford Taurus SUV.

Parameter	**Value**
m	1542
I_{xx}, I_{zz}, I_{xz}	670, 2786, 166
l_f, l_r	0.92, 1.77
h, t_w	0.55, 1.02
b_ϕ, k_ϕ	4500, 72500
C_f, C_r	106000, 88000
g	9.8

Table 3.2
SUV vehicle parameters based on [138].

Parameter	**Value**
m_s, m_{uf},, m_{ur}	1440, 40, 40
I_{xx}, I_{zz}, I_{xz}	900, 2000, 166
l_f, l_r	1.016, 1.524
h, t_w	0.75, 1.5
$b_{\phi f}$, $b_{\phi r}$	1897, 1265
$k_{\phi f}$, $k_{\phi r}$	30000, 20000
C_f, C_r	57296, 52712
J_b, b_w	1.2, 0.5
r_w, g	0.334, 9.8

Table 3.3
Heavy vehicle parameters of single truck [139].

Parameter	**Value**
m, m_s, m_u	16000, 14300, 1700
I_{xx}, I_{zz}, I_{xz}	4718, 34917, 1050
l_f, l_r	1.95, 1.54
h, t_w	1.15, 1.86
b_ϕ, k_ϕ	100000, 457000
C_f, C_r	582000, 783000
J_b, b_w	32.9, 5.5
r_w, g, ρ	0.52, 9.8, 1.292

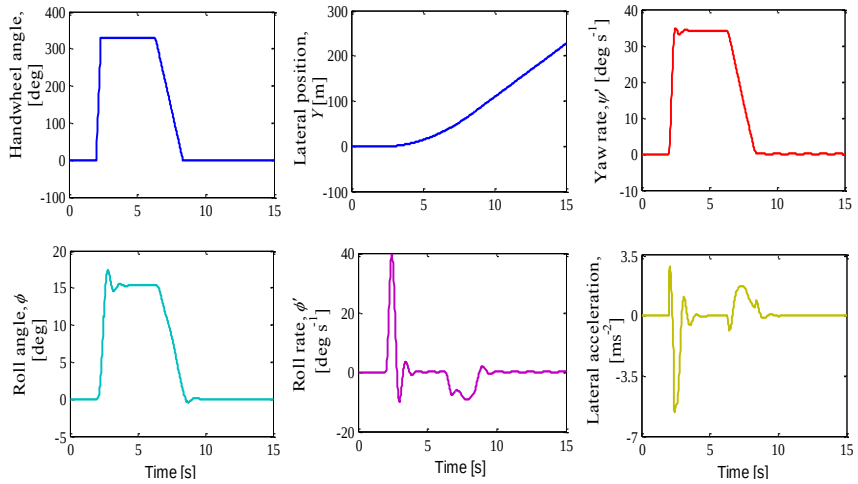

Figure 3.6: Vehicle maneuver test of J-turn at 20m/s.

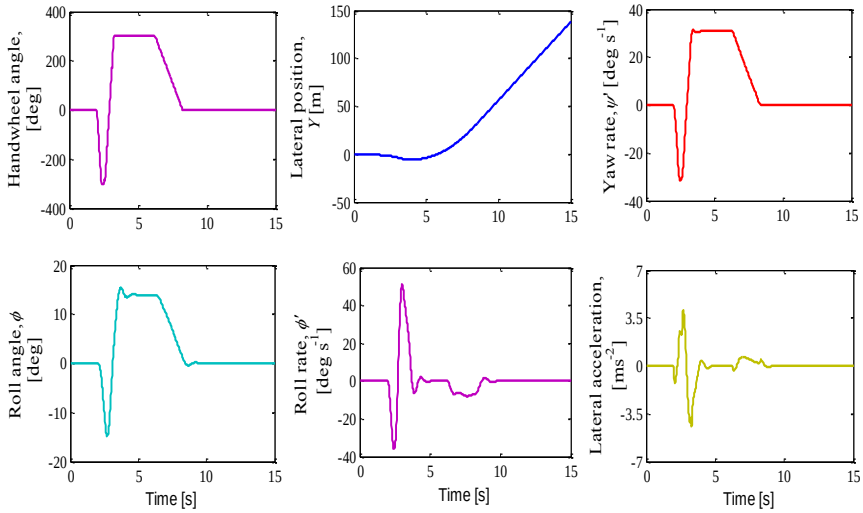

Figure 3.7: Vehicle maneuver test of roll rate feedback fishhook at 20m/s.

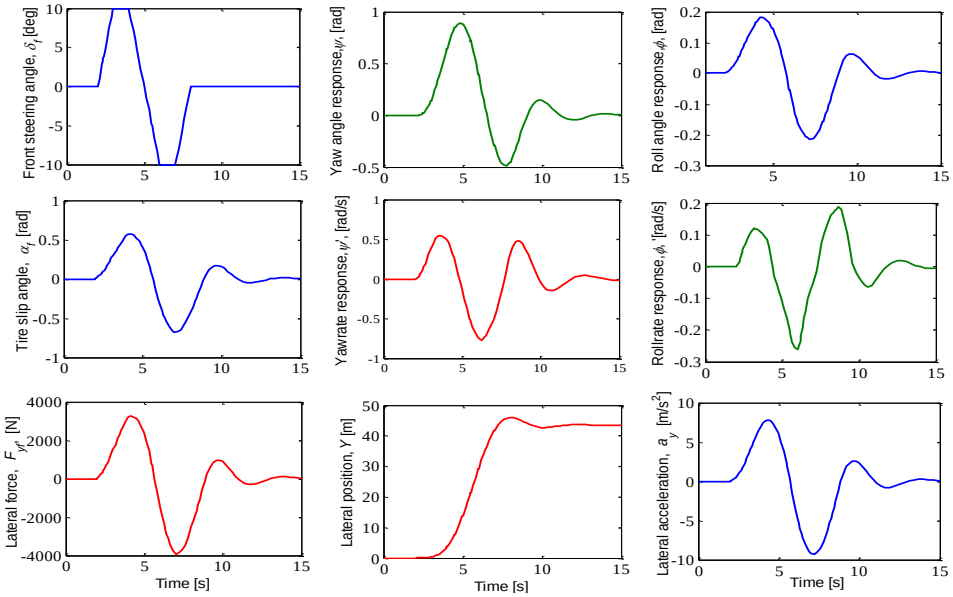

Figure 3.8: Vehicle maneuver test of single lane change at 30m/s with μ = 0.1.

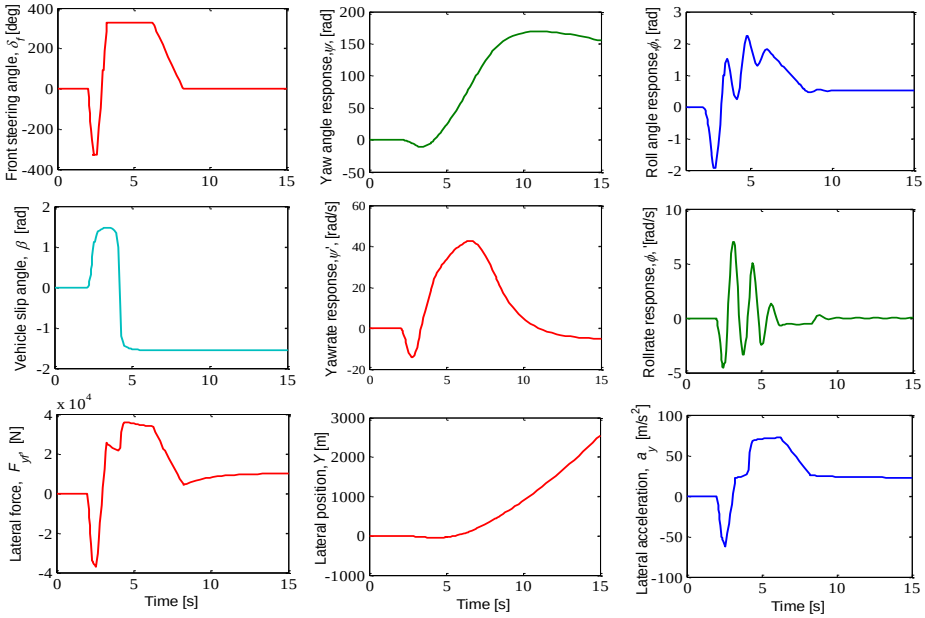

Figure 3.9: Vehicle maneuver test of roll rate feedback at 30m/s with μ = 0.1.

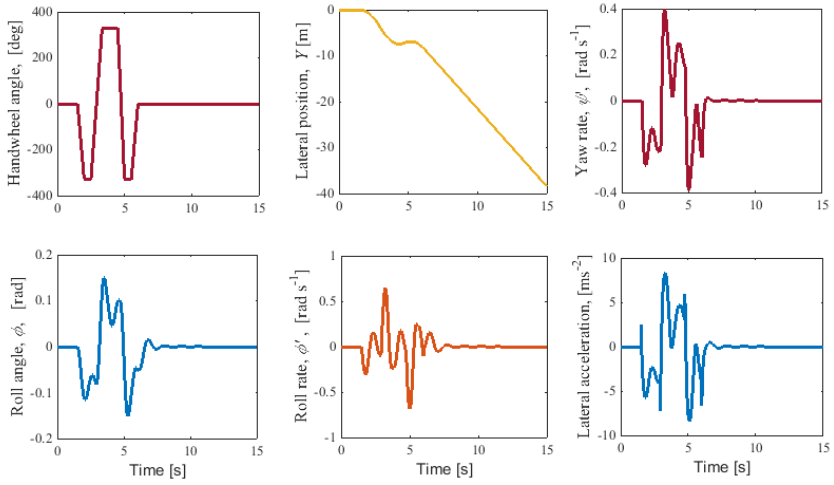

Figure 3.10: Vehicle maneuver test of double lane change at 20m/s with μ = 0.9.

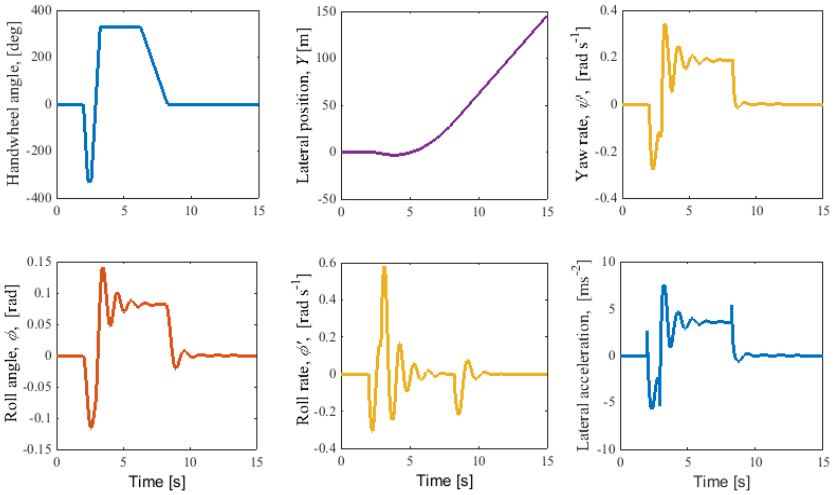

Figure 3.11: Vehicle maneuver test of roll rate feedback at 20m/s with μ = 0.9.

In the second scenarios, we perform a single lane change and roll rate feedback fishhook tests, where we set the vehicle speed at 30m/s with a road surface coefficient of 0.1 under the vehicle parameters in Table 3.2. The maneuver tests responses are shown in Figures 3.8 and 3.9. Based on the vehicle responses in yaw rate, roll rate and lateral acceleration, it's proved and shown that the vehicle model is validated and corrected, thus, can be implemented for controller design.

On the other hand, we make another vehicle test in order to validate the heavy vehicle model illustrated in Table 3.3. Table 3.3 shows the numerical data extracted from a single unit truck for model parameters and their definitions based on [139]. However, in this scenario, we performed only the double lane change and roll rate feedback test, for the purpose of testing improvement to existing vehicle and for vehicle validation purposes in the open-loop simulation, as displayed in Figures 3.10 and 3.11. The vehicle speed was set at 20m/s, which is suitable for both tests, with a road surface coefficient of 0.9.

As illustrated in Figures 3.10 and 3.11, the vehicle response in term of roll angle, roll rate, yaw rate, and lateral acceleration due to steer angle has been proven to be validated, thus suitable for other simulations.

3.7 Summary

The mathematical modeling of the sport utility vehicle, heavy vehicle system, tire model, and disturbances model has been presented. Modification of the vertical forces particularly related to roll motion and lateral acceleration are taken into account. The rollover indicator called LTR is explained with few enhancement of the indicator by considering the lateral acceleration. The development of the vehicle model is validate through standard maneuvers test. A MATLAB® 2012 and Simulink® 2012 application is used in the simulation process to validate the system. Based on the vehicle responses in yaw rate, roll rate and lateral acceleration, it has been proven and shown that the vehicle model is validated and corrected, thus, can be implemented for controller design. Therefore, obtained mathematical model can be considered well enough for the control design and simulation.

Chapter 4
Enhancing Path-Following Control of Autonomous Sport Utility Vehicle

4.1 Introduction

A vehicle capable of handling many things at once, without any human intervention, can be termed as an autonomous vehicle. Basic functions of autonomous braking and steering however are insufficient; an autonomous or driverless car is a vehicle has to have the ability to sense its surrounding or environment plus able to determine desired location, which can be achieved using variety of instrumentation and equipment such as radar, global positioning system, on-board camera for vision, and an independent operating unit.

All sensory data are then computed for obstacle identification, avoidance is then executed using advanced control system. Advanced control systems in autonomous vehicles interpret sensory information to identify obstacles and appropriate navigation paths, as well as relevant signage. In addition, there is currently a lot of interest in the use of autonomous vehicles or robots for military purposes, further increasing the relevance of advanced automotive control.

In this chapter, we limit the vehicle to a ground vehicle which related to the authors work. These vehicles are increasingly studied by several researchers either from academia, industry, and the military, by using several control methods including fuzzy logic [140], hybrid control [141], H-infinity control [142], linear quadratic regulator [143], and more. A description of the best comparative study on predictive control strategies for autonomous guidance vehicles can be found in [144-145], where a nonlinear vehicle dynamics model is used for controller design by active front steering in a double lane change scenario. Kevinczky et al. studied the effect of side wind via an active front steering maneuver for an autonomous vehicle using nonlinear MPC [130].

The first contribution of this chapter is the effect of vehicle roll dynamics motion is consider to the system, whereas most previous papers only focused on a 2DoF vehicle model (lateral and yaw motion). By including the roll dynamics in the system, we can evaluate the effectiveness of controllers, especially under high-speed

conditions. For this study, we limit the path following control of an unmanned ground vehicle that is related to the author's work and emphasizes that we assume a known trajectory for the lateral position and yaw angle based on the reference in [94]. Figure 4.1 illustrate the vehicle path-following control scenario under the cornering maneuver.

In this chapter, first, we assume there is no disturbance or crosswind will affect to the system. Next, for second scenario we assume that the crosswind effect with road adhesion coefficient on the system, then, we compare the performance of the 8DoF vehicle model for two different controllers: MPC and LQC based on a simple yaw-lateral 2DoF and roll-yaw 3DoF bicycle model. Moreover, we evaluate and compare the effectiveness and robustness of both controllers for the vehicle in path-following control and stability.

Furthermore, we extend the concept of MPC to apply it to the autonomous vehicle maneuvering problem where a trajectory optimization is solved at each time step. Based on the known trajectory, we simulate motion of the vehicle at low (10m/s), middle (20m/s), and high (25m/s) forward speeds on a low-friction surface (a wet earth road), following the trajectory as close as possible in a double lane change scenario while maintaining vehicle stability.

The control inputs for the system depend on the vehicle maneuvers, namely, front steer angle for 2WS, front and rear steer angles for 4WS, and front and rear driving or braking forces for DYC, while the control outputs are the yaw angle, yaw rate, and vehicle lateral position where we emphasize/aiming more on tracking of lateral position.

The second contribution of this chapter is to propose MPC with a FF controller and MPC with a PI controller to minimize tracking errors in the lateral position and yaw angle. To evaluate the effectiveness of the proposed control method, we compare it with LQC with a FF/PI controller.

One of the main objectives of this chapter is a comparative study of a path-following control of an autonomous vehicle employing different maneuvers. To the best of the authors' knowledge, there has been no comparative study of these three control signal maneuvers for path-following control of an autonomous vehicle using MPC and LQC techniques, which this chapter discusses (third contribution).

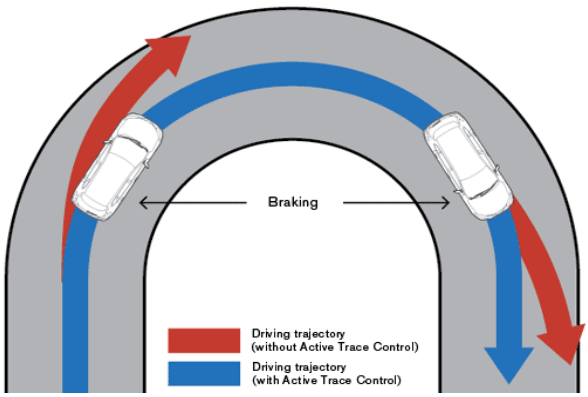

Figure 4.1: Vehicle path-following control example [94].

On the other hand, it is known that AFS has a great influence on lateral vehicle behavior under normal driving conditions [146-147], however, based on the fact that AFS is no longer able to produce enough lateral force during high acceleration because of the highly nonlinear characteristic of its tires, active braking system is utilized to overcome this drawback for limited handling conditions [148].

Therefore, we utilize ABS which focuses on DYC which produces the corrective yaw moment by using the rear braking forces between the left and the right side of the rear tire vehicle in order to avoid the interferences between AFS and DYC (which become a fourth contribution to this chapter).

4.2 Path-Following Maneuver Problem

In many applications it is of primary importance to steer an object (robot arm, vehicle, ship, galaxy class starship, etc.) along a desired path. The speed or dynamic behavior along the path may be of secondary interest. Control problems for such applications are usually approached as two separate tasks.

The first task, denoted the geometric task, is for the output y of the system (usually the position) to reach and follow a desired path y_d designed as a function of an auxiliary path variable θ, left as an extra DoF for the second task. In the second task, θ is used to satisfy an additional dynamic specification along the path. This task is denoted the dynamic task and is usually specified as an assignment for the speed.

In the common tracking problem the path variable θ is assigned to a specific time function $v_t(t)$ constructed so that $\tilde{y}_d(t) := y_d(v_t(t))$ is a moving point that satisfies the tracking objective and the dynamic limitations of the system. In this case the two tasks, the geometric and dynamic parts of the problem, are merged into a single task

with objectives often more stringent than required in applications. An example is to automatically drive a car along a road. This can be achieved by making the car track a point that moves along the road with a certain speed.

However, by instead emphasizing that the main task is to make the car stay on and follow the road, one can let the desired speed be of secondary interest and sacrificed if necessary. A less restrictive control objective is to solve a pure path following problem. In this case the output y should merely converge to and follow the desired path $y_d(\theta)$ without any specific dynamic requirements along the path. Clearly, in many cases this problem statement is too flexible. When driving the car the primary importance is to follow the road. However, it is also important to keep up the speed to arrive at the destination in reasonable time.

The idea focused on in this chapter is to bridge the gap between tracking and path following, and the control concept will be called maneuvering. This is motivated by [94] who designed a maneuver regulation control law from a tracking algorithm by converting a time parametrized desired output signal into a θ-parametrized desired output path and designing an update law to ensure proper motion for θ.

There are subtle differences in maneuvering as compared to tracking or path following. Maneuvering is by active control to achieve both convergence to the path and to satisfy the dynamic behavior along the path, approached as two separate tasks. Path following, on the other hand, is the same as solving the geometric task only (with a nonzero motion), whereas tracking is a method for strictly solving the geometric and dynamic tasks in a single task. The result is that tracking becomes a special case of maneuvering, and maneuvering becomes a special case of path following.

4.3 Control Allocation

In this section, the linear MPC and LQC are explained. The basic hierarchical control structure adopted in MPC and LQC for an autonomous SUVs path following control is shown in Figure 4.2. In the control structure illustrated in Figure 4.2, a 2WS model using front steering only, a 4WS model using front and rear steering, or a DYC model producing a reaction moment at the front and rear wheels are used to control the vehicle so that it follows a given reference trajectory.

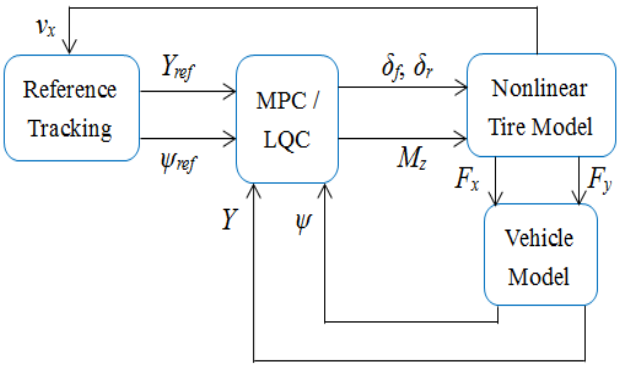

Figure 4.2: Predictive control structures.

It includes the vehicle speed, desired reference trajectory, MPC, and a linear vehicle model with a nonlinear tire model. LQC will be implemented in the same way as MPC to facilitate a fair comparison.

Then, we propose the MPC with FF and MPC with PI controller for an autonomous SUV path following control. MPC is designed to track and follow a given trajectory as close as possible, while the FF/PI controller is adopted in order to reduce the tracking errors between the desired and the real outputs, thus enhancing vehicle stability and handling under crosswind disturbance.

4.3.1 Model Predictive Control

To implement MPC with a receding horizon control strategy, the following strategies are adopted:

1. A dynamic process model is used to predict the behavior of the plant and future plant outputs based on the latest and past observations of the system inputs and outputs.
2. The control signal inputs are calculated by minimizing the tracking error between the predicted output and the desired trajectory signal to keep the process following the trajectory as closely as possible, taking into account the objective function and constraints.
3. Only the first control signal is implemented on the plant, whereas others are rejected at the next sampling instant where the future output is known.
4. Step 1 is repeated with the updated value, and all orders are updated.

For the sake of easiness, the MPC is designed based on a simple 2DoF lateral-yaw motion by linearizing the equations from the vehicle and tire models as explained

and defined in Equations (3.23) to (3.24), giving the following basic equations of free-rolling linear vehicle motion without braking or acceleration:

$$m\dot{v}_y = \frac{1}{v_x}[-\mu(C_r + C_f)v_y + (\mu(C_r l_r - C_f l_f) - m v_x^2)\dot{\psi}] + \mu[C_f \delta_f + C_r \delta_r] + F_{wy} \tag{4.1}$$

$$I_{zz}\ddot{\psi} = \frac{1}{v_x}[\mu(C_r l_r - C_f l_f)\, v_y - \mu(C_f {l_f}^2 + C_r {l_r}^2)\dot{\psi}] + \mu[C_f l_f \delta_f - C_r l_r \delta_r] + M_z + M_{wz} \tag{4.2}$$

The relationship between the cornering force and tire slip angle is linear, whereas the slip angle is small. The tire lateral forces on the front and rear tires are treated as proportional to the tire slip angle described as follows:

$$F_{yf} = \mu_f C_f \alpha_f \ , \quad F_{yr} = \mu_r C_r \alpha_r \tag{4.3}$$

where C_f and C_r are constants representing the linear front and rear tire cornering stiffness values. For the DYC, the reaction moment occurring at the front and rear wheels due to the steer-angle effect (as an external yaw moment) can be approximated as follows:

$$M_f \approx 2 l_f \mu_f C_f M_z \ , \qquad M_r \approx 2 l_r \mu_r C_r M_z \tag{4.4}$$

The vehicle motion in Equations (4.1) and (4.2) can be represented in state-space form as:

$$\dot{x}_l = A x_l + B_1 u_l + B_d w_d + B_2 r_l \ , \qquad y_l = C x_l + D u_l \tag{4.5}$$

where $x_l \in \mathbb{R}^x$, $u_l \in \mathbb{R}^u$, $w_d \in \mathbb{R}^w$, $r_l \in \mathbb{R}^r$, and $y_l \in \mathbb{R}^y$ are the state vectors, control input vectors, crosswind effects as a disturbance vectors, desired trajectory vectors, and measured output vectors, respectively. We define:

$$\begin{gathered} x_l = [v_y \ \ Y \ \ \dot{\psi} \ \ \psi]^T \ , \quad u_l = [\delta_f], \quad [\delta_f \ \ \delta_r]^T, \quad [\delta_f \ \ M_z]^T \ , \quad w_d = [F_{wy} \ \ M_{wz}]^T, \\ r_l = [Y_{des} \ \ \psi_{des}]^T \ , \quad y_l = [Y \ \ \psi]^T \end{gathered} \tag{4.6}$$

We define the front steering angle, rear steering angle, and direct yaw moment control as the inputs to the system. Thus, the vehicle motion in Equation (4.5) can be represented in discrete state-space form by neglecting an unmeasured disturbance as MPC is designed in discrete form as:

$$x_l(k+1|k) = A_l\, x_l(k|k) + B_l\, u_l(k|k) + B_2\, r_l(k|k), \qquad y_l(k|k) = C_l\, x_l(k|k) + D_l\, u_l(k|k) \tag{4.7}$$

where $x_l(k|k)$ is the state vector at time step k and $x_l(k+1|k)$ is the state vector at time step $k+1$, with $x_l(k|k) \in \mathbb{R}^{xl(k|k)}$, $u_l(k|k) \in \mathbb{R}^{ul(k|k)}$, $r_l(k|k) \in \mathbb{R}^{rl(k|k)}$, and $y_l(k|k) \in \mathbb{R}^{yl(k|k)}$ being the state vectors, control input vectors, reference vectors, and measured output vectors, respectively.

For 2WS, 4WS, and 2WS with DYC, the control signals to the systems with the same tuning control parameters are:

$$u_l(k) = [\delta_f\ ], \quad u_l(k) = [\delta_f\ \ \delta_r]^T, \quad u_l(k) = [\delta_f\ \ M_z]^T \tag{4.8}$$

Because the controller is designed based on a simple 2DoF bicycle model, neglecting roll dynamics and considering a linear tire model, it is impossible for the controller to track and follow a given or desired trajectory perfectly or accurately. However, the controller is designed to achieve the aim of a double lane change scenario for different control maneuvers through simulation.

The objective of the predictive control system is to bring the predicted output as close as possible to the reference signal within a predictive horizon, where we assume that the reference signal remains constant in the optimization window. It could also be said that the objective is to find the optimal control input vector $\Delta\hat{u}_l(k+i|k)$ such that an error function between the predicted output and the reference signal is minimized. The control objectives are typically a trade-off between how well the controller tracks the output reference and how much input action it uses. The optimization of the predictive control system will be solved by minimizing a cost function given by:

$$J_{mpc}(x(k),U_k) = \sum_{i=1}^{H_p} \left\| \hat{y}_l(k+i\,|\,k) - r_l(k+i\,|\,k) \right\|_{Q_i}^2 + \sum_{i=0}^{H_c-1} \left\| \Delta\hat{u}_l(k+i\,|\,k) \right\|_{R_i}^2 \tag{4.9}$$

Here, the first summation refers to minimizing the trajectory of the tracking error between the predicted outputs $\hat{y}_l(k+i|k)$ (i = 0, …,n) and the output reference signal $r_l(k + i|k)$ (i = 0, …, n). The second summation reflects the penalty on the control signal effort due to the front steer angle, $\Delta\hat{u}_l(k+i|k)$ (i = 0, …,n), in the case of the 2WS control maneuver. Here, $r_l(k+i|k)$ is the reference value of the lateral position and yaw angle. The variation of the front steer angle $\Delta\hat{u}_l(k+i|k)$ can be obtained by making the cost function as small as possible.

The weight matrices Q_i and R_i are semi-positive definite and positive definite respectively, which can be adjusted for the desired closed-loop performance. Terminal weights are the quadratic weights Q_i on $y(t+H_p)$ and R_i on $u(t+H_p–1)$. We apply the quadratic weights at time $k+H_p$ only, such as the prediction horizon's final step. Using terminal weights, we can achieve infinite horizon control that guarantees closed-loop stability. However, before using terminal weights, we must distinguish between

problems with and without constraints. We have defined Q_i as the state tracking weight because the error $\hat{y}_l(k+i|k) - r_l(k+i|k)$ can be made as small as possible by increasing Q_i. Similarly, R_i is defined as the input tracking weight, and the variation of the input is reduced to slow the response of the system by increasing R_i. The predictive and control horizons are usually assumed to satisfy $H_p \geq H_c$.

The inherent physical limitations on the capacity of control actuators or on the control actuators rate give rise to the hard constraints on the input and on the input rate. Both the constraints have a profound impact on the stabilization of a given initial condition and the performance of the closed-loop systems. Terminal constraints are the constraints on $y(t+H_p)$ and $u(t+H_p-1)$. We can use terminal constraints as an alternative way to achieve closed-loop stability by defining a terminal region. For the relatively simple unconstrained case, a terminal weight can make the finite-horizon MPC behave as if its prediction horizon were infinite such as it behavior is identical to a LQC.

The input constraints are usually applied to avoid actuator saturation and are imposed to arrest the aggressive control move. Thus, the second constraints add stability to the system. The optimization of the predictive control system through cost function in Equation (4.9), taking into consideration the constraints on the actuators due to physical reasons (i.e., the ranges of front tire, rear tire, and moment torques), is formulated as in Equation (4.10). The maximal tire slip angles $\alpha_{f,max}$ and $\alpha_{r,max}$ are detected where the maximal tire force is achieved in order to prevent extreme saturation of the tire lateral force.

$$
\begin{aligned}
&\min_{\Delta U_k} \quad J_{mpc}(x_l(k), \Delta U_l(k)) \\
&subject\ to: \\
&\quad \hat{x}_l(k+1|k) = A_l x_l(k|k) + B_l u_l(k|k) + B_2 r_l(k|k) \\
&\quad \hat{x}_l(k+2|k) = A_l \hat{x}_l(k+1|k) + B_l \hat{u}_l(k+1|k) + B_2 \hat{r}_l(k+1|k) \\
&\qquad\qquad \vdots \\
&\quad \hat{x}_l(k+i|k) = A_l \hat{x}_l(k+i-1|k) + B_l \hat{u}_l(k+i-1|k) + B_2 \hat{r}_l(k+i-1|k) \\
&\quad \delta_{f,\min} \leq \hat{u}_l(k+i|k) \leq \delta_{f,\max}, \ 2WS \\
&\quad \delta_{r,\min} \leq \hat{u}_l(k+i|k) \leq \delta_{r,\max}, \ 4WS \\
&\quad M_{z,\min} \leq \hat{u}_l(k+i|k) \leq M_{z,\max}, \ DYC \\
&\quad \Delta\delta_{f,\min} \leq \Delta\hat{u}_l(k+i|k) \leq \Delta\delta_{f,\max} \\
&\quad \Delta\delta_{r,\min} \leq \Delta\hat{u}_l(k+i|k) \leq \Delta\delta_{r,\max} \\
&\quad \Delta M_{z,\min} \leq \Delta\hat{u}_l(k+i|k) \leq \Delta M_{z,\max}, \ \ i = 1, \cdots H_p
\end{aligned}
\tag{4.10}
$$

By knowing an upper bound angle limit and a lower bound angle limit as functions of a vehicle slip angle and a tire slip angle limit, the maximal front and rear steering angle limits can be derived as:

$$\delta_{f,\max}(k) = \alpha_{f,\max} + \frac{v_y - l_f \dot{\psi}}{v_x} \quad , \qquad \delta_{r,\max}(k) = \alpha_{r,\max} + \frac{v_y + l_r \dot{\psi}}{v_x} \tag{4.11}$$

The inequality of tire slip angle; $-\alpha_{\lim} < \alpha_f < +\alpha_{\lim}$ indicates that the tire steer angle, δ_f, may be held within a bound of the vehicle side slip angle, β_f, to avoid the lateral tire force saturation region. Thus, these bounds are determined once at time k such that $\alpha_{f,max}$, $(k+i|k)$ is equal to constant, where before the upper and lower bounds are defined, the linearization of the nonlinear tire model in Equations (3.13) and (3.14) is investigated at the operating point $\alpha_{f,0}$, $F_{yf,0}$:

$$F_{y,f} = (\alpha_f - \alpha_{f,0}) \times k_{\alpha,f} + F_{y,f,0} \tag{4.12}$$

where $k_{\alpha f}$ denotes the linearization coefficient [149]. Same goes through for the rear steer angle. For the case of direct yaw moment control, when the front and rear lateral tire force saturation is reached, an additional yaw moment M_z is used in order to reach the yaw rate tracking goal.

The optimization problem in Equation (4.10) is based on the linear system in Equation (4.5), where the optimization problem in Equation (4.10) can be recast as a QP or linear program if the function in Equation (4.9) is convex linear or quadratic (details can be found in [94]). Then, the resulting MPC controller for the linear system will solve the problem in Equation (4.10) at each time step. Once a solution, u_k^*, to problem in Equation (4.10) has been obtained, the input command is computed as:

$$u(k) = u(k-1) + \Delta u_k^* \tag{4.13}$$

At the next time step, the linear model is computed based on new state and input measurements, which results in the new QP problem in Equation (4.10) being solved over a shifted horizon. Finally, an optimal input is then calculated for the next time step (instead of the immediate time step) by solving a convex optimization problem at each time step.

In general the stability of the presented control scheme is difficult to prove. Based on the accurate analysis of the vehicle nonlinearities, we obtained a stable and performing controller by a proper choice of the cost function and the system constraint. In particular, without the constraints, the performance of the linear MPC controller is not acceptable and sometimes unstable. This is due to the fact that a

simple linear model is not able to predict the change of slope in the tires' characteristics.

To overcome this issue we add constraints to the optimization problem, in order to prevent the system from entering into a nonlinear and possibly unstable region of the tire characteristic. Thus, the tire slip angle constraints in Equation (4.11) are used to maintain vehicle stability. It is well known that stability is not ensured by MPC law in Equation (4.10), Equation (4.12), since our problem is the linear problem. Thus, for nonlinear MPC, usually the problem is augmented with a terminal cost and terminal constraint set to ensure close-loop stability [150], and it goes beyond the scope of this work.

In order to make the MPC entirely equivalent to the LQC, we may use a control horizon equal to the prediction horizon. In an unconstrained application, we can use a short horizon and still achieve nominal stability. Thus, the horizon is no longer a parameter to be tuned. When the application includes constraints, the horizon selection becomes important. The standard (finite-horizon) MPC provides comparable performance, if the prediction horizon is long. We must tune the other controller parameters (weights, constraint softening, and control horizon) to achieve this performance.

4.3.2 Linear Quadratic Control

To allow a fair comparison of the tracking responses with those from MPC, the LQC is also based on the linearized vehicle Equations (4.1) and (4.2) with a quadratic cost function. A standard 2DoF LQC tracking control structure where a feedforward controller operating on the reference is combined with a feedback controller operating on the output.

The aim of this approach, called LQ tracking, is to track and follow the desired trajectory as close as possible, with the linear quadratic solution [151-152]. We denote the control error by $\varepsilon_{er}(t)$, the desired trajectory by $r_l(t)$, and the performance output by $y_l(t)$, with these being related by:

$$\varepsilon_{er}(t) = r_l(t) - y_l(t) \tag{4.14}$$

The integral error is then given by:

$$\varepsilon_e = \int_0^t \varepsilon_{er}(t)dt \tag{4.15}$$

Which is introduced as a new state to the dynamic system in Equations (4.1) and (4.2) as given in state space by:

$$\begin{bmatrix} \dot{\varepsilon}_e \\ \dot{x}_l \end{bmatrix} = \begin{bmatrix} 0 & -I \\ 0 & A_l \end{bmatrix} \begin{bmatrix} \varepsilon_e \\ x_l \end{bmatrix} + \begin{bmatrix} 0 \\ B_l \end{bmatrix} u_l + \begin{bmatrix} I \\ 0 \end{bmatrix} r_l \tag{4.16}$$

Which can be simplified as $\dot{x}_{lq} = A_{lq}\, x_{lq} + B_{lq}\, u_{lq} + E_{lq} r_l$. Thus, the new error for the system in Equation (4.16) can be defined as:

$$\varepsilon = \begin{bmatrix} \varepsilon_{er} \\ \varepsilon_e \end{bmatrix} = M r_l + H x_{lq} \tag{4.17}$$

Where

$$M = \begin{bmatrix} I \\ 0 \end{bmatrix}, \qquad H = \begin{bmatrix} -I & 0 \\ 0 & I \end{bmatrix} \tag{4.18}$$

With an infinite-horizon problem, where, Q_{lq} and R_{lq} are positive-definite weighting matrices on tracking error and input error, respectively. We try to find the control $u_{lq}(t)$ that will regulate the system at zero by tuning Q_{lq} and R_{lq}, the cost function is given by:

$$\begin{aligned} & J_{lqc} = \min_u \int_0^\infty (\varepsilon^T(t) Q_{lq} \varepsilon(t) + {u_{lq}}^T(t) R_{lq} u_{lq}(t))\, dt \\ & \textit{subject to}: \\ & \qquad \dot{\varepsilon}(t) = A_{lq}\varepsilon(t) + B_{lq} u_{lq}(t) \\ & \qquad \varepsilon(0) = \varepsilon_0 \\ & \qquad u_{lq}(t) \in U_{lq} \\ & \qquad U_{lq} = \{u_{lq} \in \Re^m \mid u_{lq\min} \le u_{lq} \le u_{lq\max}\} \end{aligned} \tag{4.19}$$

The set $U_{lq} \in \mathrm{R}^m$ is defined by lower and upper bounds, with u_{lqmin}, $u_{lqmax} \in \mathrm{R}^m$, $u_{lqmin} < u_{lqmax}$, where all inequalities are to be understood component wise. The LQC can be derives in the discrete time from the cost function:

$$J_{lqc}(u_{lq}) = \sum_{i=1}^{\infty} \varepsilon(k+i)^T Q_{lq} \varepsilon(k+i) + u_{lq}(k+i-1)^T R_{lq} u_{lq}(k+i-1) \tag{4.20}$$

where ε is the vector of system states in the standard state-space form as given in Equation (4.17). The LQC provides nominal stability provided matrices Q_{lq} and R_{lq} meet certain conditions. We can convert the LQC to a finite-horizon form as follows:

$$J_{lqc}(u_{lq}) = \sum_{i=1}^{\infty} \varepsilon(k+i)^T Q_{lq} \varepsilon(k+i) + u_{lq}(k+i-1)^T R_{lq} u_{lq}(k+i-1) + x(k+H_p)^T Q_p x(k+H_p) \tag{4.21}$$

where Q_p , the terminal penalty matrix, is the solution of the Riccati equation:

$$Q_p = A_{lq}^T Q_p A_{lq} - A_{lq}^T Q_p B_{lq} (B_{lq}^T Q_p B_{lq} + R_{lq})^{-1} B_{lq}^T Q_p A_{lq} + Q_{lq} \tag{4.22}$$

When the application includes constraints, the horizon selection becomes important. The constraints, which are usually softened, represent factors not considered in the LQC cost function. If a constraint becomes active, the control action deviates from the LQC (state feedback) behavior. If this behavior is not handled correctly in the controller design, the controller may destabilize the plant.

The optimal input state feedback controller K_{opt} is obtained by minimizing the cost function. The optimal input state feedback controller K_{opt} is obtained by minimizing the cost function:

$$K_{opt} = [-R_{lq}^{-1} B_{lq}{}^{T} P_{11} \quad -R_{lq}^{-1} B_{lq}{}^{T} P_{12}] \tag{4.23}$$

where P_{11} and P_{12} are the unique positive-definite solutions to the algebraic Riccati equation for an infinite-horizon LQ problem:

$$A_{lq}^{T} P_e + P_e A_{lq}^{T} - P_e B_{lq} R_{lq}^{-1} B_{lq}^{T} P_e + Q_{lq} = O \tag{4.24}$$

where,

$$Q_{lq} = \begin{bmatrix} C^{T} Q_{11} C & 0 \\ 0 & Q_{22} \end{bmatrix} \tag{4.25}$$

And O is the zero matrix. The solutions of the Riccati differential equation are:

$$P_e = P_e^{T} = \begin{bmatrix} P_{11} & P_{12} \\ P_{21}^{T} & P_{22} \end{bmatrix} > 0 \tag{4.26}$$

Here, the feedforward gain K_s, which is designed for target tracking, and the feedback gain K_f are given by:

$$K_s = [-C_{lq}(A_{lq} + B_{lq} K_{opt})^{-1} B_{lq}]^{-1}, \qquad K_f = C_{lq}(A_{lq} + B_{lq} K_{opt})^{-1} \tag{4.27}$$

With the control law being given by:

$$u_{lq}(t) = -K_s x_{lq} - K_f r_l \tag{4.28}$$

Once the algebraic Riccati equation has been solved, the optimal gains can be computed from Equation (4.27). The problem now becomes how to choose the weighting matrices Q_{lq} and R_{lq}, so that a good response is obtained without exceeding the bandwidth and position limitations of the actuators, i.e., without so-called saturation. Detailed explanation of the solution of the algebraic Riccati equation for the LQR optimal gain may be found in [152]. The constraints, which are usually softened, represent factors not considered in the LQC cost function. If a constraint becomes active, the control action deviates from the LQC (state feedback) behavior. If this behavior is not handled correctly in the controller design, the controller may

destabilize the plant. For an in-depth discussion of design issues for constrained systems see [150]. Depending on the situation, we might need to include terminal constraints to force the plant states into a defined region at the end of the horizon, after which the LQC can drive the plant signals to their targets.

4.3.3 MPC with FF/PI Controller

In this sub-section, we propose the MPC with FF controller for an autonomous SUV path-following control, for the active front steering control maneuver as shown in Figure 4.3.

MPC is designed to track and follow a given trajectory as close as possible, while the FF controller is adopted in order to reduce the tracking errors between the desired and the real outputs, thus enhancing vehicle stability and handling maneuverability. On the other word, the state feedback from the MPC is adopted with the FF controller to stabilize the vehicle about a known trajectory and to correct the errors that accumulated by non-modelled vehicle dynamics, disturbances, or parameter uncertainties as shown in Figure 4.3.

For a simple kinematic lateral motion model formulation, yaw rate can be derived from the geometric relation as shown in Figure 4.4(a), considering its limitations due to the capability of the vehicle in maximum acceleration:

$$\dot{\psi}_{des} = \frac{v_x}{R_w} = \kappa v_x , \qquad R_w = \frac{v_x^2}{\mu g} \tag{4.29}$$

The trajectory errors of lateral and yaw vehicle motions, with respect to the center lane of the road as shown in Figure 4.4(b), are given by:

$$e_\psi = \psi - \psi_{des} , \qquad \dot{e}_y = \dot{y}\cos(e_\psi) + \dot{x}\sin(e_\psi) , \qquad \dot{e}_x = -\dot{y}\sin(e_\psi) + \dot{x}\cos(e_\psi) \tag{4.30}$$

The acceleration is along the *Y*-axis and the vehicle-body side-slip angle, under small angle assumptions, is related to the lateral position error and yaw angle error by:

$$a_y = \dot{y} + \dot{\psi} v_x , \qquad \dot{y} = \dot{e}_y - e_\psi v_x \tag{4.31}$$

In Figure 4.3, the state feedback from the MPC and FF controller is adopted here to stabilize the vehicle for a known trajectory and to correct the errors that have accumulated owing to un-modeled vehicle dynamics, disturbances, or parameter uncertainties. The MPC controller is used for tracking purposes due to advantages on multivariable and constraint systems.

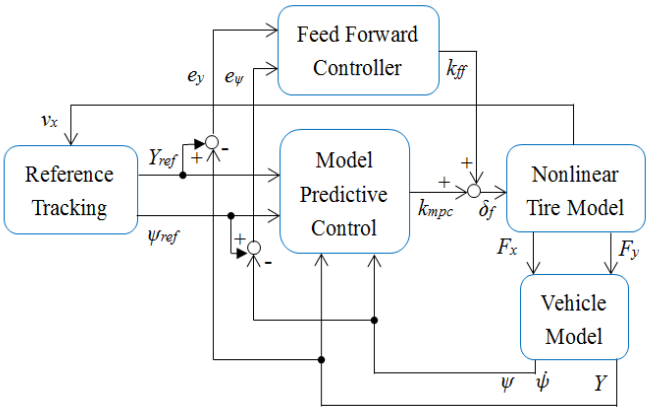

Figure 4.3: Predictive control with feedforward controller.

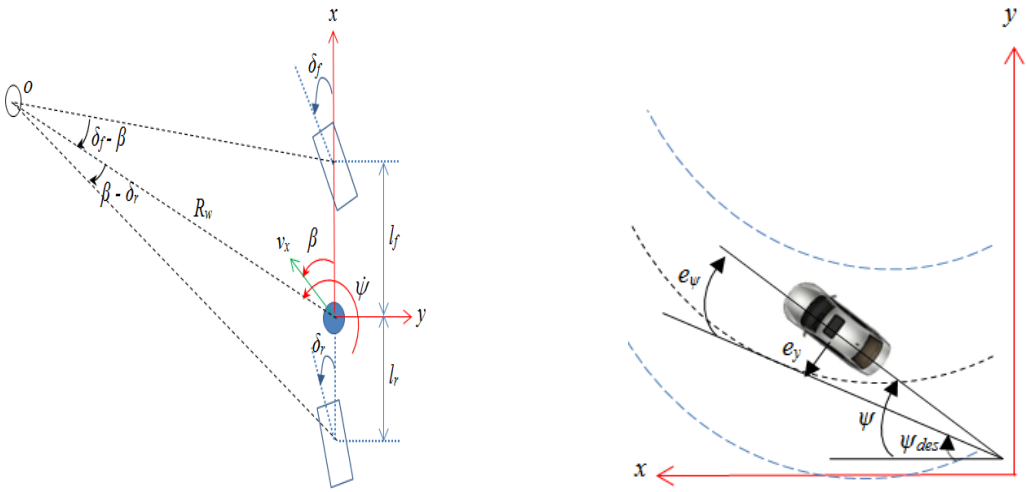

(a) (b)

Figure 4.4: SUV dynamics model (a) Vehicle kinematics motion, (b) Vehicle dynamics motion.

A FF controller is adopted for minimizing tracking errors and to ensure zero steady-state errors due to its simplicity, thus enhancing vehicle stability. A driver steering controller using a general LQR formulation was derived in [153], while MPC was employed in [154], where, the solution of a cost function results in a MPC steering control law, based on state feedback and future path preview for a discrete domain controller given as:

$$k_{mpc}(k) = [-k_k \ \Omega \qquad k_k] \cdot \begin{bmatrix} x(k) \\ T(k) \end{bmatrix} \tag{4.32}$$

where Ω is the free response matrix of dynamics system, k_k is the controller preview gain vector derived using MPC formulation, and $T(k)$ is the preview vector. The MPC cost function to be minimized is given in Equation (4.9), where $||x||_{Q(i)}^2$

means $x^T Q(i)x$, and $r(k+i)$ are the future demand values of road path lateral position and yaw angle previewed by the driver, defined in ground-fixed axes, $\Delta u = \delta_f$. $Q(i)$ is the cost function matrix associated with time step i ahead of the current time. $R(i)$ is the cost function matrix associated with the future values of the steer angle. The predicted path-following errors are penalized up to the preview horizon but the steering input is only penalized up to the control horizon; there is no penalty on the constant steering input that might exist beyond the control horizon up to the preview horizon ($H_c \leq i \leq H_p$). Rewriting equation of cost function in Equation (4.9) without summation signs gives:

$$J_{mpc}(k) = \left\| \widehat{Y}(k) - T(k) \right\|_{Q_i}^2 + \left\| \widehat{U}(k) \right\|_R^2 \tag{4.33}$$

where,

$$T(k) = \begin{Bmatrix} r(k+1) \\ \vdots \\ r(k+H_p) \end{Bmatrix}, \quad Q = \begin{bmatrix} Q(1) & & \\ & \ddots & \\ & & Q(H_p) \end{bmatrix}, \quad R = \begin{bmatrix} R(0) & & \\ & \ddots & \\ & & R(H_c - 1) \end{bmatrix} \tag{4.34}$$

The predicted error up to the preview horizon is defined as:

$$\varepsilon(k) = T(k) - \Omega x(k) \tag{4.35}$$

Following Maciejowski's analysis as mentioned in [19], it can be analyze to give:

$$Y(k) = \Omega x(k) + \Theta U(k) \tag{4.36}$$

where,

$$Y(k) = \begin{Bmatrix} y(k+1) \\ \vdots \\ y(k+H_p) \end{Bmatrix}, \quad U(k) = \begin{Bmatrix} u(k) \\ \vdots \\ u(k+H_c-1) \end{Bmatrix} = \begin{Bmatrix} \delta_f(k) \\ \vdots \\ \delta_f(k+H_c-1) \end{Bmatrix}$$

$$\Omega = \begin{Bmatrix} CA \\ CA^2 \\ \vdots \\ CA^{H_p} \end{Bmatrix}, \quad \Theta = \begin{Bmatrix} CB & 0 & \cdots & 0 \\ CAB & CB & 0 & \cdots \\ \cdots & \cdots & \cdots & \cdots \\ CA^{H_c-1}B & \cdots & CAB & CB \\ CA^{H_p-1}B & \cdots & \cdots & C\sum_{i=0}^{H_p-H_c} A^i B \end{Bmatrix} \tag{4.37}$$

Detail may refer to Maciejowski [19]. Maciejowski explains that this can be solved for $U(k)_{opt}$ using QR decomposition (invoked in Matlab using the backslash operator), so that:

$$U(k)_{opt} = K_{full}\varepsilon(k), \quad \text{where} \quad K_{full} = \begin{bmatrix} S_Q\Theta \\ S_R \end{bmatrix} \backslash \begin{bmatrix} S_Q \\ 0 \end{bmatrix} \tag{4.38}$$

$U(k)_{opt}$ is an array of future optimum steering inputs up to the control horizon. A receding horizon control strategy is used, which involves taking the first element of $U(k)_{opt}$ for the steering input $\delta(k)_{opt}$ then calculating $U(k+1)_{opt}$ and using the first element of that for the steering input $\delta(k+1)_{opt}$. The optimum steering input $\delta(k)_{opt}$ can therefore be determined using a linear time-invariant controller:

$$\delta_f(k)_{opt} = k_k(T(k) - \Omega x(k)) \tag{4.39}$$

Finally the predictive control law can be written as Equation (4.29) or as:

$$\delta_f(k)_{opt} = K_k\, x_{Y\psi}(k) \tag{4.40}$$

where,

$$\begin{aligned} K_k &= [-k_k\Omega \quad k_k] \\ x_{Y\psi}(k) &= \begin{Bmatrix} x(k) \\ T(k) \end{Bmatrix} = [v_y \;\; Y \;\; \dot{\psi} \;\; \psi \;\; e_y \;\; \dot{e}_y \;\; e_\psi \;\; \dot{e}_\psi \;\; Y_{des} \;\; \psi_{des}]^T \end{aligned} \tag{4.41}$$

From the lateral position and yaw tracking error in Equation (4.30), then, by substituting Equations (4.1) and (4.2) into Equation (4.30), it yields:

$$\begin{aligned} m\ddot{e}_y = {} & \dot{e}_y\left[-\frac{1}{v_x}\mu_f C_f - \frac{1}{v_x}\mu_r C_r\right] + e_\psi(\mu_f C_f + \mu_r C_r) + \dot{e}_\psi\left[-\frac{1}{v_x}\mu_f C_f l_f + \frac{1}{v_x}\mu_r C_r l_r\right] \\ & + \dot{\psi}_{des}\left[-\frac{1}{v_x}\mu_f C_f l_f + \frac{1}{v_x}\mu_r C_r l_r\right] + \mu_f C_f \delta_f + \mu_r C_r l_r \delta_r + F_{wy} + \frac{m_s}{m} g F_b \end{aligned} \tag{4.42}$$

$$\begin{aligned} I_{zz}\ddot{e}_\psi = {} & \dot{e}_y\left[-\frac{1}{v_x}\mu_f C_f l_f + \frac{1}{v_x}\mu_r C_r l_r\right] + e_\psi(\mu_f C_f l_f - \mu_r C_r l_r) + \dot{e}_\psi\left[-\frac{1}{v_x}\mu_f C_f l_f^2 - \frac{1}{v_x}\mu_r C_r l_r^2\right] \\ & + \dot{\psi}_{des}\left[-\frac{1}{v_x}\mu_f C_f l_f^2 - \frac{1}{v_x}\mu_r C_r l_r^2\right] - I_{zz}\ddot{\psi}_{des} + \mu_f C_f l_f \delta_f - \mu_r C_r l_r \delta_r + M_z + M_{wz} \end{aligned} \tag{4.43}$$

The state-space model in tracking error variables is therefore given by [155]:

$$\begin{aligned} \begin{bmatrix} \dot{e}_y \\ \ddot{e}_y \\ \dot{e}_\psi \\ \ddot{e}_\psi \end{bmatrix} = {} & \begin{bmatrix} 0 & 1 & 0 & 0 \\ 0 & -\frac{\mu_f C_f + \mu_r C_r)}{m v_x} & \frac{\mu_f C_f + \mu_r C_r)}{m} & -\frac{\mu_f C_f l_f - \mu_r C_r l_r)}{m v_x} \\ 0 & 0 & 0 & 1 \\ 0 & -\frac{\mu_f C_f l_f - \mu_r C_r l_r)}{I_{zz} v_x} & \frac{\mu_f C_f l_f - \mu_r C_r l_r)}{I_{zz}} & -\frac{\mu_f C_f l_f^2 + \mu_r C_r l_r^2)}{I_{zz} v_x} \end{bmatrix} \begin{bmatrix} e_y \\ \dot{e}_y \\ e_\psi \\ \dot{e}_\psi \end{bmatrix} + \begin{bmatrix} 0 & 0 & 0 \\ \frac{1}{m} & 0 & \frac{m_s}{m} g \\ 0 & 0 & 0 \\ 0 & \frac{1}{I_{zz}} & 0 \end{bmatrix} \begin{bmatrix} F_{wy} \\ M_{wz} \\ F_b \end{bmatrix} \\ & + \begin{bmatrix} 0 \\ -\frac{\mu_f C_f l_f - \mu_r C_r l_r)}{m v_x} - v_x \\ 0 \\ -\frac{\mu_f C_f l_f^2 + \mu_r C_r l_r^2)}{I_{zz} v_x} \end{bmatrix} \dot{\psi}_{des} + \begin{bmatrix} 0 & 0 & 0 \\ \frac{\mu_f C_f}{m} & \frac{\mu_r C_r}{m} & 0 \\ 0 & 0 & 0 \\ \frac{\mu_f C_f l_f}{I_{zz}} & \frac{\mu_r C_r l_r}{I_{zz}} & \frac{1}{I_{zz}} \end{bmatrix} \begin{bmatrix} \delta_f \\ \delta_r \\ M_z \end{bmatrix} \end{aligned} \tag{4.44}$$

The state space model for the lateral dynamics of the vehicle given by Equation (4.44) can be simplified as:

$$\dot{x} = Ax + B_1 u + B_d w_d + B_2 r \ , \qquad y = Cx + Du \tag{4.45}$$

where $x = \{e_y, \dot{e}_y, e_\psi, \dot{e}_\psi\}^T$, $u = \{\delta_f, \delta_r, M_z\}^T$, $w_d = \{F_{wy}, M_{wz}, F_b\}^T$, $r = \dot{\psi}_{des}$, the open loop matrix A has two eigenvalues at the origin and is unstable as shown in Figure 4.5(a). The system has to be stabilized by the control feedback. By using the state feedback law:

$$\delta_f = -Kx = -k_1 e_y - k_2 \dot{e}_y - k_3 e_\psi - k_4 \dot{e}_\psi \tag{4.46}$$

The eigenvalues of the closed-loop matrix ($A - B_1K$) can be placed at any desired location as shown in Figure 4.5 (b). Then, the closed-loop system under state feedback is given by:

$$\dot{x}_l = (A - B_1 k_{mpc})x + B_1 k_{ff} + B_d w_d + B_2 r_l \tag{4.47}$$

Due to presence of the $B_2\dot{\psi}_{des}$ term, the tracking errors will not all converge to zero when the vehicle is travelling on a curve, even though the matrix ($A - B_1K$) is asymptotically stable. Therefore, we want to investigate whether the use of a FF/PI term in addition to state feedback can ensure zero steady state errors on a curve. Thus, we assume that the steering controller is obtained by the state feedback from the MPC in Equation (4.32) plus a FF/PI term that attempts to compensate for the road curvature are as follows:

$$u_l(k) = \delta_f(k) = -k_{mpc}\, x(k) + k_{ff} \ , \qquad u_l(k) = -k_{mpc}\, x(k) + k_{pi} \tag{4.48}$$

For PI controller, from Figure 4.3, the control signal from the PI controller given in Laplace transform as:

$$k_{pi} = k_p + \frac{k_i}{s} \tag{4.49}$$

From here, we will focus only for FF controller and the PI controller will be implemented with the same approach. From the system in Equation (4.5), the eigenvalues of the closed-loop matrix $A - B_1k_{mpc}$ can be placed at any desired location. Let us assume that the longitudinal vehicle speed is constant. Then, the closed-loop system is given by:

$$\dot{x}_l = (A - B_1 k_{mpc})x + B_1 k_{ff} + B_d w_d + B_2 r_l \tag{4.50}$$

For simplicity, we assume zero initial conditions, and, taking the Laplace transform (ℓ) of Equation (4.50), we find:

$$X_l(s) = [sI - (A - B_1 k_{mpc}]^{-1} \left\{B_1\, \ell(k_{ff}) + B_d\, \ell(w_d) + B_2\, \ell(r_l)\right\} \tag{4.51}$$

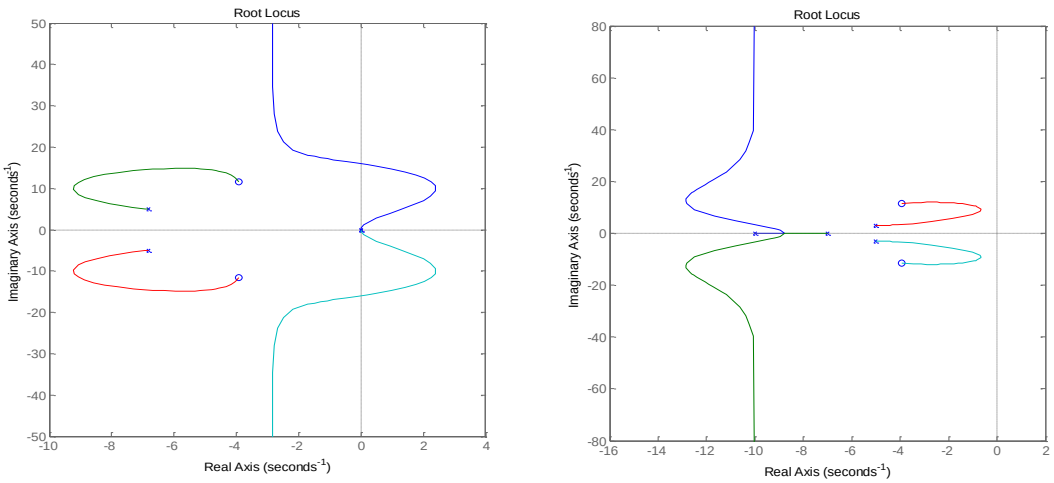

(a) (b)

Figure 4.5: Control feedback in *s*-plane (a) Uncontrolled, (b) Controlled.

For ease of understanding, let us assume here $r_l = \dot{\psi}_{des} = v_x/R_w$. Then, with a small-angle assumption, constant forward speed, and constant radius of curvature, we obtain:

$$\ell(r_l) = \frac{v_x}{sR_w}, \text{ and } \ell(k_{ff}) = \frac{k_{ff}}{s}, \text{ and } \ell(w_d) = \frac{2.5\pi v_w^2}{2s} \tag{4.52}$$

Based on the final-value theorem, the steady-state tracking error is given by:

$$x_{ss} = \lim_{t\to\infty} x(t) = \lim_{s\to 0} s\,X_l(s) = -(A - B_1 k_{mpc})^{-1} \times \left[B_1 k_{ss} + B_d \frac{2.5\pi v_w^2}{2s} + B_2 \frac{v_x}{R_w} \right] \tag{4.53}$$

Again, for the sake of simplicity, we evaluate Equation (4.53) using the symbolic toolbox in Matlab, yielding the steady-state errors:

$$x_{ss} = \begin{bmatrix} \dfrac{k_{ff}}{k_{mpc1}} - \dfrac{(l - l_r k_{mpc3})}{k_{mpc1} R_w} + \left(\dfrac{m v_x^{\,2}}{k_{mpc1} R_w l} - \dfrac{F_w}{k_{mpc1} l} \right) \left(\dfrac{l_f}{\mu_r C_r} - \dfrac{l_r}{\mu_f C_f} - \dfrac{l_f k_{mpc3}}{\mu_r C_r} \right) \\ 0 \\ \dfrac{(-\mu_f C_r l_f l_r - \mu_r C_r l_r^{\,2} + l_f m v_x^{\,2} + F_{wy} R_w l_f)}{\mu_r C_r R_w l} \\ 0 \end{bmatrix} \tag{4.54}$$

The steady-state lateral position error can be made zero if the feedforward steering angle is chosen as:

$$k_{ff} = \frac{(l - l_r k_{mpc3})}{R_w} - \left(\frac{m v_x^{\,2}}{R_w l} - \frac{F_{wy}}{l} \right) \left(\frac{l_f}{\mu_r C_r} - \frac{l_r}{\mu_f C_f} - \frac{l_f k_{mpc3}}{\mu_r C_r} \right) \tag{4.55}$$

However, k_{ff} cannot influence the steady-state yaw angle error no matter how the k_{ff} steering angle is chosen, as can be seen from Equation (4.54). The steady-state yaw angle error from Equation (4.54) can be written as:

$$e_{\psi ss} = \frac{(-\mu_r C_r l_f l_r - \mu_r C_r l_r^{\,2} + l_f m v_x^{\,2})}{\mu_r C_r R_w l} = \frac{m v_x^{\,2} l_f}{\mu_r C_r R_w l} - \frac{l_r}{R_w} \tag{4.56}$$

If we rearrange the Equations (4.55) and (4.56), then the feedforward steering angle is given by:

$$k_{ff} = \frac{l}{R_w} + k_{mpc3}\, e_{\psi ss} + \frac{v_x^{\,2}}{R_w}\left(\frac{m l_r}{\mu_f C_f l} - \frac{m l_f}{\mu_r C_r l}\right) \tag{4.57}$$

This upon closer inspection is seen to be:

$$k_{ff} = \frac{l}{R_w} + k_{mpc3}\, e_{\psi ss} + a_y K_v \tag{4.58}$$

where

$$a_y = \frac{v_x^{\,2}}{R_w}, \qquad K_v = \left(\frac{m_f}{\mu_f C_f} - \frac{m_r}{\mu_r C_r}\right), \quad m_f = \frac{m l_r}{l}, \quad m_r = \frac{m l_f}{l} \tag{4.59}$$

where a_y is the lateral acceleration, K_v is called the understeer gradient steering, m_f and m_r represent the portion of the vehicle mass carried on the front and rear axle. Thus, the steady-state steering angle for zero lateral position error is given by:

$$k_{ss} = \frac{l}{R_w} + a_y K_v \tag{4.60}$$

From Equation (4.56), we may rewrite and rearrange the equation in order to achieve zero steady-state yaw angle error if the vehicle parameters and the vehicle speed are chosen as:

$$\frac{l_r}{R_w} = \frac{m v_x^{\,2} l_f}{2\mu_r C_r R_w l} \tag{4.61}$$

Then, the steady-state yaw angle error of Equation (4.56) can be zero. However, this only happens at one particular speed and road adhesion coefficient, and this speed and road adhesion coefficient are independent of the radius of the path.

Since the vehicle has a fixed length, both the lateral position error and yaw angle error cannot be made zero simultaneously unless the condition of Equation (4.61) is satisfied. This also proved that no matter what control law is used, the yaw angle error $e_{\psi ss}$ will have the steady-state value. The vehicle slip angle is given by:

$$\beta = \arctan\left(\frac{\dot{y}}{v_x}\right) \approx \frac{1}{v_x}(\dot{e}_y - v_x\, e_\psi) \tag{4.62}$$

Since the steady-state of the lateral position error can be made zero, this gives:

$$\beta = -e_{\psi} = -(\psi - \psi_{des}) \tag{4.63}$$

Hence:

$$\beta + \psi = \psi_{des} \tag{4.64}$$

The main aim here is not about the steady-state error of the yaw angle but what is wanted is the heading angle of (β+ψ) to converge with the desired yaw angle.

4.3.4 Rear Braking Control

In this sub-section, the desired direct yaw moment control is adopted from the differences between the two sides of the vehicle torque as denoted in Equation (3.5). Let us assume the vehicle mass is asymmetric and all available torque is transmitted to the ground; thus, the corrective direct yaw moment can be expressed as:

$$M_z = \frac{t_w (F_{xr,r} - F_{xr,l})}{2} \tag{4.65}$$

Based on [156], the right and left wheel brake distribution is more effective than the distribution of front and rear wheels for vehicle steering maneuvers. Thus, the corresponding torque difference between the left and right sides can be denoted in term of M_z as:

$$T_{b,rl} - T_{b,rr} = \frac{2 M_z r_w}{t_w} \tag{4.66}$$

In our study, the braking torque is activated only according to the e_{ψ}; i.e. only used when the vehicle goes toward instability or emergency maneuvers because of its direct affects on the longitudinal motion, while the steering angle is considered for the entire maneuver to be in control or in normal driving maneuvers.

This means we consider two control inputs: front steering angle, and direct yaw moment, but only a single control input is activated at one time. The control law is designed to select the most effective wheels to apply the brake torque, which depends on the steering condition.

Oversteering happens when the vehicle yaw rate is larger than the desired yaw rate, thus, the outer wheels will be selected to generate a contra-cornering yaw moment. Understeering happens when the vehicle yaw rate is smaller than the desired yaw rate, thus, the inner wheels will be chosen to generate a pro-cornering yaw moment as shown in Figure 4.6.

In this study, we use only one wheel at the time to generate the control moment or break torque because the vehicle is not as much decelerated as when brake torque is applied at more than one wheel to generate the same amount of yaw moment.

Thus, to avoid overlapping with front steering angle command, only rear wheels are involved in the control law, as follows:

$$T_{b,rl} = \frac{2M_z r_w}{t_w}, \quad e_\psi < 0, \quad \dot{\psi} < 0 \tag{4.67}$$

$$T_{b,rl} = \frac{2M_z r_w}{t_w}, \quad e_\psi > 0, \quad \dot{\psi} > 0 \tag{4.68}$$

$$T_{b,rr} = \frac{-2M_z r_w}{t_w}, \quad e_\psi < 0, \quad \dot{\psi} > 0 \tag{4.69}$$

$$T_{b,rr} = \frac{-2M_z r_w}{t_w}, \quad e_\psi > 0, \quad \dot{\psi} < 0 \tag{4.70}$$

(a) (b)

Figure 4.6: Individual rear braking wheels: (a) Understeering, (b) Oversteering.

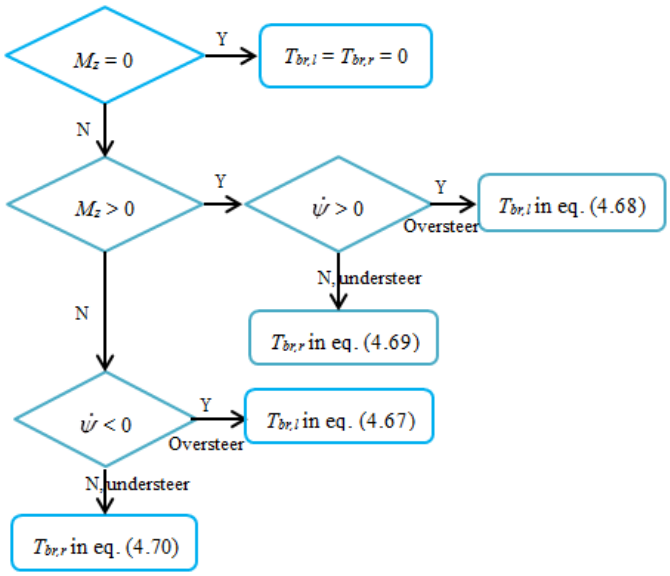

Figure 4.7: Direct yaw moment control logic algorithm.

Figure 4.7 illustrates the flow chart of the braking torques algorithm for the selection of the most appropriate control action based on calculation Equations in (4.68) to (4.70).

4.4 Simulation

The linear MPC and LQC with the proposed methods controller, as described in Section 4.3 have been implemented in a simulation for a path-following vehicle control in a double lane change scenario.

4.4.1 Scenario Description

The double lane change maneuver approximates an emergency maneuver case and generally demonstrates the agility and capabilities of a vehicle in terms of lateral dynamics. During such a maneuver, understeering, oversteering, or even rollover may occur. For these scenarios, we used model parameters for a Ford Taurus SUV and sports utility passenger car based on [138] as illustrated in Table 3.1 and Table 3.2.

Simulations were performed using the MPC Toolbox in Matlab and Simulink software. In this chapter, the predictive controller was used to minimize the deviation of the vehicle from the target path to achieve the main aim, namely, to follow the desired or reference trajectory as close as possible.

In the first scenario, the controllers based on simple 2DoF vehicle motion were compared with each other for a nonlinear vehicle system at a low forward speed (10m/s) and high forward speed (25m/s), on an ideal road friction surface, and medium forward speed (20m/s) on a low-road-friction surface (wet earth with snow, μ = 0.3). In this scenario, there is no disturbances to the system, both controllers (MPC and LQC) were designed and implemented in the simulation scenarios, with the parameters and conditions given in Tables 4.1 and 4.2. The path-following tracking error is a measure of how closely the output responses follow the reference trajectory, and is a measure of the deviation from the benchmark. In this chapter, we use the root-mean-square formula for the standard deviation of the tracking error:

$$e_t = \sqrt{Var\ (y - r_i)} = \sqrt{\frac{1}{(n-1)} \sum (y - r_i)^2} \tag{4.71}$$

where n is the number of time periods, and y and r_i are the measured output and the reference, respectively.

For the second scenario, the vehicle is considered to be travelling horizontally following the path with a constant velocity at 10m/s and 25m/s without braking or accelerating. The drag force and torque given by Equation (3.20) under the initial driving conditions is assumed to act in the direction of the path at t = 1sec with v_w = 10m/s, acting as a disturbance on the vehicle. Table 4.3 illustrates the MPC and MPC with PI controller parameters with weighting matrices that were designed and implemented in AFS maneuver scenario. Table 4.4 lists the MPC and PI controller parameters with weighting matrices that were designed and implemented in AFS and AFS with the DYC maneuver scenarios.

In the third scenario, the vehicle is considered travelling on the horizontal following the path with v_x = 20m/s, and with road adhesion coefficient is set at μ = 0.5 (wet earth road). The drag force and torque given by Equation (3.20) in the initial driving condition is assumed to act in the direction of the path at t = 1sec with v_w = 10m/s. The forces and torques arising from this sidewise acting wind gust is assumed to be persistent and are applied as a step functions throughout the simulation time. Here, we compare the effectiveness of MPC with the PI controller for AFS, and AFS with DYC control maneuvers under the same forward speed, with crosswind effect consideration and with μ = 0.5. Table 4.5 illustrates the MPC with the PI controller parameters with weighting matrices that were designed and implemented in the scenarios.

In the last scenario, the effects of the vehicle roll dynamics motion was considered and studied. The drag force and torque given by the Equation (3.19) in the initial driving conditions are assumed to act in the direction of the path at time t = 1 sec with a wind velocity of v_w = 10m/s. The predictive controller was implemented by minimizing vehicle deviation from the target path. The controllers are compared against each other for 2DoF and 3DoF bicycle models, which discludes vehicle roll dynamics at high speed specifically, high (30m/s); also with wet concrete (μ = 0.7) and wet icy (μ = 0.1) road surfaces. Table 4.6 illustrates the MPC controller parameters with weighting matrices that were designed and implemented in the scenarios.

Table 4.1
Parameters of controller.

Parameter	**Value**
H_p, H_c	20, 9
T_s, T	0.05, 15
δ_f, δ_r	± 0.5
$\Delta\delta_f$, $\Delta\delta_r$	± 0.35
M_z, ΔM_z	± 2000, ± 1500

Table 4.2
Parameters of controller weighting matrices.

Control maneuvers		**MPC**	**LQC**
2WS	v_x = 10m/s, μ = 1	R_1 = 0.1, ΔR_1 = 0.03 Q_{11} = 2.05, Q_{22} = 0.5	R_{lq} = 5, ΔR_{lq} = 0.5 Q_{lq1} = 10, Q_{lq2} = 1.5
	v_x = 25m/s, μ = 1	R_1 = 0.1, ΔR_1 = 0.03 Q_{11} = 5.25, Q_{22} = 0.5	R_{lq} = 5, ΔR_{lq} = 0.5 Q_{lq1} = 20, Q_{lq2} = 2.5
	v_x = 20m/s, μ = 0.3	R_1 = 0.1, ΔR_1 = 0.03 Q_{11} = 2.65, Q_{22} = 0.65	R_{lq} = 5, ΔR_{lq} = 0.5 Q_{lq1} = 12, Q_{lq2} = 2.8
4WS	v_x = 10m/s, μ = 1	R_1, R_2 = 0.1, ΔR_1, R_2 = 0.03 Q_{11} = 2.85, Q_{22} = 0.2	R_{lq1}, R_{lq2} = 5, ΔR_{lq1}, R_{lq2} = 0.5 Q_{lq1} = 4.65, Q_{lq2} = 1.55
	v_x = 25m/s, μ = 1	R_1, R_2 = 0.1, ΔR_1, R_2 = 0.03 Q_{11} = 3.15, Q_{22} = 0.5	R_{lq1}, R_{lq2} = 5, ΔR_{lq1}, R_{lq2} = 0.5 Q_{lq1} = 14.5, Q_{lq2} = 2.55
	v_x = 20m/s, μ = 0.3	R_1, R_2 = 0.1, ΔR_1, R_2 = 0.03 Q_{11} = 3.55, Q_{22} = 3.05	R_{lq1}, R_{lq2} = 5, ΔR_{lq1}, R_{lq2} = 0.5 Q_{lq1} = 9.5, Q_{lq2} = 4.15
2WS + DYC	v_x = 10m/s, μ = 1	R_1, R_2 = 0.1, ΔR_1, R_2 = 0.03 Q_{11} = 2.15, Q_{22} = 0.5	R_{lq1}, R_{lq2} = 5, ΔR_{lq1}, R_{lq2} = 0.5 Q_{lq1} = 5, Q_{lq2} = 1.5
	v_x = 25m/s, μ = 1	R_1, R_2 = 0.1, ΔR_1, R_2 = 0.03 Q_{11} = 4.55, Q_{22} = 0.5	R_{lq1}, R_{lq2} = 5, ΔR_{lq1}, R_{lq2} = 0.5 Q_{lq1} = 10.4, Q_{lq2} = 2.55
	v_x = 20m/s, μ = 0.3	R_1, R_2 = 0.1, ΔR_1, R_2 = 0.03 Q_{11} = 5.15, Q_{22} = 1.05	R_{lq1}, R_{lq2} = 5, ΔR_{lq1}, R_{lq2} = 0.5 Q_{lq1} = 8.5, Q_{lq2} = 2.35

The weighting matrices for the inputs and outputs of MPC and LQC were based on a trial and error process, where the main target here is to achieve zero lateral position error rather than zero yaw angle error.

Table 4.3
Controller parameter conditions in AFS maneuver.

Parameter	**MPC**	**MPC + PI**
H_p, H_c	20, 9	20, 9
δ_f, $\Delta\delta_f$	± 0.35, ± 0.17	± 0.35, ± 0.17
R_1	0.1	0.1
Q_{11}, Q_{22} (v_x = 10m/s)	2.15, 0.5	1.95, 0.5
k_{p1}, k_{i1}	-	1.5, 0.2
k_{p2} k_{i2}	-	1.5, 0.1

Table 4.4
Controller parameters for MPC with PI controller.

Parameter	**AFS**	**AFS + DYC**
H_p, H_c	20, 9	20, 11
δ_f , $\Delta\delta_f$	± 0.35, ± 0.17	± 0.35, ± 0.17
M_z, ΔM_z	-	± 1500, ± 500
R_1	0.1	0.1
Q_{11}, Q_{22} (v_x = 25m/s)	4.1, 0.5	3.5, 0.5
k_{p1}, k_{i1}, k_{p2} k_{i2}	0.5, 0.1, 0.1, 0.1	0.9, 0.3, 0.9, 0.2

Table 4.5
Controller Parameters for MPC with PI Controller.

Parameter	**AFS**	**AFS + DYC**
H_p, H_c	20, 9	20, 11
δ_f, $\Delta\delta_f$	± 0.35, ± 0.17	± 0.35, ± 0.17
M_z, ΔM_z	-	± 1500, ± 1000
R_1, ΔR_1, R_2, ΔR_2	0.1, 0.03, -, -	0.1, 0.03, 0.1, 0.03
Q_{11}, Q_{22} (v_x = 20m/s)	1.95, 0.5	2.05, 0.5
k_{p1}, k_{i1}, k_{p2} k_{i2}	0.5, 0.2, 0.25, 0.15	0.4, 0.55, 0.5, 0.6

Table 4.6
Model predictive control weighting matrices parameters for v_x = 30m/s.

Control maneuvers		2DoF	3DoF
2WS	v_x = 30m/s, μ = 0.7	$R_1 = 0.1, \Delta R_1 = 0.03$ $Q_{11} = 5.65, Q_{22} = 0.5$	$R_1 = 0.1, \Delta R_1 = 0.03$ $Q_{11} = 3.55, Q_{22} = 0.5$
	v_x = 30m/s, μ = 0.1	$R_1 = 0.1, \Delta R_1 = 0.03$ $Q_{11} = 0.083, Q_{22} = 0.042$	$R_1 = 0.1, \Delta R_1 = 0.03$ $Q_{11} = 0.03, Q_{22} = 0.45$
4WS	v_x = 30m/s, μ = 0.7	$R_1 = 0.1, \Delta R_1 = 0.03$ $R_2 = 0.1, \Delta R_2 = 0.03$ $Q_{11} = 1.55, Q_{22} = 2.5$	$R_1 = 0.1, \Delta R_1 = 0.03$ $R_2 = 0.1, \Delta R_2 = 0.03$ $Q_{11} = 1.35, Q_{22} = 3.5$
	v_x = 30m/s, μ = 0.1	$R_1 = 0.1, \Delta R_1 = 0.03$ $R_2 = 0.1, \Delta R_2 = 0.03$ $Q_{11} = 0.005, Q_{22} = 0.001$	$R_1 = 0.1, \Delta R_1 = 0.03$ $R_2 = 0.1, \Delta R_2 = 0.03$ $Q_{11} = 0.04, Q_{22} = 0.5$
2WS+DYC	v_x = 30m/s, μ = 0.7	$R_1 = 0.1, \Delta R_1 = 0.03$ $R_2 = 0.1, \Delta R_2 = 0.03$ $Q_{11} = 5.05, Q_{22} = 0.5$	$R_1 = 0.1, \Delta R_1 = 0.03$ $R_2 = 0.1, \Delta R_2 = 0.03$ $Q_{11} = 3.5, Q_{22} = 0.5$
	v_x = 30m/s, μ = 0.1	$R_1 = 0.1, \Delta R_1 = 0.03$ $R_2 = 0.1, \Delta R_2 = 0.03$ $Q_{11} = 0.092, Q_{22} = 0.04$	$R_1 = 0.1, \Delta R_1 = 0.03$ $R_2 = 0.1, \Delta R_2 = 0.03$ $Q_{11} = 0.5, Q_{22} = 2.5$

Here, the weighting matrices were selected based on the best-response outputs by first tuning the outputs gain parameter, than follow by tuning input gains parameter.

4.4.2 Result and Discussion

Since our research is conducted through a simulation process, it is necessary to validate the vehicle model through maneuver tests. Another way to strengthen the proposed control methods is to compare the proposed controller with another controller. This way, we are comparing two different controls for the same aims and target, in order to validate and prove the methods used are accurate enough. Currently, we are developing the vehicle prototype for our next study on the real implementation. To facilitate a comparison of the robustness and performance of both controllers in stabilizing the vehicle at a chosen speed along the desired trajectory, the controller

tuning parameters from Tables 4.1 to 4.6 were selected for all situations and conditions of vehicle maneuvers.

In the first scenario, first, we performed a vehicle simulation test under ideal road surface friction coefficients, asphalt dry (μ = 1), at a constant low forward speed of 10m/s without disturbances. The MPC and LQC weight tuning parameters are listed in Table 4.2. We evaluated the controller's robustness for the output responses by comparing the performance of 2WS, 4WS, and 2WS with DYC manoeuvres at a forward speed of 10m/s, as shown in Figure 4.8 to Figure 4.10. The controller tracking error, based on Equation (4.71) for lateral position and yaw angle responses, are summarized in Table 4.7. From Figure 4.8, for the lowest speed manoeuvres and with a high road adhesion coefficient, there was not much difference between the manoeuver controllers; both controllers gave a perfect response when following a given trajectory and maintaining vehicle stability. It can be seen that for 4WS and 2WS with DYC manoeuvres, the rear steering angle and the direct yaw moment are almost unused, since the front steering can provide sufficient control ability. This may be partly due to the fact that the rear steering and DYC were not used in lower speed manoeuvres.

In these scenarios, among the three control maneuvers, the 2WS with DYC performed slightly better especially in yaw angle and yaw rate responses followed by 4WS, and finally 2WS, in which lateral position and yaw angle look almost identical. In this situation the figures show that, the rear steering of the 4WS maneuver is going in the opposite direction with front steering in order to stabilize the vehicle along the trajectory.

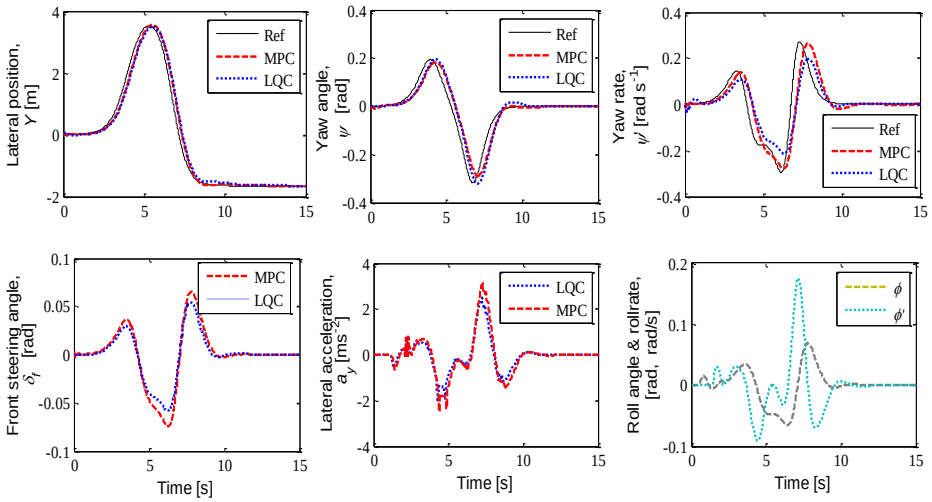

Figure 4.8: Vehicle maneuver by 2WS at 10m/s.

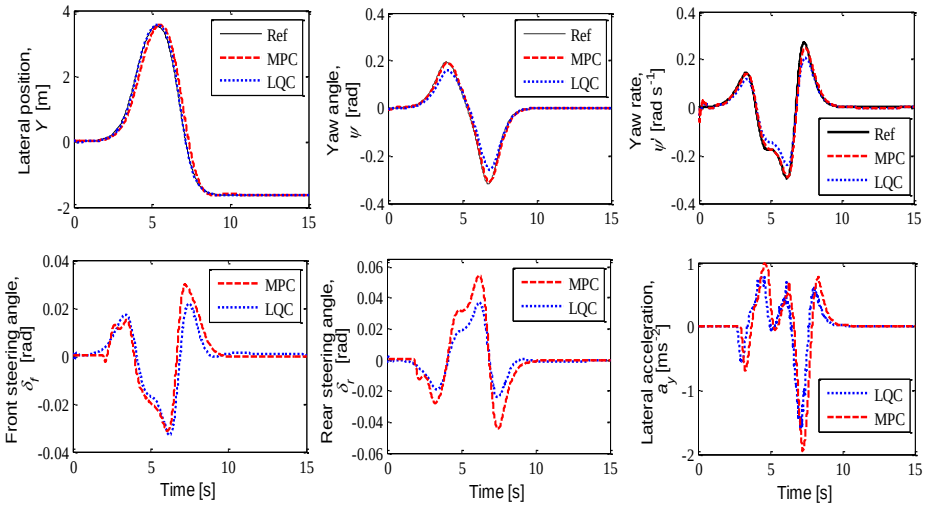

Figure 4.9: Vehicle maneuver by 4WS at 10m/s.

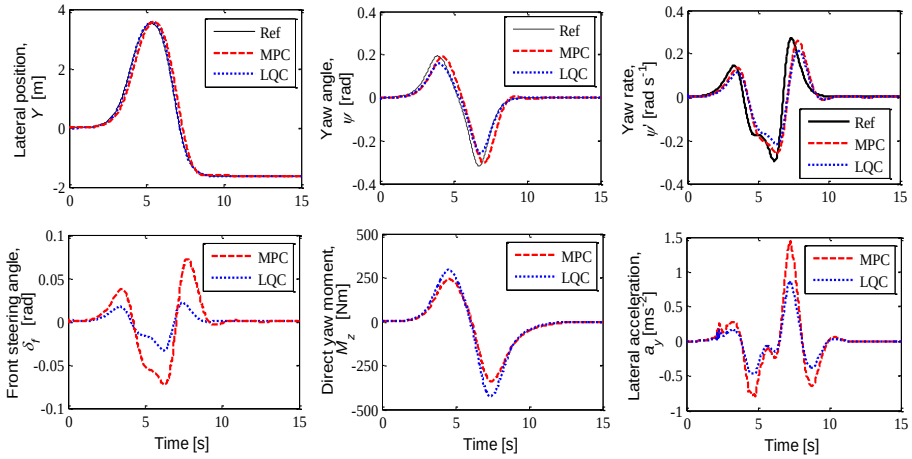

Figure 4.10: Vehicle maneuver by 2WS+DYC at 10m/s.

While, for direct yaw moment controls under 2WS with DYC maneuver, it is used with a very little amount of torque because yaw outputs were successful to track and follow a given trajectory closely. In low forward peed scenario, both controllers were successfully implemented for all maneuver controls due to the fact that, roll dynamics will not have much influence during low speed maneuvers. Furthermore, at low vehicle speed, all manipulated inputs are under the constraints of the front steering angle, rear steering angle, or direct yaw moment control.

Next, we simulated the motion of the vehicle at high forward speed (chosen as 25m/s) and neglected the road surface friction (which was chosen as dry concrete, μ = 1). We evaluated the controllers robustness for the output response by comparing performances of 2WS, 4WS, and 2WS with DYC maneuvers as shown in Figures 4.11 to 4.13. It can be seen clearly from these figures that for the MPC controller, the

trajectory tracking responses for lateral position and yaw angle were similar for all control maneuvers and it was possible to successfully track and follow a given trajectory. The lateral position responses were similar for LQC, but it can be seen that LQC did not perform well in terms of yaw angle and yaw rate tracking responses. This shows that LQC is not suitable for control implementation in multivariable systems.

Moreover, Figures 4.12 and 4.13 illustrate that for a high forward speed of the vehicle, the maneuver response was much better for 4WS and for 2WS with DYC than for 2WS: the rear steering and DYC were fully utilized. We can therefore conclude that for 4WS, the rear wheels helped the vehicle to steer by improving its handling at high speed and decreasing the turning radius at low speed. In 2WS vehicles, the rear set of wheels are always directed forward and do not play an active role in controlling the steering. To illustrate our point, the tracking error result based on Equation (4.71) for all the maneuvers from Figures 4.11 to 4.13, are tabulated in Table 4.7, from which it can be seen that, among the three maneuver controls, 2WS with DYC gives the best performance by reducing the tracking error for lateral position, yaw angle, and yaw rate responses compared with 4WS and with 2WS only. However, in some cases; particularly at high speeds with neglected road friction, lateral position is much lower under 4WS of the MPC controller compared to the other maneuver controls.

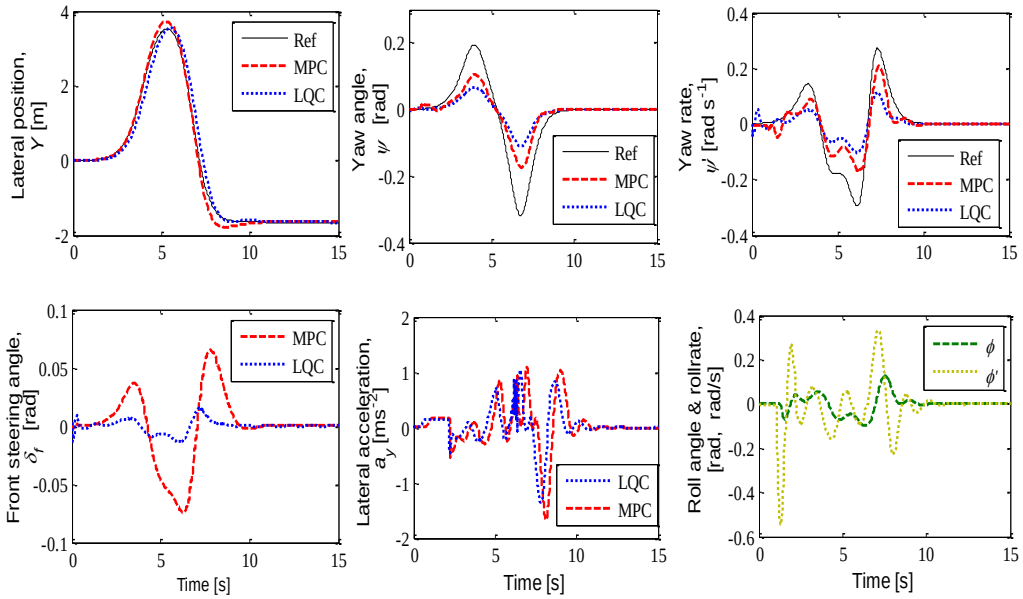

Figure 4.11: Vehicle maneuver by 2WS at 25m/s.

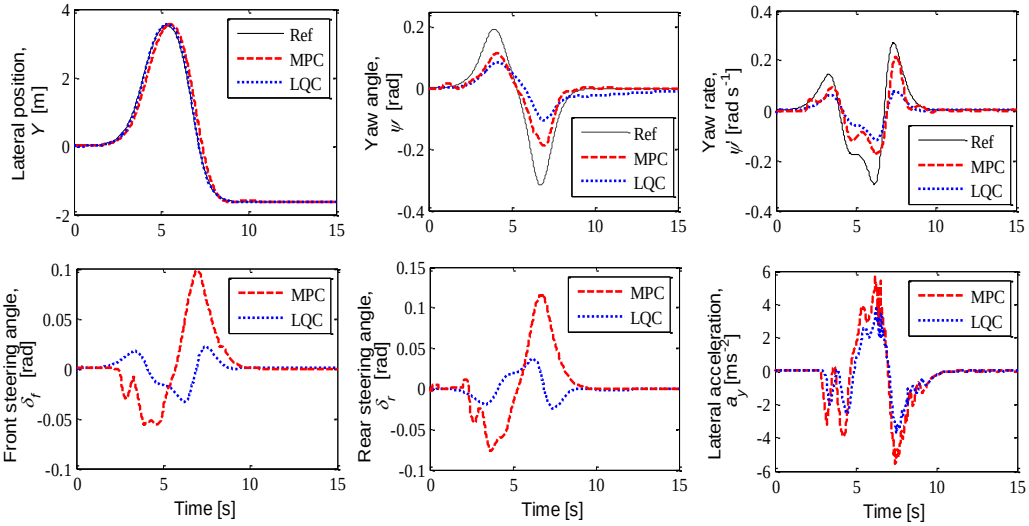

Figure 4.12: Vehicle maneuver by 4WS at 25m/s.

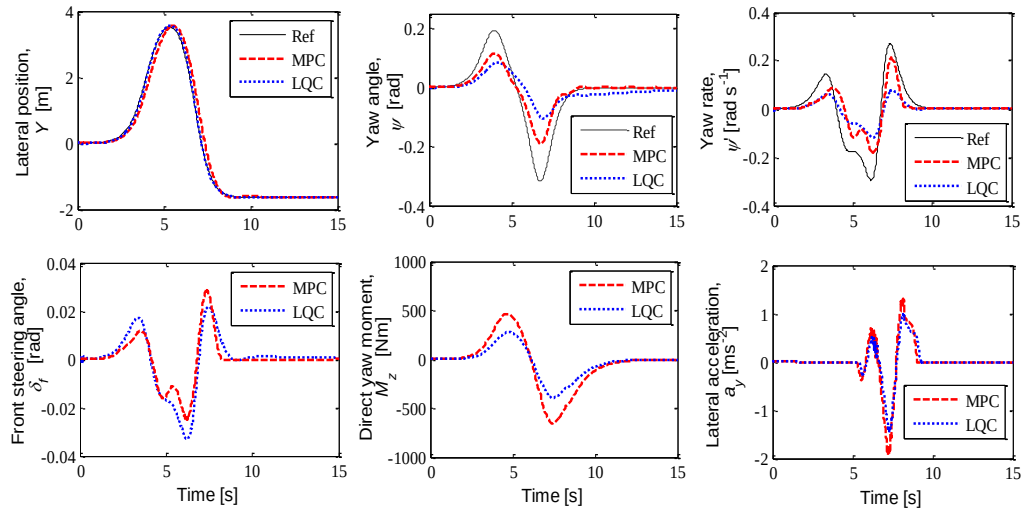

Figure 4.13: Vehicle maneuver by 2WS+DYC at 25m/s.

Table 4.7

Path-following tracking errors without road surface friction $\mu = 1$.

Vehicle speed	**Maneuver control**	**LQC**		**MPC**	
		Y [m]	ψ [rad]	Y [m]	ψ [rad]
10m/s	2WS	0.0798	0.0198	0.0812	0.0081
	4WS	0.0768	0.0165	0.0810	0.0058
	2WS +DYC	0.0772	0.0163	0.0810	0.0054
25m/s	2WS	0.0882	0.7645	0.0994	0.2146
	4WS	0.0834	0.8484	0.0838	0.0782
	2WS +DYC	0.0826	0.6242	0.0908	0.0524

Next, we tested the vehicle at 20m/s forward speed and taking the road friction coefficient to be that for wet earth with snow (μ = 0.3), with the tuning parameters for MPC and LQC as tabulated in Table 4.2. In these scenarios, we ignored the simulation under low forward speed because we believe that, the vehicle response is not really influenced at low speed. Thus, we compare the simulation results for 2WS, 4WS, and 2WS with DYC for both controllers in middle forward speed with low road friction coefficient, as shown in Figures 4.14 to 4.16. These results show that at 20m/s, and when μ varies from its values for asphalt and dry concrete to wet earth with snow, 4WS and 2WS with DYC maneuvers give much better tracking performances than 2WS only. It can be noted that for 4WS and 2WS with DYC, MPC performed much better than LQC in terms of the yaw angle and yaw rate tracking responses. However, the MPC and LQC tracking responses for the 2WS maneuver were unstable, with the result that the vehicle would lose control and spin away from the trajectory.

In these scenarios, we can see clearly see that for 4WS, the rear wheels helped the vehicle to steer by improving its handling at low friction adhesion, while its the same for 2WS with DYC, where direct yaw control is fully utilized to stabilize the vehicle along the trajectory at middle speed, as shown from the yaw angle and yaw rate vehicle responses. Furthermore, the simulation results in Figures 4.15 and 4.16 also demonstrate that, for both controllers, at μ = 0.3 and 20m/s, the tracking performances for lateral and yaw rate were better, but not perfect and still allowed the vehicle to track and follow the trajectory compared with Figure 4.14. Table 4.8 shows the robustness of the controller performance and the tracking errors for all types of maneuvers at a vehicle speed of 20m/s with road surface friction.

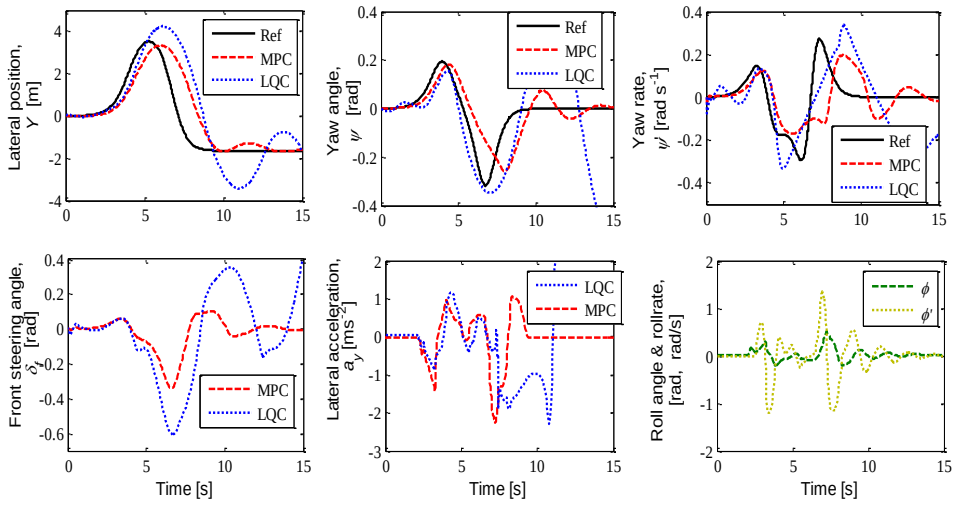

Figure 4.14: Vehicle maneuver via 2WS at 20m/s with μ = 0.3.

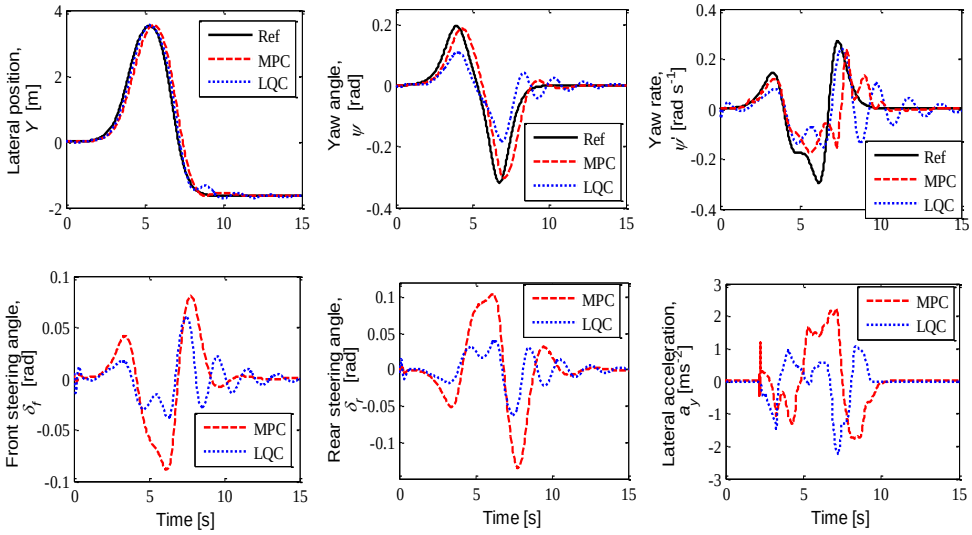

Figure 4.15: Vehicle maneuver via 4WS at20 m/s with μ = 0.3.

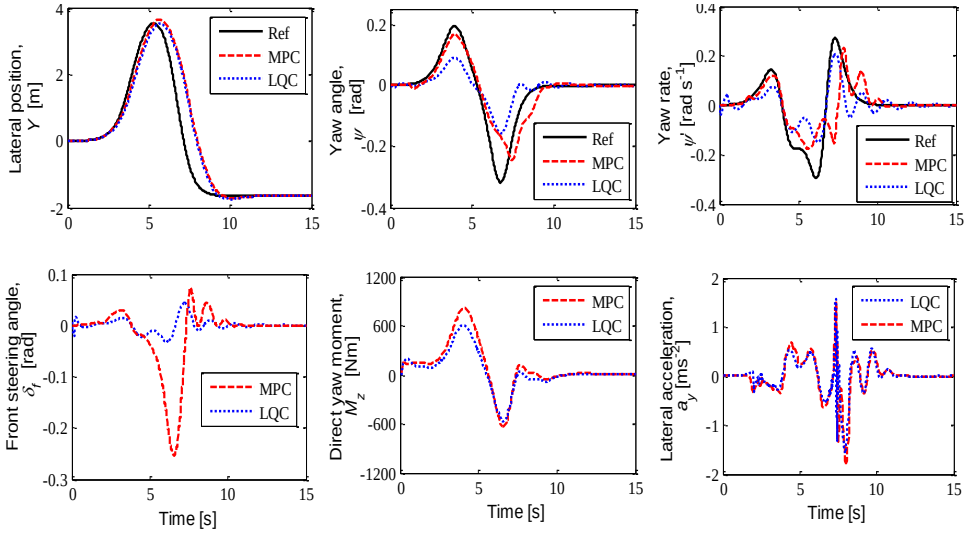

Figure 4.16: Vehicle maneuver via 2WS+DYC at 20m/s with μ = 0.3.

Table 4.8

Path-following tracking errors with road surface friction μ = 0.3.

Vehicle speed	**Maneuver control**	**LQC**		**MPC**	
		Y [m]	ψ [rad]	Y [m]	ψ [rad]
20m/s	2WS	0.8424	0.5654	0.5876	0.3014
	4WS	0.1048	0.0676	0.0954	0.0184
	2WS+DYC	0.1487	0.0986	0.1394	0.0268

Finally, we simulated the vehicle's behavior at a high forward speed of 25m/s with ideal road surface friction coefficients, asphalt dry (μ = 1), and at middle forward speed of 20m/s taking the road surface friction condition to be wet earth with snow (μ

= 0.3), in a double lane change scenario to minimize tracking errors. We used MPC with FF controller and compared the results with those from LQC with FF controller described in Sections 4.3.2 and 4.3.3. Table 4.9 illustrates the weighting matrices for MPC and LQC with FF controller gain parameters, for each control maneuver. We compared the performance of both controllers for the lateral position and yaw angle output responses to an AFS maneuver only, as shown in Figures 4.17 and 4.18. The idea for this scenario was selected because we wanted to see the effect of the feedforward controller compared with the results in Figures 4.10 and 4.13 without FF term. From Figures 4.17 and 4.18, it can be clearly seen that for the MPC with FF controller, trajectory tracking responses for lateral position and yaw angle in 2WS were slightly better than for LQC with FF controller. Figure 4.17 demonstrates that both controllers performed very well for lateral position, but MPC with FF controller performed much better than LQC with FF controller for yaw angle and yaw rate responses. Moreover, the lateral position and yaw angle errors are greatly reduced by adding the FF controller to either MPC or LQC.

Furthermore, when the vehicle behavior is simulated on a low-road-adhesion surface, as shown in Figure 4.18, MPC with FF controller still behaves better than LQC with FF controller for both output responses.

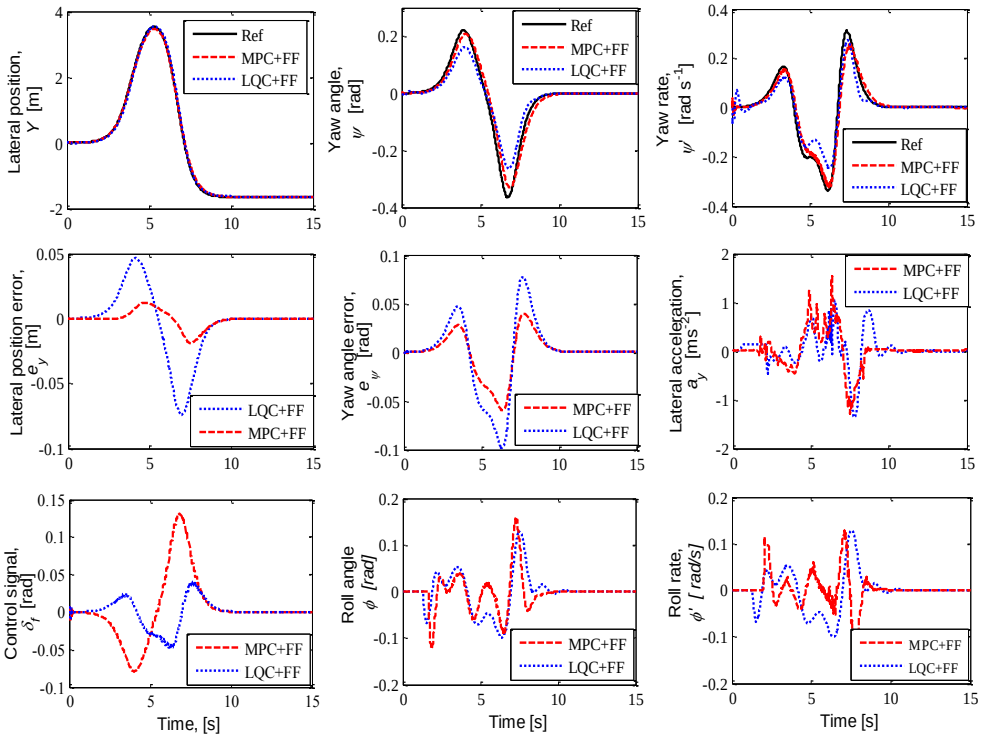

Figure 4.17: Vehicle tracking errors for maneuver via 2WS at 25m/s.

However, in this situation, we can notice that for the yaw angle and yaw rate responses: the vehicle does not follow the trajectory very well; it has some vibrations or oscillations for both controllers, which deteriorates the vehicle performances which, based on the authors knowledge, comes from the FF controllers tuning gain parameter or inertial conditions of the system. However, for a low friction coefficient, MPC with FF controller still gives better responses than LQC with FF controller. It also can be noticed that when the FF controller is added to MPC or LQC, the trajectory tracking response is again much better than with MPC or LQC alone.

Table 4.9
Parameters of controller weighting matrices.

Control maneuvers		**MPC + FF**	**LQC + FF**
2WS	v_x = 25m/s, μ = 1	$R_1 = 0.1$, $\Delta R_1 = 0.01$	$R_{lq} = 5$, $\Delta R_{lq} = 0.5$
		$Q_{11} = 4.25$, $Q_{22} = 1.5$	$Q_{lq1} = 18.5$, $Q_{lq2} = 3.5$
		$k_{ff1} = 2.45$, $k_{ff2} = 1.25$	$K_f = 1.25$, $K_s = 1.45$
	v_x = 20m/s, μ = 0.3	$R_1 = 0.1$, $\Delta R_1 = 0.01$	$R_{lq} = 5$, $\Delta R_{lq} = 0.5$
		$Q_{11} = 3.85$, $Q_{22} = 1.25$	$Q_{lq1} = 12.5$, $Q_{lq2} = 2.8$
		$k_{ff1} = 1.95$, $k_{ff2} = 0.75$	$K_f = 0.95$, $K_s = 1.15$

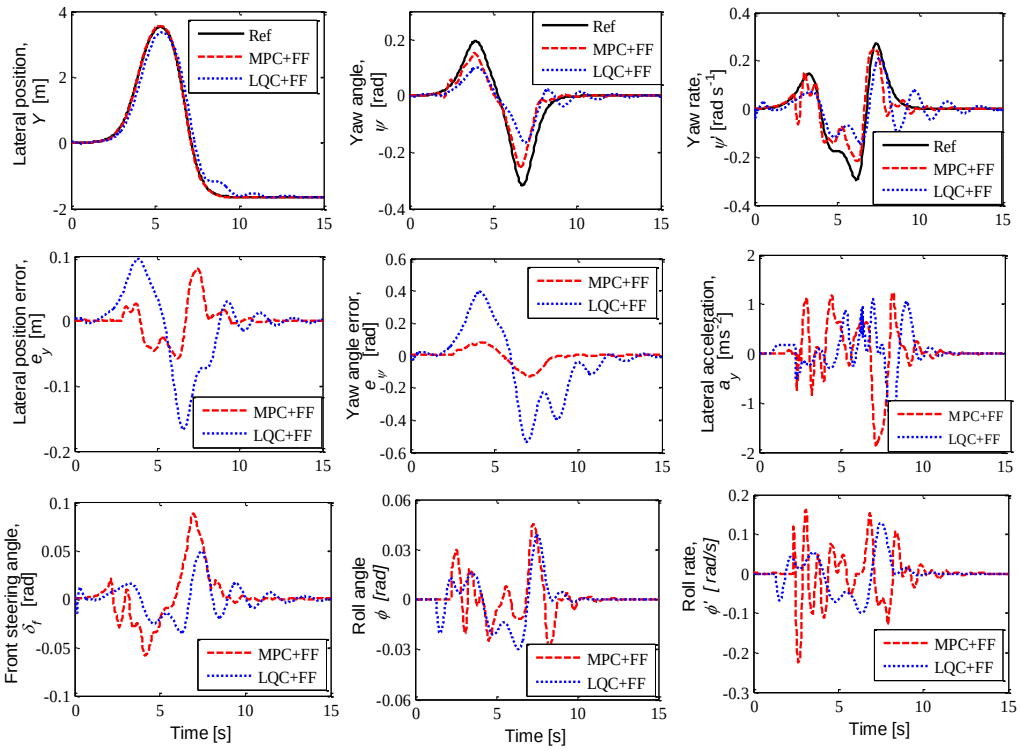

Figure 4.18: Vehicle tracking errors for maneuver via 2WS at 20m/s with μ = 0.3.

In the second scenario, first, we simulated the vehicle's behavior at a low forward speed of 10m/s on a double lane change scenario to minimize tracking errors. We used an MPC with PI controller and compared the results with those from MPC only, as described in Sections 4.3.1 and 4.3.3. We compared the performance of both controllers for the lateral position and yaw angle output responses to an AFS maneuver, as shown in Figure 4.19. From Figure 4.19, it can be clearly seen that for the MPC with PI controller, the trajectory tracking responses for the lateral position and yaw angle were slightly better than for the MPC controller. However, the MPC with PI controller has a high increase in lateral position by minimizing the trajectory error, as can be seen from the lateral position error. The vehicle stability also can be enhanced with an additional PI controller; the results proved that yaw rate response under the MPC with PI controller is very closely correlated with the desired trajectory, as opposed to the MPC only.

Figure 4.19 also demonstrates that both controllers performed very well for lateral position and yaw angle, even under the crosswind effect, because a vehicle does not feel much effect from crosswind in low forward speed. The crosswind effect can be seen through the lateral forces at the front and rear wheels where the steady-state of front lateral forces without the crosswind was particularly at zero.

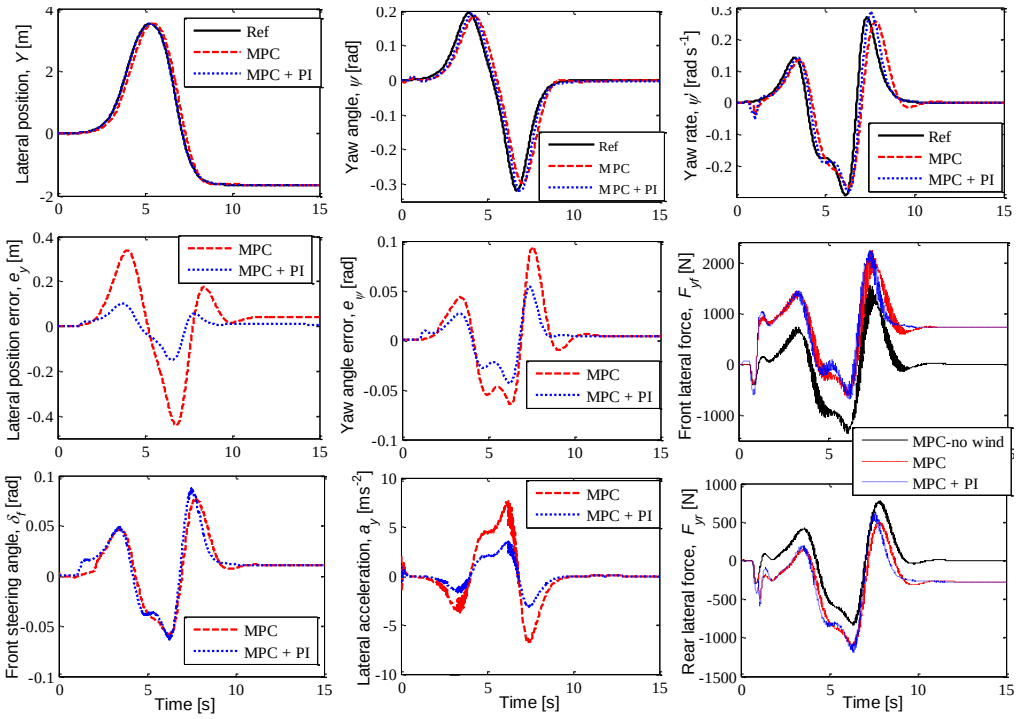

Figure 4.19: Vehicle maneuver via AFS at 10m/s under crosswind.

As mentioned in Section 4.1, most of the tracking responses are influenced in the beginning of the crosswind effect where it is decided at one second. In this scenario, the front steering angle is within the constraint for both controllers, and the proposed controller showed that the steady-state control signal was ended at zero.

On the other hand the MPC controller only has a little steady-state error along the simulation time. The selection of PI gain parameters are guided and constraint within the Equation (4.55). Moreover, we neglected the DYC maneuver because it will not affect the vehicle control maneuver in lower speeds, since the tracking performances were better with an integrated control approach.

Next, we tested the vehicle's behavior at a high forward speed of 25m/s, in the same scenario. Since it is proved that MPC with PI controller provides tracking response closer to the desired references, whilst successfully minimizing the tracking errors, in this scenario, we compared the performance of the MPC with PI controller for lateral position and yaw angle errors to both an AFS, and AFS with DYC maneuvers, as shown in Figure 4.20. We like to see the effectiveness of the proposed braking control allocation, as described in Section 4.3.4, at high forward speed under the crosswind effect. From the Figure 4.20, it can be seen clearly that both maneuvers performed well for lateral position response, but AFS with DYC can minimize more of the lateral position error than AFS maneuver. For yaw angle and yaw rate responses, both maneuvers cannot follow a given trajectory as closely as possible; however, it can be seen that AFS with DYC maneuver provides much better yaw angle and yaw rate tracking responses than AFS maneuver- especially as indicated in yaw angle error response. It shows that, by adding one more control input to the system, particularly in this case, we add the direct yaw moment control as shown in Figure 4.21, where it may enhance vehicle stability and handling even under crosswind disturbance effects.

Moreover, the crosswind effect to the system can be seen through the lateral forces at the front and rear wheels, as shown in Figure 4.20. In this scenario, the front steering angle and angle rate are within the constraints for both maneuvers control. An AFS with DYC maneuver showed that the steady-state control signal was ended at zero, while the AFS maneuver has a little steady-state error throughout the simulation time. The control signals of AFS with DYC can be seen through the front steering angle and direct yaw moment control as shown in Figure 4.21, where the rear braking

torque on the right wheels was much more used than the left wheels to stabilize the vehicle maneuver control.

The results showed that at high forward speed, an AFS maneuver is not able to stabilize the vehicle for the yaw rate response, especially under crosswind disturbance. It can therefore be improved by adding another control input to the system, such as active rear steering, braking system, or torque distribution at the front and/or rear wheels. Thus, with a combination of AFS and DYC, rear braking torque distribution between left and right wheels may enhance vehicle stability.

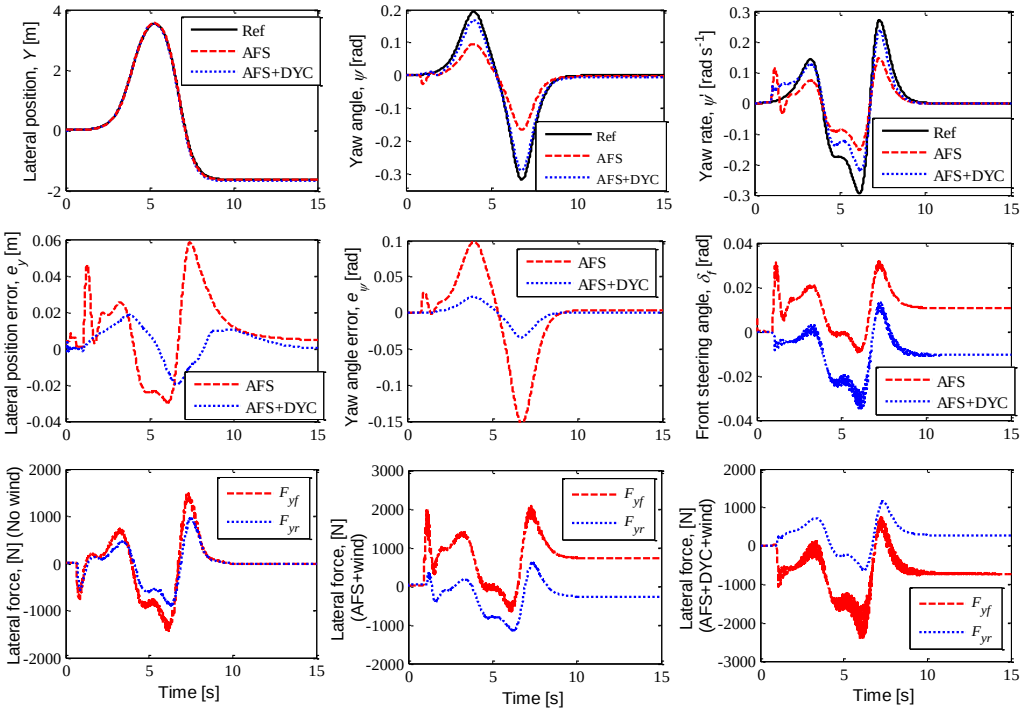

Figure 4.20: Vehicle maneuver via AFS and AFS+DYC at 25m/s with crosswind.

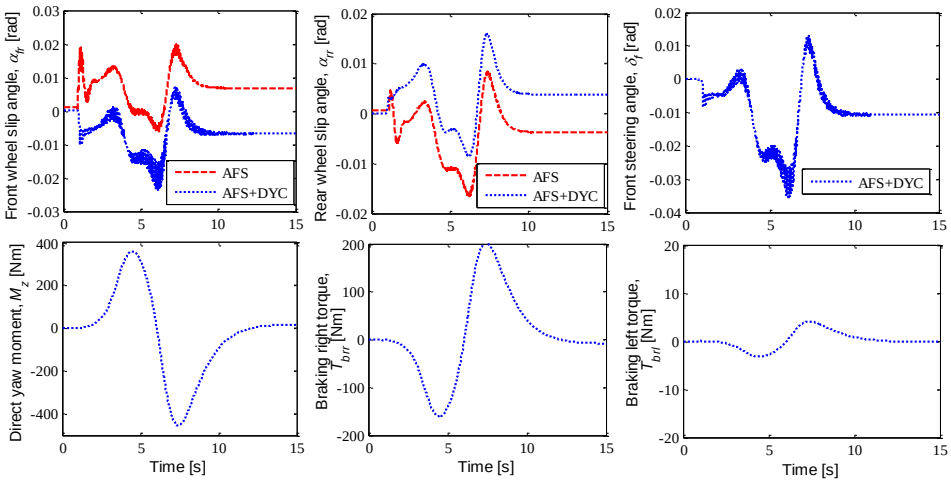

Figure 4.21: Control signal of a vehicle maneuver via AFS and AFS+DYC at 25m/s with crosswind.

In our study, when the DYC is applied, the velocity is increased from 0 to 0.5m/s, and the DYC is dependent on the output weighting matrices from the MPC controller. Thus, we need to tune the input and output weighting matrices as well as possible in order for the DYC to usefully enhance the yaw rate response which refers to the vehicle stability, while AFS is used mainly for tracking purposes.

For the third scenario, we simulated the vehicle's behavior at a forward speed of 20m/s with road surface friction wet earth road (μ = 0.3), in a double lane change scenario to minimize tracking errors. In order to see the effectiveness of the proposed method in Sections 4.3.3 and 4.3.4, we used MPC with the PI controller and compared the results with those from AFS and AFS with DYC maneuvers. We also compared the vehicle performances of AFS (front steer wheel with PI controller) with 2WS (front steer wheel) which was without the PI controller to evaluate the advantages of the PI controller. We compared the performance of the controller for the lateral position, yaw angle, yaw rate, lateral position error, and yaw angle error output responses as shown in Figure 4.22. We like to see the effectiveness of the proposed braking control allocation as described in Section 4.3.4 on wet earth road under the crosswind effect.

From the Figure 4.22, it can be clearly seen that AFS and AFS with DYC maneuvers performed well in the lateral position rather than the 2WS maneuver. However, if we see the vehicle's responses of lateral error, we might notice that the AFS with DYC maneuver can minimize the lateral position errors more than the AFS maneuver. In the vehicle's yaw angle and yaw rate responses, both maneuvers (2WS and AFS) cannot follow a given trajectory as close as possible, which saw 2WS perform worse than the AFS maneuver. However, it can be seen that the AFS with DYC maneuver provided a much better yaw angle and yaw rate tracking responses than the AFS maneuver, especially as indicated in the yaw angle error response. It shows that, by adding one more control input to the system, particularly in this case we added the direct yaw moment control as shown in Figure 4.23, may enhance vehicle stability and handing even though under the disturbances of crosswind and road adhesion. From Figure 4.22, it proved that the proposed braking control algorithm was successful to enhance the vehicle stability through yaw angle and yaw rate responses.

Moreover, the crosswind effect on the system can be seen through the lateral forces at the front and rear wheels as shown in Figure 4.22. In this scenario, the front steering angle and angle rate are within the constraints of both maneuvers control. An AFS with DYC maneuver showed that the steady-state control signal ended at zero, while the AFS maneuver has a little steady-state error throughout the simulation time. The control signals of AFS with DYC can be seen through the front steering angle and direct yaw moment control as shown in Figure 4.23. It was observed that the rear braking torque on the right wheels were used more than the left wheels to stabilize the vehicle maneuver control.

Furthermore, Figure 4.23 illustrates the response of the driver control signal, PI controller signal, and steering angle generated by the AFS signal for all maneuvers control. The results showed that at middle forward speed, an AFS maneuver is not able to stabilize the vehicle for the yaw rate response under crosswind and road adhesion disturbances.

Therefore, it can be improved by adding another control input to the system such as active rear steering, braking system, or torque distribution at the front and/or rear wheels. With the combination of AFS and DYC, rear braking torque distribution between left and right wheels may enhance the vehicle's stability. However, when the vehicle speed is increased or when the road surface coefficient becomes lower, the SUV that has a high CoG becomes more difficult to control and stabilize. Therefore, a new control technique is needed to maintain the vehicle's stability while following the reference path in the above scenarios.

For the last scenario, we tested the vehicle under a high forward speed of 30m/s at road friction coefficients of wet, concrete (μ = 0.7) and icy surface (μ = 0.1) with consideration of crosswind effect. The same MPC design was used, of which the parameter controls are listed in Table 4.6. We compared the simulation results for 2WS, 4WS, and 2WS with DYC control maneuvers for both controllers (2DoF and 3DoF), and present the comparison in Figures 4.24 to 4.27. The simulation results show that for 2DoF controller at 30m/s, and on wet concrete, all control maneuvers give slightly similar outputs performances. Better response were achieved in lateral positioning, and although the tracking performance of yaw angle and yaw rate deteriorated, the system still allowed the vehicle to track and follow the trajectory, successfully rejecting the effects of wind gust that impact the vehicle.

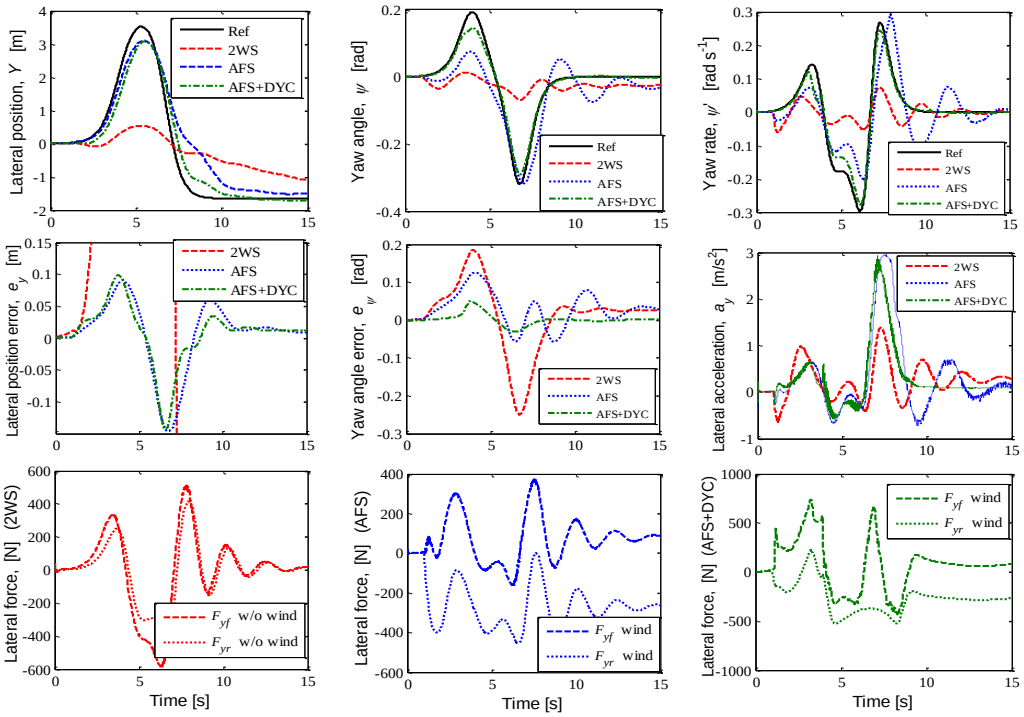

Figure 4.22: Vehicle maneuver via AFS and AFS+DYC at 20m/s with μ = 0.3 under crosswind.

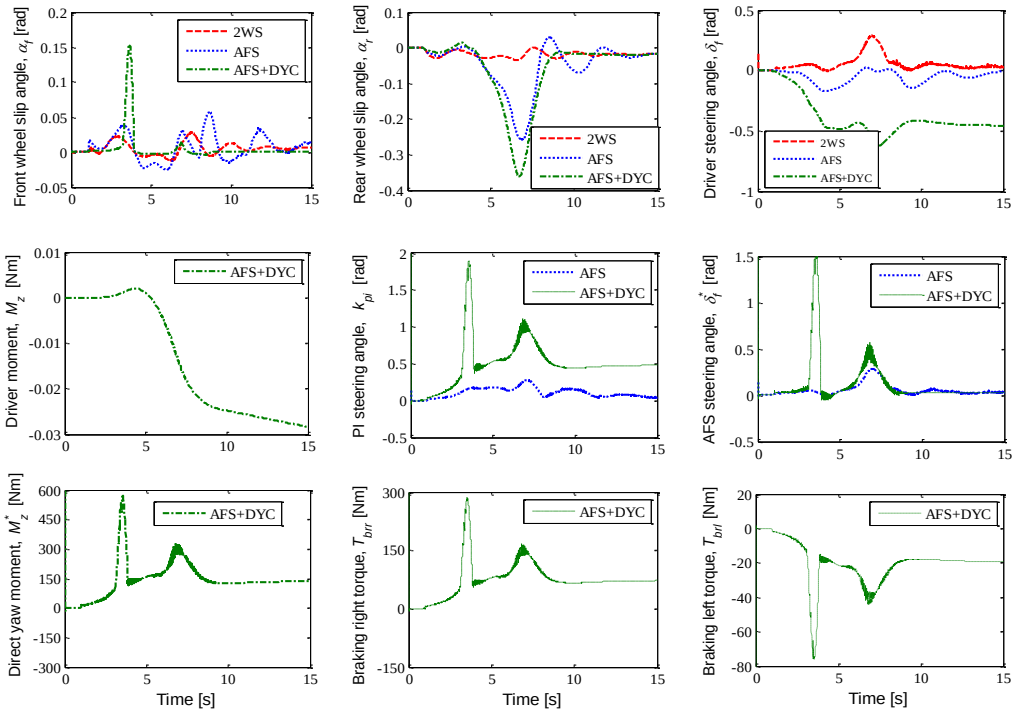

Figure 4.23: Control signal of a vehicle maneuver via AFS and AFS+DYC at 20m/s with μ = 0.3 under crosswind.

As tabulated in Table 4.10, 4WS and 2WS with DYC show slightly better tracking performance compared to 2WS only. However, in the case of the 3DoF controller, it can be clearly seen that 2WS with DYC and 4WS control maneuvers

offered a much higher performing response, especially in yaw angle and yaw rate response, than 2WS. This is shown in Figure 4.25. In this scenario, the rear steering and direct yaw moment control was fully utilized to control and enhance vehicle stability. It is therefore very important to consider roll dynamics in order to enhance vehicle stability and to follow the path trajectory. From Figures 4.24 and 4.25, there are some strong frequency oscillations in front of some responses, i.e. front lateral force, vehicle side slip angle, and lateral acceleration trace, which based on authors' knowledge, come from the numerical calculation, or associated glitches, and initial condition of the system.

Furthermore, when we simulated vehicle maneuver for 30m/s and icy road condition for 2DoF controller, it can be seen that all maneuvers control simulation, the tracking responses become unstable, and impossible to control, especially under the crosswind effect as shown in Figure 4.26. Most probable cause is the roll dynamic motion neglect in the 2DoF controller design, when the vehicle itself was modeled by including roll dynamic factor. It can be said that the inclusion of roll dynamic factor is important for vehicle maneuver, in term of stability and controllability, at high speed and icy road condition. Since high speed coupled with icy road condition will render the equation to become highly nonlinear, it is impossible for a linear tire model to react positively, since the handling properties may be significantly different from those generated by the linear tire model.

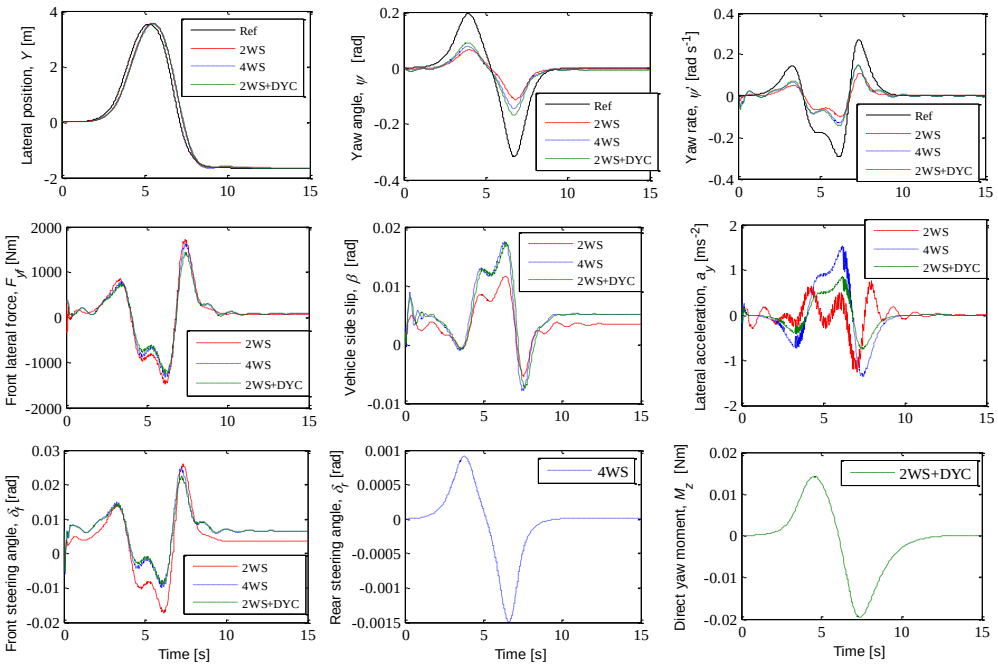

Figure 4.24: 2DoF controller at 30m/s and μ = 0.7 by 2WS, 4WS, and 2WS + DYC.

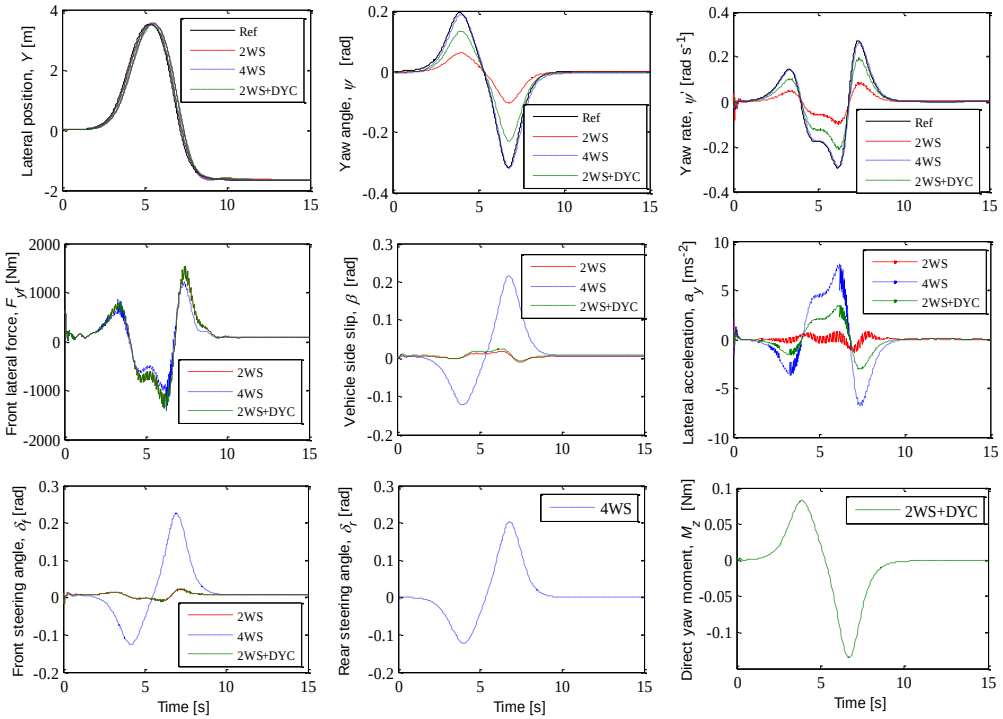

Figure 4.25: 3DoF controller at 30m/s and μ = 0.7 by 2WS, 4WS, and 2WS + DYC.

These results show that linear tire model is only suitable for analyzing a stable vehicle behavior under the assumption of small steering and acceleration.

Next, for the 3DoF controller simulation, the 2WS with DYC maneuvers provide a much better tracking responses in comparison to 4WS, particularly in the case of lateral output. On the contrary, 4WS maneuver demonstrates a much better tracking response in the yaw angle and yaw rate responses, as tabulated in Table 10. With appropriate weight tuning gain, the rear steering angle and direct yaw moment control are fully optimized in order to become stable along the given trajectory. However for the 2WS maneuver, the vehicle responses become unstable, despite several instances where the weighting tuning gains adjusted for output and input gains.

With the inclusion of another input control to the controller design, we can enhance the vehicle responses for both 2WS with DYC and 4WS control maneuvers show. This means that for 2WS controller design, it may have to use more than just front steering to stabilize the vehicle under the effects of wind gusts. Figure 4.27 shows that rear steering angle and direct yaw moment are fully utilized in order to stabilize the vehicle for 2WS with DYC and 4WS maneuvers control.

In contrast to the 2DoF controller as shown in Figure 4.26, in the 3DoF controllers, the 2WS control maneuver can still be used to track a given trajectory, despite not perfectly following the trajectory in a satisfactory manner, especially under crosswind effects. In Figure 4.27, we can see some oscillations in few traces responses, at the end of the responses. Based on the authors' knowledge, these oscillations may come from the vehicle model and some initial conditions of the system with imperfect controllers tuning weighting gains. In these conditions, neither 2WS nor 4WS control maneuvers for lateral response, nor 2WS and 2WS with DYC control maneuvers for yaw angle or yaw rate response performed well, causing an increase in vehicle instability, increased vibration, and tracking responses deterioration. We will next focus on how to enhance the controller in order to stabilize vehicle maneuverability and handling stability.

We can therefore conclude that for 4WS, the rear wheels were helping the car to steer by improving the vehicle handling at high speed, while decreasing the turning radius at low speed. Meanwhile for 2WS with DYC, active front steering was used in low speed maneuvers for lateral acceleration, while inclusion of DYC was adopted for high lateral acceleration when the tires were saturated, and could not produce enough lateral force for vehicle control and stability as intended. In 2WS vehicles, the rear set of wheels do not play an active role in controlling the steering.

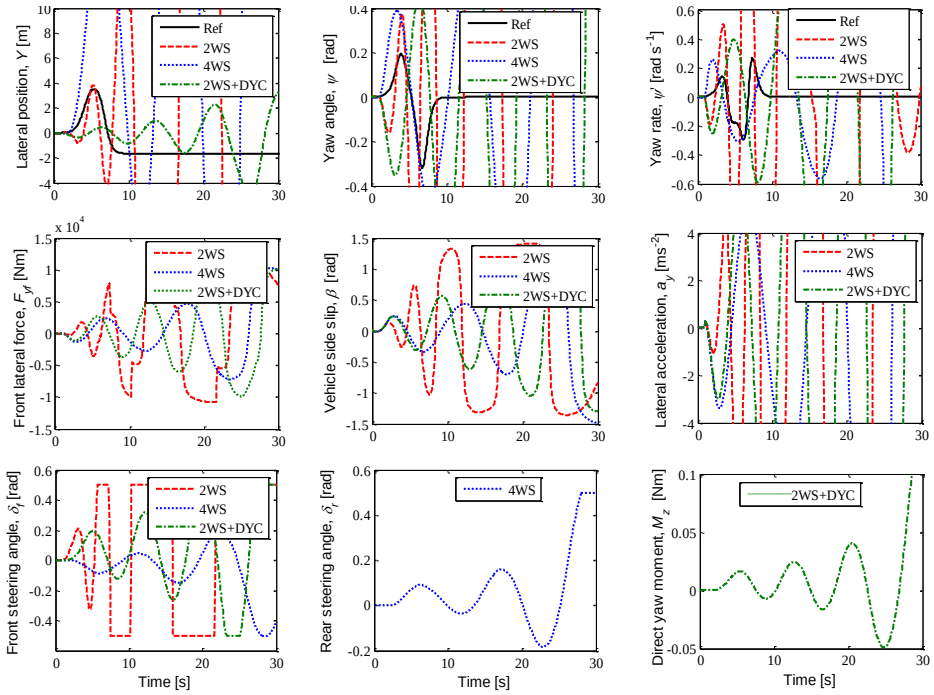

Figure 4.26: 2DoF controller at 30m/s and μ = 0.1 by 2WS, 4WS, and 2WS + DYC.

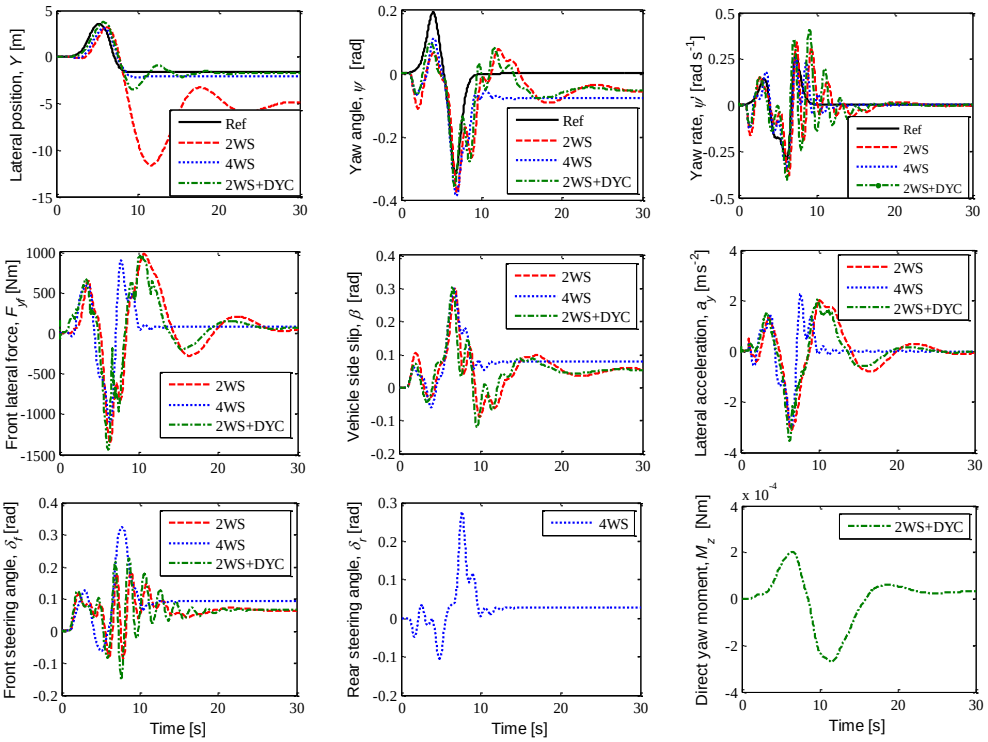

Figure 4.27: 3DoF controller at 30m/s and μ = 0.1 by 2WS, 4WS, and 2WS + DYC.

Table 4.10
Path-following tracking errors with vehicle speed at 30m/s.

Road friction surface	Maneuver control	Controller 2DoF		Controller 3DoF	
		Y [m]	Ψ [rad]	Y [m]	Ψ [rad]
μ = 0.7	2WS	0.0639	0.5348	0.0616	0.5215
	4WS	0.0558	0.5239	0.0528	0.0023
	2WS + DYC	0.0549	0.5226	0.0524	0.0254
μ = 0.1	2WS	Uncontrolled	Uncontrolled	2.1352	0.5264
	4WS	Uncontrolled	Uncontrolled	0.8824	0.2982
	2WS + DYC	Uncontrolled	Uncontrolled	0.9964	0.4580

From Table 4.10 it can be seen that among the three controllers, 4WS gave the best performance by reducing the tracking error for lateral and yaw angle responses when compared with 2WS with DYC, and 2WS only. Table 4.10 tabulated the MPC robustness and the tracking errors in Equation (4.71) for all types of maneuver at 30m/s vehicle speed, and under various road surfaces. Furthermore, all control maneuver signals for both controllers were within the input constraints.

We would like to highlight that in MPC approaches, although there was an advantage in multivariable systems, in this study there was a trade-off between the

weighting tuning parameter, either to focus on lateral position or yaw angle trajectory. In this chapter, we have chosen lateral position as the weighting tuning priority, so we may get a better response on yaw angle and yaw rate response by sacrificing lateral position precision.

Last but not least, we would like to address the issue of improving the tracking responses, by using the appropriate tuning weighting matrices and prediction and control horizons for MPC and LQC. A proper adjustment of the weighting matrices should provide a better response, and so in this chapter, we have tuned the parameters using a trial-and-error procedure and then selected the best tuning weighting matrices based on the best performances.

4.5 Summary

This chapter has presented a comprehensive study of MPC and LQC of an autonomous vehicle in path-following control. The study focused on different control maneuvers (2WS, 4WS, and 2WS with DYC) at low, middle, and high forward speeds on a road surface with a high friction coefficient; dry concrete and a low friction coefficient; wet earth with snow, in a double lane change scenario. The effectiveness of the propose controllers also have been evaluated without and within the disturbance particularly with crosswind effect. The controllers were designed based on a simple 2DoF vehicle model with a linear tire model, and the system was based on yaw-roll motion with a nonlinear tire model. Based on a known trajectory for lateral position and yaw angle, we evaluated the effect of roll dynamics at low speed (10m/s), middle speed (20m/s), and high speed (25m/s), and at high (μ = 1) and low (μ = 0.3) road frictions to follow the trajectory as close as possible while maintaining vehicle stability. Moreover, we evaluated and compared the efficiency of front steer, rear steer, and direct yaw moment as control inputs to the system. We have also proposed MPC with FF controller and MPC with PI controller to minimize the trajectory errors for lateral position and yaw angle and thus enhance vehicle stability. We have shown that, by adding the FF/PI controller, it may enhance vehicle stability and improves lateral position tracking.

The simulation results showed that, by including roll dynamics in the linear vehicle model leads to considerable improvements in the stability and trajectory performance of the vehicle. Furthermore, the results showed that use of the rear

wheels and the direct yaw moment are beneficial in helping to steer the vehicle, improving its handling at high speed, decreasing the turning radius at low speeds, and reducing the tracking errors for lateral position and yaw rate responses. The simulations also proved that MPC is more useful than LQC for multivariable systems and systems with constraints.

Moreover, this study presented an integrated control approach for AFS and DYC maneuver based on MPC and the PI controller in order to track and follow a given trajectory as close as possible, while minimizing the output trajectory errors. The simulation result showed that by adding the PI controller with MPC, it proved that the vehicle stability, handling, and maneuverability can be enhanced and the lateral position tracking can be improved for a four-wheeled SUV. The results also proved that the right and left wheels' brake distribution in DYC are more effective and successfully implemented with the combination of AFS for vehicle steering maneuver even under the crosswind effect and on low road adhesion coefficient to the lateral and yaw motions.

However, we have highlighted that there is a trade-off for the controllers to achieve the target for two tracking outputs with one control signal. Thus, MPC is very useful when implemented for multivariable systems with constraints compared with LQC. Currently, we are seeking to solve the trade-off between the lateral position and yaw rate responses to achieve better responses for both trajectories. Comparison of the performances for real nonlinear models is left for further work.

Chapter 5
Enhancing Yaw Stability and Rollover Prevention Control of Heavy Duty Vehicle

5.1 Introduction

Heavy vehicle stability safety systems are currently available from a number of manufacturers of heavy road transport equipment. Advisory systems to warn the driver of impending rollover were developed over a decade ago and have been superseded by technology development [157-158]. Advisory systems were not considered in this research, nor were systems in the experimental stages such as those that pump up air bags.

Stability safety technology is claimed to be highly effective in potentially dangerous situations like overestimating curve speed limit (e.g. narrowing curves, highway exits); obstacle avoidance maneuvers with sudden steering input (e.g. steering from the shoulder back onto the road and skidding); and laden semi-trailer in narrow curves on slippery surface (jackknifing on turns).

Each crash was a stability related crash to ensure that adequate numbers of crashes of that type were analyzed. Not all stability related crashes can be eliminated or reduced by HVSST. In particular, the following crash types would still occur: rollover crashes when the vehicle enters a curve so fast that it cannot be slowed sufficiently to prevent rollover; human factor accident such as fatigue related crashes or similar where the driver simply does not perceive a curve and drives straight ahead; and crashes where the vehicle is tripped causing a rollover.

In Section 5.2, the heavy vehicle problem is addressed particularly focusing on yaw stability and rollover prevention control. The objective of this chapter is also mentioned. Next, the control allocation by using the model predictive control and the switching technique are described in Section 5.3. In Section 5.4, the description scenario of heavy vehicle system is explained. Finally, simulation comparison with nominal or conventional method is discussed in Section 5.4.

5.2 Heavy Duty Vehicle Problem

In this study, we focus on the application of threat avoidance scenario in emergency maneuver control as shown in Figure 5.1. Such simple threat avoidance without fast safe lane change maneuver and front wheel's reaction as disturbance to the system through MPC have been published and discussed in [159-160]. However, in this chapter, we illustrate a scenario where the driver needs to make a safe lane change trajectory due to threats such as a front vehicle making an emergency brake, an animal suddenly appearing, or a divider or kinematic threat.

The appearance of these sudden threats force the controller to react as fast as possible to make a safe lane change before the vehicle crash by taking into account the constraint of the steering angle and the braking torque. Due to the lane change maneuverer, the rollover might happen in fast speed, fast lane change with consideration of the lateral force that might attack the vehicle. Based on these harsh scenarios, the controller is designed to avoid crash from happening. Due to the high CoG, heavy weight, collisions avoidance maneuver, disturbances with great effect such as gust of wind, irregular road surfaces or split friction, bumpy road, emergency maneuver, excessive speed, and abrupt maneuver; heavy vehicles have a tendency to yaw and rollover instability, thus accidents will happen.

A hard braking on mu-split road surface will cause vehicle to spin and lose the steering control. In a straight route under the inclement environmental conditions, drivers can compensate continuously for small directional deviations from the desired course by controlling the handle. However, when making an emergency or abrupt lane change, especially in the strong wind condition, drivers does not have enough time to make the compensation for adjusting the handle and this will initiate a vehicle to spin, leading to instability, and then rollover.

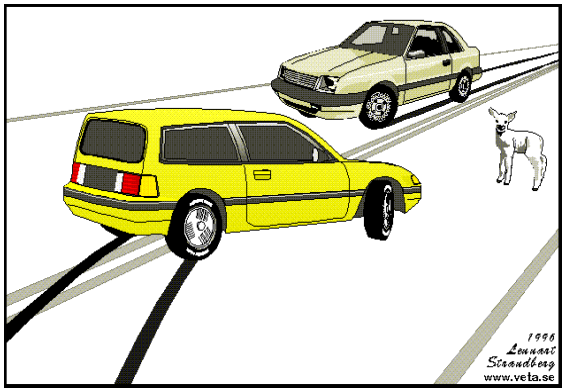

Figure 5.1: Simple example of threat avoidance scenario [144].

Therefore, it is required and urgently to establish a rapid and safety with secure control techniques systems to discover and prevent the yaw motion instability; in doing so vehicle stability will enhanced.

This chapter contributes to increase knowledge about the directional yaw stability control of heavy vehicles under the inclement scenario on emergency thread avoidance maneuver. We limit the heavy vehicles to the standard single truck that related to the authors work [139]. There are few work by several researcher either from academia or industry by using several control methods such as proportional integral derivative [161], neural networks control [162], feedforward and feedback control [163], H-infinity control [164], and linear quadratic regulator [165] for heavy vehicle system with various aims, conditions and scenarios (mostly for rollover prevention).

In this study, we expand and enhance the concept of MPC for applications in heavy vehicle maneuvering where a control optimization problem is solved and fixed at single time step. The first contribution of this study is we enhanced the MPC and then we proposed the SMPC technique for stabilizing the vehicle under the thread avoidance scenario with switching technique to 1) avoid an obstacle in emergency maneuver, 2) follow the safe trajectory closely, 3) prevent the rollover, and 4) improve the heavy truck vehicle stability and maneuverability. We compare the performance ability of the two different controllers in term of lateral displacement/lane change, and yaw rate through i) MPC and ii) SMPC. Moreover, we compared both controllers for two different control maneuvers; i) ARS with DBC and ii) ARS with DYC. We evaluated and compared the effectiveness of proposed method under the disturbances in i) front steering angle, ii) gust of wind, iii) road bank angle, and iv) mu-split scenarios.

5.3 Control Allocation

The block diagram of the controller design of switching MPC is illustrated in Figure 5.2. Figure 5.2 illustrates the control structure for ARS that use rear steering, active braking system that uses the reaction moment at front and rear wheels (DYC), and differential torque distribution of left and right of rear wheels (DBC) as a control input to the system.

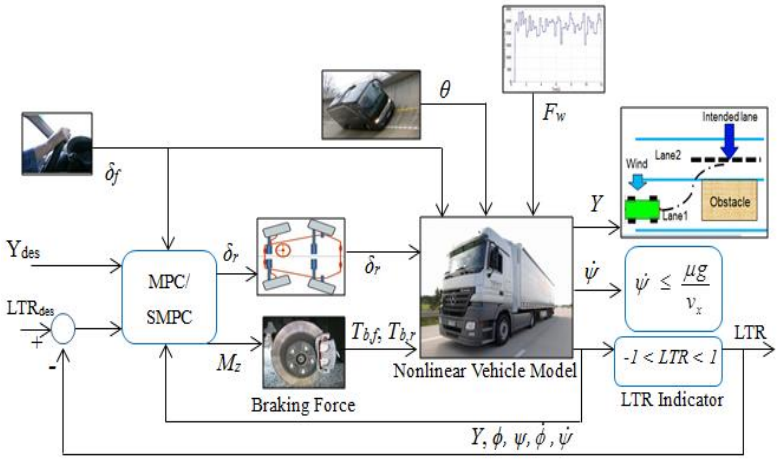

Figure 5.2: MPC via active rear steering with active braking system.

These control inputs are used to control the vehicle in order to avoid the avoidance, prevent the rollover, and able to make a safe lane change maneuver by following a given reference trajectory, while enhancing vehicle yaw stability. It comprises a constant vehicle speed, safety reference trajectory, the controllers (MPC or switching MPC), vehicle model with nonlinear tire model, the crosswind effect, road bank angle, and mu-split as disturbances to the system. MPC will be implemented in the same way of switching MPC in order to compare fairly.

5.3.1 Model Predictive Control

Model predictive control scheme is constructed concerning on 3DoF lateral-roll dynamic through linearized vehicle and tire model as explained and defined in Equations (3.23) and (3.24), where the simple characteristic equations of free rolling ($v_x = w_w r_w$) linear vehicle dynamic which is no accelerating or braking is expressed as follows:

$$\hat{m}\dot{v}_y = \frac{1}{v_x}[-(C_r + C_f)v_y + ((C_r l_r - C_f l_f) - \hat{m}v_x^2)\dot{\psi}] - \frac{1}{I_{xx}}[\hat{m}(hb_\phi)\dot{\phi} - \hat{m}h(mgh - k_\phi)\phi] + C_f\delta_f + C_r\delta_r \quad (5.1)$$

$$\hat{I}_{zz}\ddot{\psi} = \frac{1}{v_x}[(C_r l_r - C_f l_f)\, v_y - (C_f l_f^{\,2} + C_r l_r^{\,2})\dot{\psi}] + C_f l_f\, \delta_f - C_r l_r\, \delta_r + M_z + I_{zz}\rho_r \quad (5.2)$$

$$\hat{I}_{xx}\ddot{\phi} = \frac{h}{v_x}[(C_r l_r - C_f l_f)\,\dot{\psi} - (C_f + C_r)v_y] - \hat{I}_{xx}b_\phi\dot{\phi} + \hat{I}_{xx}(mgh - k_\phi)\phi + C_f h\,\delta_f + C_r h\,\delta_r \quad (5.3)$$

where the normalized vehicles mass and vehicle moment of inertia parameters are indicated by:

$$\hat{m} = m/\mu, \quad \hat{I}_{zz} = I_{zz}/\mu, \quad \hat{I}_{xx} = I_{xx}/\mu \quad (5.4)$$

For the DYC, the reaction moment occurring at the front and rear wheels due to the steer-angle effect (as an external yaw moment) can be approximated as follows:

$$M_f \approx 2l_f C_f M_z, \quad M_r \approx 2l_r C_r M_z \tag{5.5}$$

The vehicle motions in Equations (5.1) to (5.3) could be expressed in a state-space form as follow:

$$\dot{x} = Ax + B_1 u + B_2 w_d + B_3 r_{des}, \qquad y = Cx + Du \tag{5.6}$$

where $x \in \mathbb{R}^x$, $u \in \mathbb{R}^u$, $w_d \in \mathbb{R}^w$, $r_{des} \in \mathbb{R}^r$, and $y \in \mathbb{R}^y$ are the state vectors, control input vectors, disturbance vectors, desired trajectory vectors, and measured output vectors, respectively. We define:

$$\begin{aligned} x &= [v_y \;\; Y \;\; \dot{\psi} \;\; \psi \;\; \phi \;\; \dot{\phi}]^T, \qquad u = [\delta_r \;\; \rho_r \;\; \rho_l]^T, \qquad [\delta_r \;\; M_z]^T \\ w_d &= [\delta_f \;\; \theta \;\; \mu \;\; F_{wy} \;\; M_{wz}]^T, \;\; w_{des} = [Y_{des} \;\; \psi_{des}]^T, \;\; y = [Y \;\; \dot{\psi} \;\; \psi]^T \end{aligned} \tag{5.7}$$

Since MPC is created via a mathematical model of the plant in discrete time in order to predict the future control behavior, we discretize a linear vehicle dynamics in Equation (5.6) by neglecting an unmeasured disturbance to earn:

$$\begin{aligned} x_l(k+1|k) &= A_l\, x_l(k|k) + B_l\, u_l(k|k) + B_2\, w_{dl}(k|k) + B_3\, r_l(k|k) \\ y_l(k|k) &= C_l\, x_l(k|k) + D_l\, u_l(k|k) \end{aligned} \tag{5.8}$$

where $x_l(k|k)$ act the state vector of dynamical variables at time step k, while at time step k+1, $x_l(k+1|k)$ hold the state vector, with $x_l(k|k) \in \mathrm{R}^{xl(k|k)}$ and $u_l(k|k) \in \mathrm{R}^{ul(k|k)}$ indicates the state and control input vectors respectively. Whilst $w_{dl}(k|k) \in \mathrm{R}^{\omega d(k|k)}$ and $y_l(k|k) \in \mathrm{R}^{yl(k|k)}$ are the measured disturbance and measurement output vectors respectively. We define:

$$\begin{aligned} x_l(k) &= [v_y \;\; Y \;\; \dot{\psi} \;\; \psi \;\; \dot{\phi} \;\; \phi]^T, \quad u_l(k) = [\delta_r \;\; M_z \;\; \rho_{br,l} \;\; \rho_{br,r}]^T, \\ w_{dl}(k) &= [\delta_f], \qquad y_l(k) = [Y \;\; \psi]^T \end{aligned} \tag{5.9}$$

Since the controllers is constructed and designed via 3DoF linear vehicle model along linear tire model, it is difficult for the controller to make a safe lane change trajectory of thread avoidance scenario by tracking and following a given trajectory accurately. Because of the aim is to avoid a collision in emergency situation, thus, the controller is created and designed as best as possible through simulation.

The main target of the MPC at sample time k is to lead the predicted output closely or nearly to the set point signal about a predictive time horizon, by assuming the reference signal remains constant throughout the length of the optimization

window. This objective is then translated into a design to find the optimal or best control signal vector $\Delta \hat{u}_l(k+i|k)$ such that results in the best predicted behavior in order to minimizing the tracking error between the reference signal and the predicted plant output.

The control objectives are typically a trade-off between how well the controller tracks the output reference and how much input action it uses. The optimization at each control interval of the predictive controller can be solved by decreasing the quadratic finite objective function expressed as:

$$J_{mpc}(x(k),U_k) = \sum_{i=1}^{H_p} \left\| \hat{y}_l(k+i|k) - r_{ref}(k+i|k) \right\|_{Q_i}^2 + \sum_{i=0}^{H_c-1} \left\| \Delta \hat{u}_l(k+i|k) \right\|_{R_i}^2 \qquad (5.10)$$

where quadratic structure in Equation (5.10) comprising two terms. The first term is the summation of the objective function which is refers to the penalizes the deviations on path tracking error amongst the predicted outputs $\hat{y}_l(k+i|k)$, ($i = 0,\ldots H_p$-1) and the reference trajectory at certain time $r_{ref}(k+i|k)$, ($i = 0,\ldots H_p$-1) that occur within the prediction horizon.

The second term, is the summation of the objective function, it reflects to penalize the magnitude of each control value in the control history, particularly control signal effort of the rear steer angle $\Delta \hat{u}_l(k+i|k)$, ($i = 0,\ldots H_c$-1) of the ARS control maneuver. Here, $r_{ref}(k+i|k)$ exists of the reference value of the safe lane change trajectory or lateral position.

The variation of the control input i.e. rear steer angle $\Delta \hat{u}_l(k+i|k)$ can be attained meanwhile the objective function is created anticipated as small as possible. The constant symmetric weight Q_i and R_i are semi-positive definite state matrix and positive definite control input matrix respectively. These weighting matrices can be automatically or manually tuned or adjusted as accurate as possible from the desired closed-loop performance. We designated R_i is the input tracking weight and the input variation of the control signal is diminished to make the performance of the system fast by shrinking the value of R_i. In addition, Q_i is defined as state tracking weight on account of the error $\hat{y}_l(k+i|k) - r_{ref}(k+i|k)$ could be formed as small as possible by increasing the size of Q_i.

The control and predictive horizon is normally expected to be $H_p \geq H_c$ and the control input signal is assumed constant for all $H_c \leq i \leq H_p$. The control horizon H_c is

used to dictating the number of parameters used to capture the future control trajectory. We formulate the optimization of the predictive control system while satisfying a given constraints of vehicle actuators (physical bounds), i.e. the range of rear tire angle and moment torque accounting as:

$$
\begin{aligned}
&\min_{\Delta U_k} \quad J_{mpc}(x_l(k), \Delta U_l(k)) \\
&subject \quad to: \\
&\quad \hat{x}_l(k+1|k) = A_l x_l(k|k) + B_l u_l(k|k) + B_2 w_{dl}(k|k) + B_3 r_l(k|k) \\
&\quad \hat{x}_l(k+2|k) = A_l \hat{x}_l(k+1|k) + B_l \hat{u}_l(k+1|k) + B_2 \hat{w}_{dl}(k+1|k) + B_3 r_l(k+1|k) \\
&\quad \vdots \\
&\quad \hat{x}_l(k+i|k) = A_l \hat{x}_l(k+i-1|k) + B_l \hat{u}_l(k+i-1|k) + B_2 \hat{w}_{dl}(k+i-1|k) + B_3 r_l(k+i-1|k) \\
&\quad \delta_{r,\min} \le \hat{u}_l(k+i|k) \le \delta_{r,\max}, \ ARS \\
&\quad M_{z,\min} \le \hat{u}_l(k+i|k) \le M_{z,\max}, \ DYC \\
&\quad \rho_{br,\min} \le \hat{u}_l(k+i|k) \le \rho_{br,\max}, \ DBC \\
&\quad \Delta\delta_{r,\min} \le \Delta\hat{u}_l(k+i|k) \le \Delta\delta_{r,\max} \\
&\quad \Delta M_{z,\min} \le \Delta\hat{u}_l(k+i|k) \le \Delta M_{z,\max} \\
&\quad \Delta\rho_{br,\min} \le \Delta\hat{u}_l(k+i|k) \le \Delta\rho_{br,\max} \\
&\quad Y_{\min} \le \hat{y}_{1l}(k+i|k) \le Y_{\max} \\
&\quad \psi_{\min} \le \hat{y}_{2l}(k+i|k) \le \psi_{\max}, \quad i = 1, \cdots H_p
\end{aligned}
\tag{5.11}
$$

Once the optimal control is chosen, an optimal input is then calculated for the next time step through determining and solving a convex quadratic problem at every time step, giving the state feedback control law as follows:

$$u_l(k, y_l(k)) = u_l(k-1) + \Delta u_l(y_l(k)) \tag{5.12}$$

At the next time step, the linear model is computed based on new state and inputs measurement, and the new quadratic programming problem in Equation (5.11) is solved over a shifted horizon. Finally, an optimal input is then calculated for the next time step (instead of the immediate time step) by solving a convex optimization problem at each time step.

It is well known that stability is not ensured by MPC law in Equation (5.11), however, since our problem is the linear problem, thus for nonlinear MPC, usually the problem is augmented with a terminal cost and terminal constraint set to ensure close-loop stability [166], and it goes beyond the scope of this work.

5.3.2 Active Rear Steering and Differential Braking Control

For the braking control technique, the direct yaw moment control of the vehicle torque, which is needed, is selected from the differences between the left and right parts of wheels as designated in Equation (3.5). From the previous study in sub-

chapter 4.3.3, we have design such that the braking torque or traction force will be mobilized or triggered according to the response of yaw rate only; i.e. adopted when the vehicle goes outside the stable region toward instability. This instability scenario happens such as in emergency thread avoidance maneuvers or driving on a low road adhesion due to mainly its direct effects on the longitudinal motion, where, the braking control is the best way to deal with it.

As we expect the front steering wheel act as the measured disruption to the system, thus, the rear steering angle is treated and considered to be in control (braking will turn off) for the entire maneuver (except emergency maneuvers) or in normal driving maneuvers, since the steering control is an efficient method to control lateral dynamics motion by applying additive steering angle. In the other words, only a single control input is used and activated at one time based on the maneuver situation, where in our control design, we have considered two control inputs: rear steering angle, and differential braking at altering between the rear left and right tire.

The designed objective of the control law is to choose the most competent tire axles to generate the brake torque that rely on the wheel steering condition. Understeering occurs when the front tires have a reduction in traction during a cornering situation ($\psi < \psi_{des}$), i.e. positive steering angle (toe-in) on the rear axle will increases the cornering radius, hence, the inner wheels will be selected to apply a pro-cornering yaw moment. On the other hand, an over steering occurs when the slip angle of the rear tires exceeds that of the front tires ($\psi < \psi_{des}$), the vehicle's angular velocity is larger than the desired vehicle's heading, i.e. positive steering angle on a front wheel will decreases the cornering radius, hence, the outer wheels will be selected to apply a contra-cornering yaw moment.

For the braking control law design, we employ only rear wheels at a time to produce the control moment by applying the difference in braking among the two axles e.g. $\Delta T_{b,r} = T_{b,rl} - T_{b,rr}$. This is because the vehicle is not slowing down or so much decelerated compared to when the brake torque is enforced at more than one wheel to create the same quantity of yaw moment. Since front steering angle command act as driver abrupt maneuver disturbance (driver staring at mobile phone), thus, the braking torque is only applied to the rear wheels and the control law is designed as:

$$T_{b,rr} = 0, \quad T_{b,rl} = \frac{-2M_z r_w}{t_w}, \qquad \text{if } \Delta T_{b,r} < 0, \quad \dot{\psi} > 0 \tag{5.13}$$

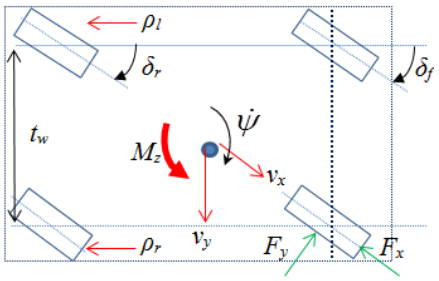

Figure 5.3: Differential braking control.

$$T_{b,rr} = \frac{2M_z r_w}{t_w}, \quad T_{b,rl} = 0, \qquad \text{if } \Delta T_{b,r} > 0, \quad \dot{\psi} < 0 \tag{5.14}$$

The Equations (5.13) and (5.14) are chosen because of the brake torque applied to the rear wheel must be positive. We use only braking force ρ to realize rollover prevention by considering the differential braking force acting either in left or right side of the wheel as:

$$\rho_i = \frac{t_w}{2J_{zz}} \tag{5.15}$$

We define that the braking force exerted on the left side is the forward direction, while an anticlockwise yaw moment is yielded as shown in Figure 5.3. The difficulty and issue now turn into how to tune and determine the controller weighting matrices Q and R in order to avoid poor response by surpass control input saturation (beyond the location and bandwidth limitations of the actuators).

5.3.3 Switching Model Predictive Control

There are some key points regarding the designs of the switching MPC such as all the controllers use the same nominal condition, the values of the plant inputs and outputs at the initial steady-state except for all unmeasured disturbance inputs must have zero nominal values. However, each controller employs a different prediction model where the model structure is the same in each case i.e. input and outputs are identical in number and type, but each model represents a particular steady-state vehicle dynamics model. The controllers also must use the same constraint either in input or output. The switching MPC controller uses the all controllers sequentially as expected (see the switching signal) that designate which one of the controllers is to perform the

calculation (the controller will active at one time based on the switching signal that trigger the controller).

In this chapter, the switch control law presented aims to activate ARS to track the driver's intended lane by make an emergency single lane change for thread avoidance scenario. Control of DYC or DBC is flipped to ARS under lateral position-based switching control, when the trajectory overpasses the intended path. Here, the switching signal of the two controllers is set based on lateral position limit and can be described as:

$$T_{b,rl} = \begin{cases} DYC\ off & (0 < Y \le 10m) \\ DYC\ on & (Y > 10m) \end{cases} \tag{5.16}$$

Under the rear steering control in ARS maneuver, the vehicle does not spin over because of rear steer angle controlled is strictly constrained. Same goes to DYC maneuver control where the brake torques of the rear tires is also limited by the constrained. The input and input rate constraints of rear steer angle and brake torques of DYC are set as following:

$$\begin{aligned} -0.5\ rad\ \le \delta_r \le\ 0.5\ rad\ , \\ -0.4\ rad/s\ \le \Delta\delta_r \le\ 0.4\ rad/s \end{aligned} \tag{5.17}$$

$$\begin{aligned} -1500\ \ Nm \le M_z \le\ 1500\ \ Nm, \\ -1000\ \ Nm/s\ \le \Delta M_z \le\ 1000\ \ Nm/s \end{aligned} \tag{5.18}$$

As mentioned in Section 4.3, if output weight matrix Q_i is enlarged, the vehicle can be controlled to converge to the reference lane trajectory immediately. On the other hand, if input weight matrix R_i is enlarged, the variation of rear wheel steer is restrained and the convergence will be slowed.

In the case of the measured yaw angle exceeds the threshold value as stated in Equations (5.13) and (5.14), the switching signal control will be turned on and the braking force is controlled to revise yaw moment. As the response delay of MPC is taken into consideration, we set the threshold value to 0.4 radian which is smaller than the constraint of yaw angle presented. The constraint of *Y*-axis placement and yaw angle are set as following:

$$-0.4\,rad\ \le \psi \le 0.4 rad\,, \quad 0\ \le Y\ \le\ 10\,m \tag{5.19}$$

5.4 Simulation

The effectiveness of the suggested controllers are assessed and implemented for a heavy vehicle yaw stability control and rollover prevention control on a thread avoidance scenario.

5.4.1 Scenario Description

First, the vehicle is treated and advised to be moving horizontally at constant speed with a v_x = 15m/s by following the safe lane change trajectory in normal driving aside from accelerating or braking. The common and regular emergency obstacle avoidance or single lane change maneuver is simulated with the peak value of the steering input for driver to be at 100deg. As a result, front steer angle under the stationary travelling environments is assumed to be acting in the direction of the route at t = 2sec representing as a measurable disturbance on the vehicle motion.

This disturbances represent the real situation when the driver staring at mobile phone, reading a new e-mails message, texting a friend or others activities instead of looking at the road or the car in front. That is because so many people make phone calls, text, manipulate GPS units, and fiddle with infotainment systems when they should be concentrating on their driving. And even the most diligent drivers can choose the wrong moment to glance at a navigation screen. According to the NHTSA, driver distraction is a factor in almost 20% of crashes in which someone is injured. This interruption of front steer angle is considered to be continuous during the simulation process time as apparent in Figure 5.4.

The starting drag force and torque on the driving axle expressed in the Equation (3.19) with wind velocity v_w = 10m/s in the stationary driving circumstances is affected to happen in the direction of the path at time t = 1sec. The action of forces and torques activating from this lateral position acting wind gust is considered always remains constant and are enforced as a step functions all over the simulation process as displayed in Figure 5.4.

On the other hand, the inclusion of bank angle as a linear disturbance to the system is consider by setting the angle to 10deg as shown in Figure 5.4 at time t = 1.5sec. Here, the bank angle of the terrain is assumed to remain constant. A constant bank angle would be present in driving situations when the vehicle is going around a

highway turn or when the vehicle has left the road and is driving on the shoulder or median.

Moreover, mu-split scenario is setting happen at time t = 2sec, where exactly at same time with the front steer disturbance. We set the road adhesion coefficient at right wheel into wet, asphalt (μ_r = 0.7), and at left wheel into dry, asphalt (μ_r = 0.9). Here, the mu-split scenario is assumed to remain constant throughout the simulation process as shown in Figure 5.4. All simulations were tested and running by using the Model Predictive Control Toolbox and other basics tool given in MATLAB and Simulink software. We will employ numerical data extracted from a single unit truck for model parameters and their definitions based on [139] as listed in Table 3.3.

In this study, the predictive controllers was carried out through reducing the vehicle deflection from the preferred path to attain the main goal which is to avoid emergency avoidance by following the given trajectory indicates as safe lane change trajectory as close as possible. Both controllers have been designed based on linear 3DoF vehicle motion to the nonlinear vehicle system at; middle (15m/s) and high forward speed (25m/s).

In this desired vehicle speeds, we evaluated and compared the achievement of the controller design for thread avoidance of lateral displacement, vehicle heading stability control, and rollover prevention control to both without the controller, and with propose method. We also compared the proposed controller in different maneuverers control i.e. ARS, ARS with DYC, and ARS with DBC. Here, we define a safe single lane change maneuver at 10deg step input represent 10m which is start from t = 0.5sec or Y_{ref} = 10m. We define also the vehicle heading angle ψ_{ref} = 0, and the vehicle's yaw rate must satisfy the stability criteria of the Equation (3.6) given approximated ≈ 0.654rad/sec (for v_x = 15m/s) and 0.392rad/sec (for v_x = 25m/s).

Table 5.1 and Table 5.2 list the MPC and SMPC control parameters with weighting matrices. Both controllers were designed and implemented in ARS, ARS with DYC, and ARS with DBC control maneuver scenarios. Again, the weighting matrices for input and outputs of the controllers are chosen through trial and error method from the best vehicle output performances, where, first we need to tune the gain of MPC under ARS, and then tune MPC under braking maneuver later until we satisfy the result performances.

Table 5.1
Model predictive control parameters.

Parameter	**Value**
H_p, H_c	11, 7
T_s, T	0.05, 15
δ_r, $\Delta\delta_r$	± 0.5, ± 0.35
ρ_r, ρ_l, M_z	± 2000
$\Delta\rho_r$, $\Delta\rho_l$, ΔM_z	± 1500

Table 5.2
Controller weighting matrices parameters.

Control maneuvers		**MPC**	**SMPC**
ARS + DYC	v_x = 15m/s	R_1, ΔR_1 = 0.1, 0.03	R_1, ΔR_1 = 0.1, 0.03
		R_2, ΔR_2 = 0.1, 0.03	R_2, ΔR_2 = 0.1, 0.03
		Q_{11} = 0.0052	Q_{11} = 0.0031, Q_{22} = 0.0456
		Q_{22} = 0.01505	Q_{33} = 0.1151, Q_{44} = 0.0155
	v_x = 25m/s	R_1, ΔR_1 = 0.1, 0.03	R_1, ΔR_1 = 0.1, 0.03
		R_2, ΔR_2 = 0.1, 0.03	R_2, ΔR_2 = 0.1, 0.03
		Q_{11} = 0.0043	Q_{11} = 0.0043, Q_{22} = 0.0456
		Q_{22} = 0.0456	Q_{33} = 6.4115, Q_{44} = 3.9595
ARS + DBC	v_x = 15m/s	R_1, ΔR_1 = 0.1, 0.03	R_1, ΔR_1 = 0.1, 0.03
		R_2, ΔR_2 = 0.1, 0.03	R_2, ΔR_2 = 0.1, 0.03
			R_3, ΔR_3 = 0.1, 0.03
		Q_{11} = 0.0022	Q_{11} = 0.0033, Q_{22} = 0.0015
		Q_{22} = 0.0015	Q_{33} = 0.0952, Q_{44} = 0.0015
	v_x = 25m/s	R_1, ΔR_1 = 0.1, 0.03	R_1, ΔR_1 = 0.1, 0.03
		R_2, ΔR_2 = 0.1, 0.03	R_2, ΔR_2 = 0.1, 0.03
			R_3, ΔR_3 = 0.1, 0.03
		Q_{11} = 0.4522	Q_{11} = 2.0852, Q_{22} = 5.9523
		Q_{22} = 0.1225	Q_{33} = 0.7869, Q_{44} = 0.3499

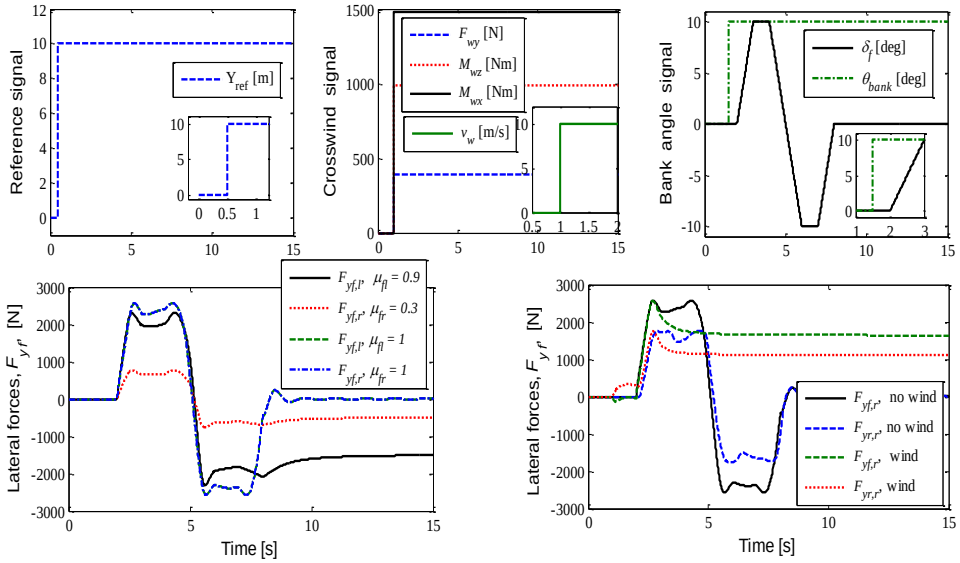

Figure 5.4: Reference and disturbances signal.

5.4.2 Results and Discussions

Prior to proposed simulations, we carried out standard vehicle maneuvers tests to validate our model in the open-loop simulation scenario. In this chapter, we performed only the double lane change and roll rate feedback fishhook test, for the purpose of testing improvement to existing vehicle and for vehicle validation purposes in the open-loop simulation, as displayed in Figures 3.10 and 3.11.

The first simulation revolves with a constant forward speed of 15m/s on a single lane change scenario through a nominal MPC method. The MPC weighting tuning parameters for all condition are listed in Table 5.2. In the first simulation process, we employed MPC only and compared the results of the controller for the lateral displacement, vehicle heading angle, and lateral acceleration output responses to an ARS, ARS with DYC, and ARS with DBC maneuvers, as demonstrated in Figure 5.5.

From the Figure 5.5, it can be seen clearly that for ARS with DYC or ARS with DBC maneuver, trajectory tracking responses of thread avoidance for lateral displacement was much better than for ARS maneuver control. It shows that under ARS maneuver control, the lateral position is oscillating few time before it achieve the desired path. However, the overshoot is too high under ARS with DYC maneuver for lateral position response which is around 80% compared to ARS with DBC which is 10%. These highest percentage overshoot indicates that the lane change made for thread avoidance is not safe trajectory where it might goes to third lane before

returning to the desired path. Thus, under ARS with DYC, the collision might happen with others vehicle in other lane although it can avoid the emergency thread in the initial lane. Moreover, since the lane change is decided at t = 0.5sec, both control maneuvers need at least 2sec to 3sec to make a safe change lane before the vehicle hit the thread. Moreover, for the yaw rate responses, both control maneuvers are able to maintain the vehicle stability at steady-state condition compared to ARS only. In ARS control maneuver, vehicle responses become unstable and spin after 12sec.

On the other hand, for ARS with braking control, at t = 1.5sec and t = 2.15sec, the vehicle stability is surpassing the limit at 0.8rad/sec of an ARS with DYC maneuver; this indicates at starting of bank angle with wind effect influence the performance. While, for an ARS with DBC maneuver, the vehicle stability is under the limit and much safe performance. Thus, with coordination of ARS and DBC; rear braking torque distribution between right and left axles be capable of enlarge and increased the vehicle stability. The crosswind, mu-split, and bank angle effects can be examined around the lateral forces at front and rear wheels, and roll angle responses, where the steady-state of front lateral forces without crosswind was particularly at zero.

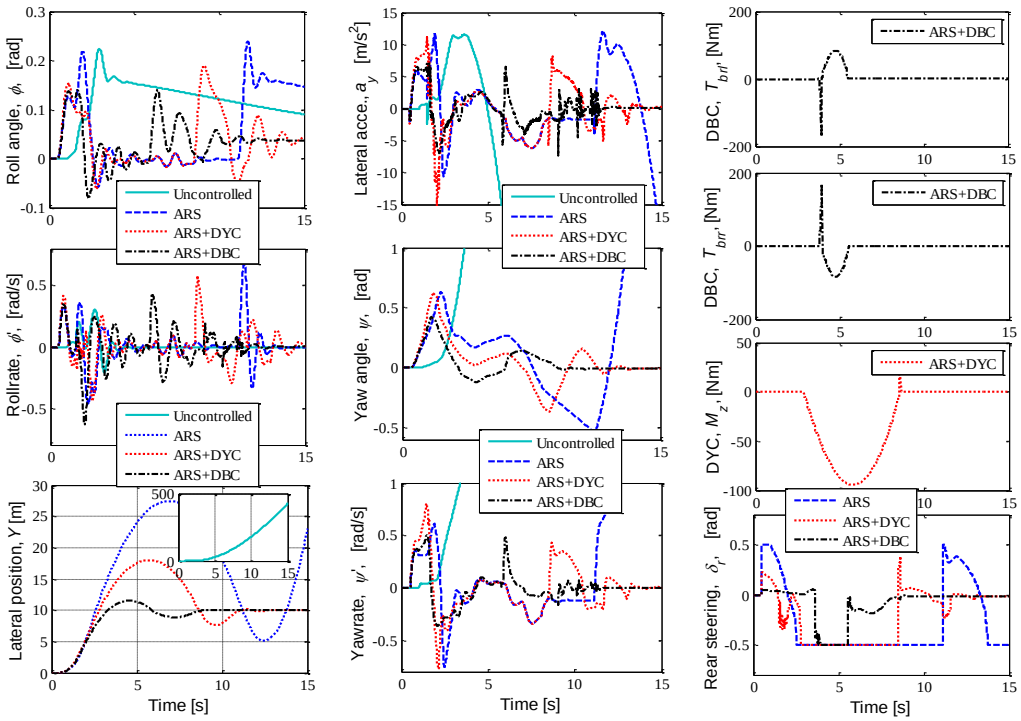

Figure 5.5: Vehicle maneuver via ARS, ARS+DYC, and ARS+DBC at 15m/s with disturbances.

In this scenario, the rear steering angle was constrained for both maneuvers; at this time, the braking control take control while the rear steering was constrained. In these simulation, it is illustrated that with single control input, it was impossible to control, the vehicle thus to achieve the aim in multivariable system.

Next, we would like to investigate the effectiveness of proposed SMPC method compare to MPC. Since previous discussion described that DBC is much effective and influence the vehicle stability than DYC, thus, here, we would only discuss on ARS with DBC maneuver for SMPC and MPC control. Based on same scenario, we simulated the heavy vehicle with the same speed at 15m/s for both controllers as shown in Figure 5.6. Figure 5.6 indicates that both controllers behaved and acted very well for lateral position and yaw angle even under disturbances effect.

However, if we scrutinize in lateral position response, we might find that the SMPC controller can decrease the overshoot to 3% from 10%; which indicates more accurate and safe lane change compared to MPC. However, both controllers need at least 3sec to 3.5sec to make a safe change lane from its initial condition at 0.5sec before the vehicle hit the thread.

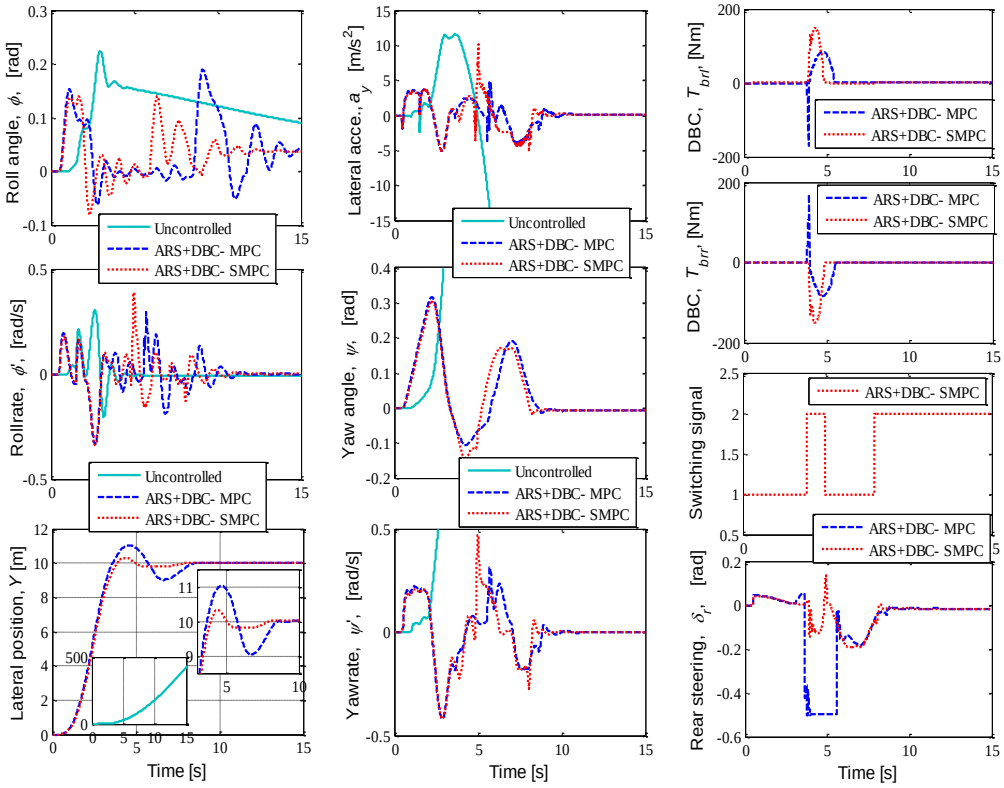

Figure 5.6: Vehicle maneuver via ARS+DBC at 15m/s with disturbances.

On the other hand, for the yaw rate responses, both controllers are able to maintain the vehicle stability below the stability limit and manage to achieve steady-state condition. However, for yaw rate response, MPC controller is performed lower than SMPC especially at 5sec.

Moreover, the rear steering angle was constrained for MPC controller, where at this time, the braking control take over to control the vehicle. Whereas for SMPC, the rear steering was within the constraint over the simulation process, here, we may see the switching method between ARS and DBC through switching signal. From the switching signal, it shows that DBC maneuver will take over control the vehicle when the lateral position responses surpass the constraint of 10m at 3.8sec. DBC maneuver maintain control until the vehicle lateral response back to it trajectory at 5sec, then DBC is off and ARS take over the command back again. After a few second manage to maintain the lateral position less than 10m, at 8sec, the vehicle try to overpass again the lateral constraint, then ARS is switch to DBC to maintain the vehicle stability along the safe path.

Furthermore, we would like to investigate the effectiveness of proposed SMPC method for both control maneuvers. Here, we tested the vehicle at 15m/s for ARS with DYC and ARS with DBC maneuvers as shown in Figure 5.7.

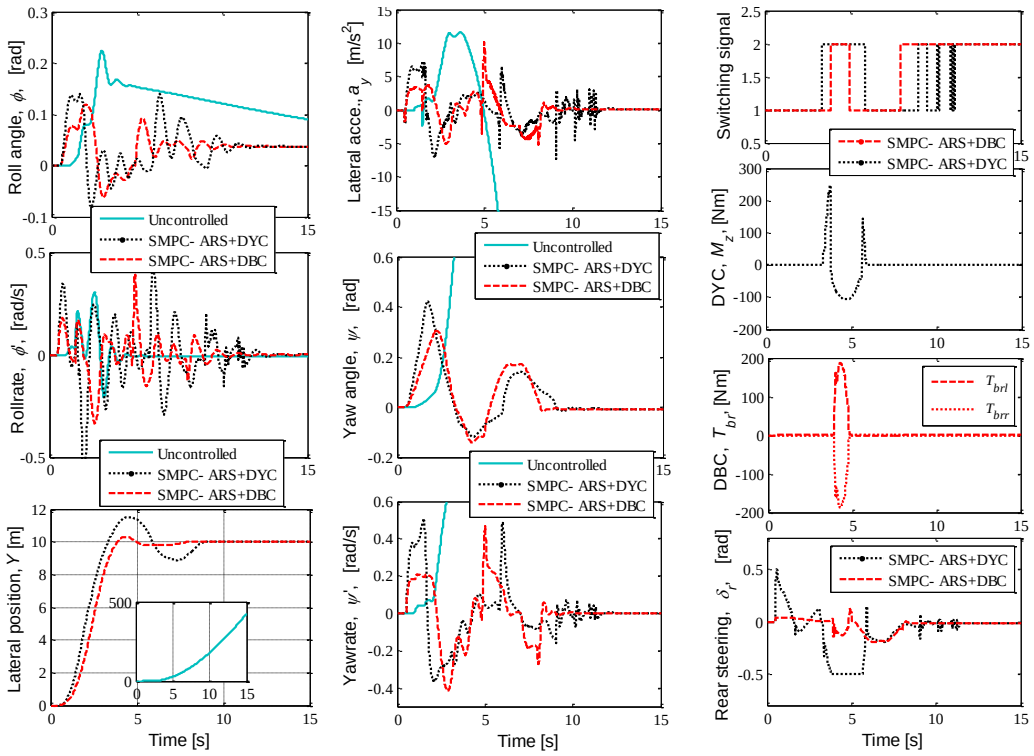

Figure 5.7: Vehicle maneuver via ARS+DYC and ARS+DBC at 15m/s with disturbances through SMPC.

Figure 5.7 illustrates that switching method for both maneuvers control performed very well than MPC as shown in Figures 5.5 and 5.6. From Figure 5.7, it reduced to 15% overshoot through SMPC compared to MPC of ARS with DYC maneuver for lateral position. Through SMPC of ARS with DYC, it took around 2.7sec to make a lane change for thread avoidance; faster than MPC. However, lateral position response, ARS with DBC is much better than ARS with DYC, but slightly same on yaw rate response of SMPC method. From the Figure 5.7, it shows that the rear steering command of SMPC of ARS with DYC was constrained for MPC controller, and the braking control take over to control the vehicle. The switch techniques from the ARS to DYC/DBC or vice versa are based on output constraint on lateral position, and it clearly can be seen from the switching signal.

Next, we tested the vehicle behavior at a high forward speed of 25m/s, in a same scenario to investigate the effectiveness of proposed SMPC method compare to MPC for ARS with DYC maneuver control as shown in Figure 5.8. Figure 5.8 indicates that both controllers behaved and acted well for lateral position and yaw angle even under disturbances effect. However, if we scrutinize in lateral position response, we might find that the SMPC controller can decrease the undershoot instead of overshoot to 1% from 5%; which indicates more accurate and safe lane change compared to MPC. However, both controllers have a high undershoot response between 5sec to 8sec that will influence the vehicle to make the crash avoidance. Both controllers have a steady-state condition around 8.5sec at 10m. On the other hand, for the yaw rate responses, both controllers are not able to maintain the vehicle stability below the stability limit (0.39rad/sec) and manage to achieve steady-state condition. However, for yaw rate response, SMPC controller is performed better than MPC especially at 0.5sec. Therefore, emphasize need to be focus on yaw rate response that indicate the vehicle stability in order not to surpass the vehicle stability limit.

Moreover, the rear steering angles were within the constraint over the simulation process for MPC and SMPC controller. However, for SMPC controller, we may see the switching method between ARS and DYC through switching signal where particularly at 2sec, the direct yaw moment control take over from the rear steering to control the vehicle when the lateral position responses surpass the constraint of 10m. Braking control maneuver in SMPC is used to maintain control the vehicle until the vehicle lateral response back to it trajectory at 10m around 3sec, then

DYC is off and ARS take over the command back again. After the vehicle achieved the steady-state condition at 8.5sec, then the control variable back to DYC again in order to maintain the vehicle stability along the safe path.

Finally, we would like to investigate the effectiveness of proposed SMPC method for both control maneuvers. Here, we tested the vehicle at same forward speed of 25m/s for ARS with DYC and ARS with DBC maneuvers as shown in Figure 5.9. Figure 5.9 illustrates that switching method for ARS with DBC maneuvers control performed very well compared than ARS with DYC for lateral position. From Figure 5.9, it reduced from 2% overshoot of ARS with DYC to 0% of ARS with DBC control maneuver for lateral position. There is no undershoot response (never close to avoidance crash) under the ARS with DBC and the lateral position achieve his steady-state condition very earlier around 3sec compared to ARS with DYC at 8sec. However, under ARS with DYC control maneuver, the lateral. This response showed that ARS with DBC control maneuver provide better and safe lane change trajectory in order to avoid emergency thread avoidance response is 1sec early than ARS with DBC to achieve a given trajectory at 10m.

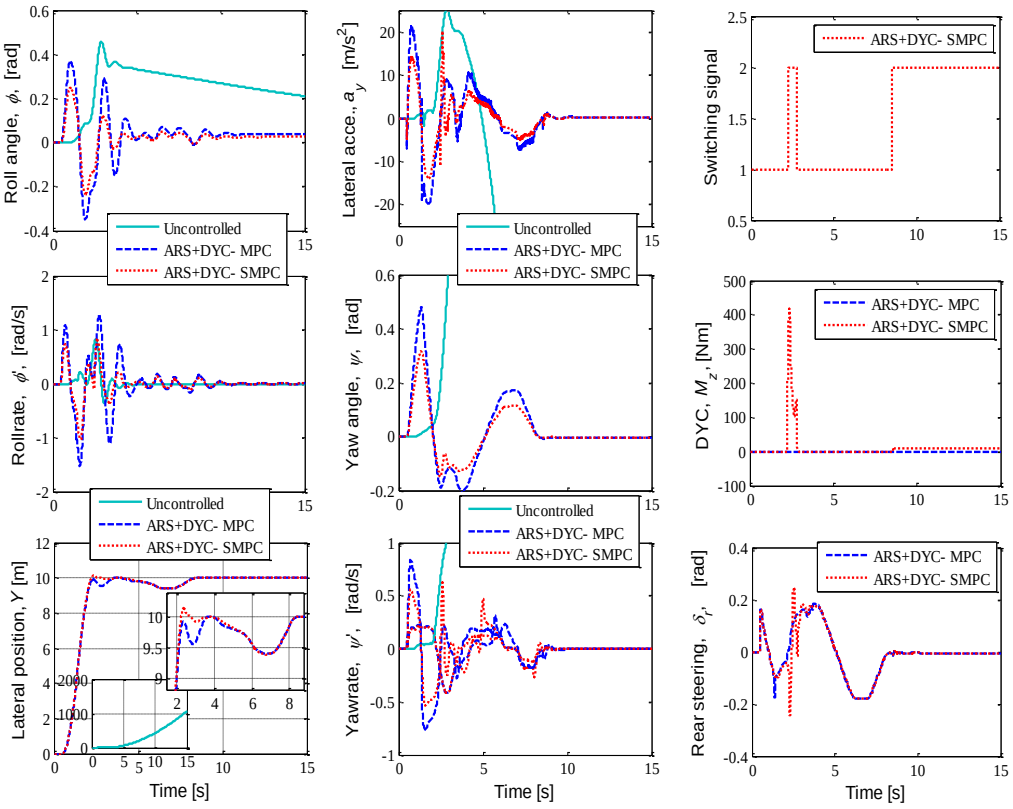

Figure 5.8: Vehicle maneuver via ARS+DYC at 25m/s with disturbances.

On the other hand, for the yaw rate responses that indicate the vehicle stability, both control maneuver are not able to maintain the vehicle stability below the stability limit (0.39rad/sec), where both control maneuver exceed the limit at 0.5rad/sec – 0.7rad/sec. The yaw rate responses show that at particular point (when the vehicle arrive at 10m), the vehicle become exceed the limit before the vehicle manage to get controlled. In overall, both control maneuvers perform almost same yaw rate response.

Moreover, from the Figure 5.9, it shows that the rear steering command of SMPC of ARS with DBC was constrained at beginning process where the vehicle start to make a lane change from 0 to 10m at 0.5sec. Whereas for ARS with DYC, the rear steering was within the constraint over the simulation process. Here, we may see the switching method between ARS and DBC through switching signal response at 5sec. This switched signal showed that the ARS is fully used to control the vehicle to avoid the emergency avoidance by make a lane change, while DBC is fully activated when the vehicle already become stable indicate through the steady-state condition. This happen because in ARS with DBC control maneuver, the lateral vehicle response never exceed the output constraint at 10m, thus DBC not really used in the beginning vehicle motion.

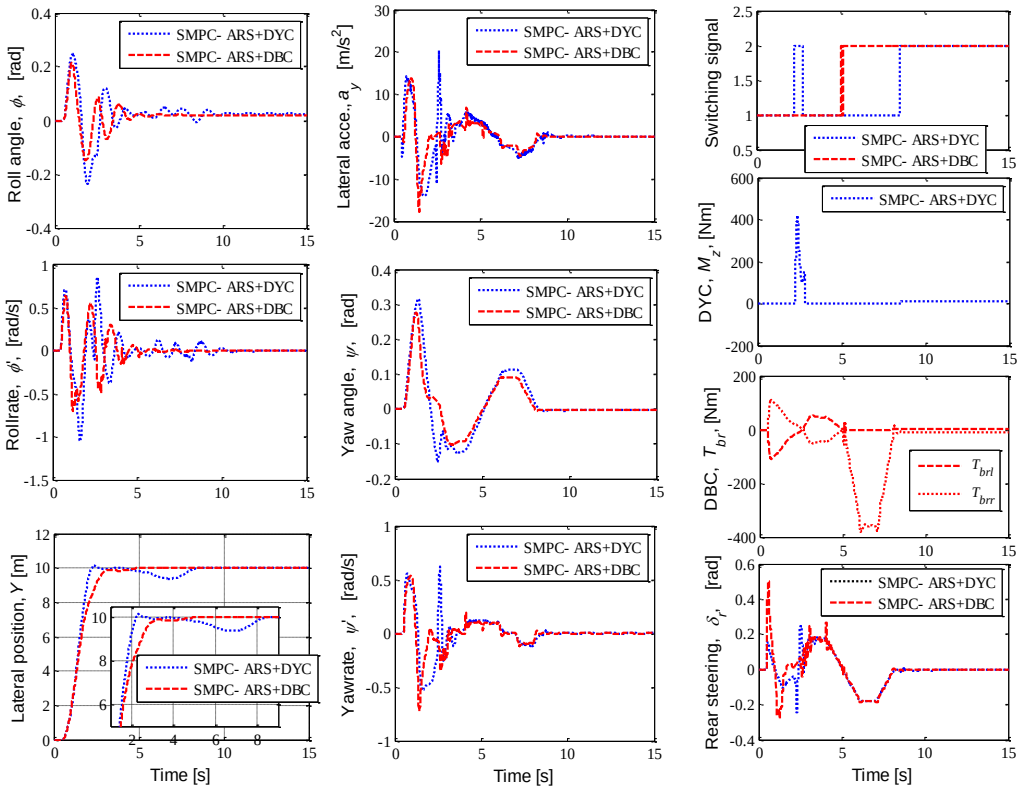

Figure 5.9: Vehicle maneuver via ARS+DYC and ARS+DBC at 25m/s with disturbances through SMPC.

It contrast to ARS with DYC where the DYC maneuver will take over control the vehicle when the lateral position responses surpass the constraint of 10m at 2sec. DYC maneuver maintain control the vehicle until the vehicle lateral response back to it trajectory at 3.5sec, then DYC is off and ARS take over the command back again. After a few second manage to maintain the lateral position less than 10m, at 8sec, the vehicle try to overpass again the lateral constraint, then ARS is switch to DYC to maintain the vehicle stability along the safe path. This can be seen through the switching signal response.

Finally, we would like to highlight in this chapter that particular research are focusing on threat avoidance for lateral position and yaw stability response. For the vehicle speed of 25m/s, we might noticed that the roll angle and roll rate motions are higher compared when the vehicle at 15m/s vehicle speed. This motion is really important if we are consider the rollover problem, since the rollover might happen due to high response in roll and roll rate motion including the lateral acceleration responses. We might say that from both motions, the high magnitude happen at beginning vehicle response when the vehicle starts to make a safe lane change trajectory at 0.5sec. Thus rollover might happen at this point, so particular solution has to make to manage the switching technique between the lateral, yaw, and roll motions. Therefore, this problem and the solution will be considered in our next research.

Furthermore, we also would like to mention that the vehicle stability and thread avoidance performances would be better with the appropriate and accurate tuning parameters of prediction horizon, control horizon, and weighting matrices for MPC and SMPC. The fines adjusting and fixing of the controller parameters would provide more excellent response, thus in this study, we tune the controller parameters by trial and error method. After a several time tuning start with prediction and control horizon parameters, continue with weighting matrices on output and input, then we adjusted and selected the best tuning parameters which corresponding and depend on the best output responses.

5.5 Summary

This study demonstrated switching model predictive control approach for active rear steering, differential braking control, and direct yaw moment control maneuvers of the heavy vehicle in thread avoidance. Disturbances of gust of wind, mu-split, and bank

angle under abrupt scenario at middle and high forward speed were considered. ARS is utilized the rear steering command, while DYC and DBC are utilized for driving and braking force distribution of rear wheels. Model predictive control is used to make a safe lane change trajectory by tracking and following an emergency given trajectory as accurate as possible. On the other hand, the switching method is employed to enhance the yaw vehicle stability and minimize the output trajectory errors through coordination between the steering and braking system.

The simulation result showed and elaborated that the vehicle stability, driver handling, and maneuverability can be improved through switching MPC instead of nominal MPC. Emergency braking of the front vehicle or obstacle appeared suddenly without warning can be avoid and refrain from collision happen through proposed method by minimizing the lateral position tracking error for a heavy vehicle. The results also demonstrated that the brake pressure distribution between the difference braking torque at the right and the left rear axles that provide the DBC are more sufficient and adequately applied with combination of ARS rather than mixture of ARS with DYC. Simulation outcome also proved that the proposed control scheme are successfully implemented for vehicle steering maneuvers even under mu-split and gust of wind effect to the lateral and yaw motions.

Chapter 6
Conclusions and Recommendation

6.1 Conclusion

The main objective of this study is to enhance and improve the existing MPC controller and its design process so that the improved MPC controller can be used effectively for vehicle dynamics control systems particularly focuses on autonomous ground vehicle and heavy duty vehicle. The first chapter describes the overall system that covers in the thesis. It consists of background, problem statement, research objectives, research methodology, scope of research, and the thesis outline.

Chapter 2 discusses the literature survey generally on research and development of vehicle dynamic control systems and with the focus on path-following control, yaw stability control, and roll stability control of autonomous ground vehicle and heavy duty vehicle. The basic concept of MPC control theory is also described and its design is explained. The design covers the MPC rule, cost function and the optimization problem. Related literature reviews regarding implementation of MPC to the vehicle dynamics control are studied.

Chapter 3 explains the modeling of complete nonlinear vehicle model, nonlinear tire model, disturbances model i.e. crosswind, bank angle, and mu-split for simulation purpose. Modification of the vertical forces particularly related to roll motion and lateral acceleration are taken into account. The rollover indicator called LTR is explained with an enhancement of the indicator by considering the lateral acceleration and un-sprung vehicle mass. The development of the vehicle model is validate through standard maneuvers test. Based on the vehicle responses in yaw rate, roll rate and lateral acceleration, it's proved and shown that the vehicle model is validated and corrected, thus, can be implemented for controller design.

In Chapter 4, an autonomous ground vehicle of path-following control under consideration of disturbances through MPC and LQR has been explained. Term of FF/PI controller has been proposed with combination of MPC to minimizing the trajectory tracking error, enhance vehicle stability and maneuverability. Deep discussion of MPC structure, PI/FF control design, control allocation between the AFS and ABS maneuver are also presented in this chapter. The simulation results

showed that, by including roll dynamics in the linear vehicle model leads to considerable improvements in the stability and trajectory performance of the vehicle.

It is also highlighted that the MPC structure capable of keeping the actuators within the limited boundaries during a lane change is the important component of the control system. Furthermore, the results showed that by adding the PI/FF controller with MPC, it is proven that the vehicle stability, handling, and maneuverability can be enhanced and the lateral position tracking can be improved. The simulations also proved that MPC is more useful than LQC for multivariable systems and systems with constraints. The results also proved that the right and left wheels' brake distribution in DYC are more effective and successfully implemented with the combination of AFS for vehicle steering maneuver.

On the other hand, the improvement of yaw stability and rollover prevention control of heavy duty vehicle under consideration of disturbances through SMPC has been studied and explained in Chapter 5. Switching technique of the MPC controller and the trade-off between the path tracking, yaw stability, and rollover are discussed. The controller design process using the linear vehicle into the nonlinear heavy system is presented. Switching technique of MPC has been proposed in order to minimize the trade-off between the emergency lane change maneuver, vehicle stability, and rollover due to threat avoidance scenario. The simulation result showed that the vehicle stability, driver handling, and maneuverability can be improved through switching MPC instead of nominal MPC.

Emergency braking of the front vehicle or due to obstacle appeared suddenly without warning can be avoided and refrained from collision happening through proposed method by minimizing the lateral position tracking error for a heavy vehicle. The results also demonstrated that the brake pressure distribution between the different braking torque at the right and the left rear axles that provide the DBC are more sufficient and adequately applied with combination of ARS rather than mixture of ARS with DYC. The braking control method through direct yaw moment and differential braking control by using the torque distribution of the left and right wheel instead of using the front and rear wheel also have been proposed and validated through simulated process.

6.2 Future Work and Recommendation

There are still open spaces for the further improvement of the vehicle stability control either through MPC controller or others controller. Since the main maneuver control are based on steering and braking control, thus, further improvement to current research are the issues with under and over steer towards an extremely cornering and counter steering to prevent a spin. Developing haptic feedback to inform the driver of the augmented steering command can be explored and it may likely improve the interpretation by the driver, leading to better acceptance of the system by drivers.

Next, the vehicle used in most of the experimental or real application has no independent braking, and only throttle and engine torque were available for control stabilization, whereas, in commercial ESC, many production vehicles have independent braking for each wheel. Through individual adjustment of the brakes, a corrective yaw torque is generated on the vehicle. This torque is the primary yaw stabilizer for all commercial ESC. It is recommended that for future experiments, four-wheeled braking is installed on the vehicle.

Moreover, based on independent in-wheel motor and integration of active steering for robust yaw motion control can be further studied in order to track and follow the desired vehicle trajectory without road preview information or advanced knowledge. Acceleration performances during cornering for driver's comfort ability take into account frequent torque control of driving motors may be future research interest.

For the vehicle stability control, most researchers are focused on yaw and roll stability control of the vehicle system. Even though the vehicle model showed good correlation with the test data, the roll rates and roll angles were under predicted. This could be due to un-modeled phenomena like tire deformation during severe maneuvers, bushing stiffness not being accounted for, and many other reasons. If those factors are incorporated in the vehicle model, the correlation would be better; consequently the results will be even more representative of the actual vehicle.

Furthermore, if vehicle test data for a fully loaded expedition in condition which might induce rollover is available, the rollover threshold might be determined more accurately. To make this model more effective, additional variables could be included in the control function. For example, in the yaw stability mode, vehicle slip angle could be included in addition to the vehicle slip rate while in the roll stability

mode a rollover index which is a function of roll rate and roll angle could be formulated. Understandably, there will always be a trade-off between the complexity and robustness of the ESC model on one hand, and the time and resources required to build and tune it, on the other.

Another interesting topic which influences the researcher and the manufacturing sector are the suspension control system. The interest of the previous method is that it can be extended to a more complex suspension models, including more specific nonlinearities according to the employed technology for further study. Moreover, the future trend of automotive suspensions systems such as electromagnetic suspensions need to be considered due to it simple structure, flexible, accurate, high bandwidth operation, energy regeneration, and good handling and riding performance.

Another important aspect to be considered is the additional uncertainty on the estimate of the state for suspension control design caused by the delayed measurements. Furthermore, significance of uncertainties in sensor measurement, influence of time-delay in the control loop architecture, effect of actuator band-limit, and enhancement of the MPC control strategy are among the areas that have to be explored and investigated.

Lastly, the improvement of the control method with different combinations such as active rear steering, active suspension, and active braking with front and rear wheels can be considered and left for further work. Moreover, the proposed method is suggested to be implemented as a real application soon.

6.3 Disturbance Observer Rejection Control

Bad environmental conditions are considered an important factor in fatal rollovers. A strong lateral wind or significant road bank may harass the behavior of heavy vehicles, and can even initiate rollover accidents, since the roll stability is easily affected by these disturbances. Thus, the development of a control system for disturbance detection and rollover prevention is extremely important while the vehicle is moving on an uneven surface or through strong lateral winds.

The DOB is known to be an effective compensation mechanism that reduces the influence of disturbances, uncertainties and nonlinearities within the plant, and that enforces the nominal input/output behavior on the actual plant, especially in the low frequency range in which the frequency of the reference signal is concentrated.

Accordingly, the DOB has the ability to asymptotically reject high-order and stepwise disturbances. During the last few years, the force of wind and moment acting on a vehicle body has been regarded as an unmeasured disturbance that can be estimated and suppressed without changing the input-output behavior by a DOB [128]. The road bank angle can also be precisely estimated using a DOB from the GPS and inertial navigation system [132], or from low-cost onboard sensors [167]. Moreover, Yu et al. presented road bank estimation using a dynamic simplex method that was applied for rollover prediction [168].

Since the MPC does not handle disturbances directly by the controller design, it cannot achieve satisfactory effects in controlling vehicle stability in the presence of strong disturbances and large uncertainties. Therefore, DOB with DRC acts as an observer and a compensator, and thus improves vehicle performance. The DOB-MPC based approaches for improving tracking performance in the control system have been proposed in [169-170]. However, its application in rollover prevention is rarely demonstrated, and its comparison is rarely mentioned.

In this sub chapter, a DOB and MPC based on DRC are proposed for rollover prevention control, particularly for heavy duty vehicle systems. Different from a conventional DOB that is only suitable for the minimum-phase system with (or without) time delay, the enhanced DOB with DRC can deal with a disturbance observer for the non-minimum-phase delay systems in a single lane change scenario. Several simulations are performed to demonstrate the effectiveness of the proposed method. We evaluate the effectiveness of the proposed method by means of a comparison with the standard LQC and DOB with DRC. This comparison is the main novelty of this chapter. To the best of the author's knowledge, previous work has not provided such a comparison for rollover prevention control of heavy vehicles.

The study focuses on the comparative investigation of the MPC and LQC with DRC for an autonomous control without the driver's intention in which AFS is demonstrated for rollover prevention. Here, the MPC and LQC are designed with DOB in order to estimate and suppress the influence of unmeasured disturbances, uncertainties, and nonlinearities. In the DRC design, the estimated wind and road bank are used as cancellation signals to provide steering assistance to the driver.

In this study, the comparison of the MPC and LQC controller for rollover prevention and roll damping is our main focus; keeping occupants safe is considered

top priority in the worst-case environmental conditions. The autonomous steering control of a heavy vehicle that is travelling in a straight line is simulated in two different environmental conditions: step wind of typhoon, and the combination of the sinusoidal wind of a typhoon with a random road bank angle.

The vehicle model is described for the controller design as shown in Figures 3.1(d) and 3.4(d). Considering the influence of the wind and road bank angle, we used vehicle motion as in Equations (3.1) to (3.5) with an improved the vehicle model motions related to roll motion as:

$$\begin{aligned}\sum M_x : (I_{xx} + m_s h^2)\ddot{\phi} + m_s h(\ddot{y} + \dot{x}\dot{\psi}) - I_{xz}\ddot{\psi} &= m_s gh(\phi + \theta) \\ - (k_{\phi f} + k_{\phi r})\phi - (b_{\phi f} + b_{\phi r})\dot{\phi} + M_{wx} + \dot{P}_b &\end{aligned} \tag{6.1}$$

where $\dot{P}_b$ represents the changing rate of the roll rate disturbance of the road bank, which can be obtained through the vehicle frame fixed coordinates based on euler angles [132]. If the pitch angle and pitch rate are regarded to be small, $\dot{P}_b$ can be simplified as:

$$\dot{P}_b \approx \ddot{\theta} \tag{6.2}$$

When the road vehicle is running through strong wind, aerodynamic forces and moments are produced in all directions about the axles, as shown in Figure 3.4(a). However, the drag forces and pitch moment due to wind are neglected in this study. Thus, the wind force, yaw moment, and roll moment exerted by the wind are described in Equation (3.19) by the following formula. We use the results of C_F from a typical wind tunnel test performed by [128]. This wind force and yaw moment coefficient are resolved with respect to the mass center of gravity of the vehicle.

The wind attack angle is given as the following function:

$$\beta_w = \arctan\left(\frac{v_w}{v_x}\right) \tag{6.3}$$

This is regarded as a constant value due to negligence of the small variation of the running state of the vehicle.

In this sub-section, we design the controllers based on linearizing vehicle and tire models explained in Chapter 3, with the assumption of constant forward speed. The controllers are designed based on 3DoF lateral-roll motions without disturbances parameters as we assume that the disturbances are unmeasured disturbances:

$$m\dot{v}_y = \frac{1}{I_{xx}v_x}[-(C_r + C_f)J_{xq}\,v_y + ((C_r l_r - C_f l_f)J_{xq} - I_{xx}mv_x^2)\dot{\psi}] - \frac{1}{I_{xx}}[m(hb_\phi)\dot{\phi} - mh(mgh - k_\phi)\phi - C_f J_{xq}\delta_f] \quad (6.4)$$

$$I_{zz}\ddot{\psi} = \frac{1}{v_x}[(C_r l_r - C_f l_f)\,v_y - (C_f l_f{}^2 + C_r l_r{}^2)\dot{\psi}] + C_f l_f\,\delta_f \quad (6.5)$$

$$I_{xx}\ddot{\phi} = \frac{h}{v_x}[(C_r l_r - C_f l_f)\,\dot{\psi} - (C_f + C_r)v_y] - b_\phi\,\dot{\phi} + (mgh - k_\phi)\phi + C_f h\,\delta_f \quad (6.6)$$

The vehicle model in Equations (6.4) to (6.6) with disturbances can be transferred to a state-space function as follows:

$$\dot{x} = Ax + B_1 u + B_d\,w_d\,, \qquad y = Cx + Du \quad (6.7)$$

$A \in \mathbb{R}^{6x6}$ is the known state matrix, $B_1 \in \mathbb{R}^{6x1}$ is the input matrix, $C \in \mathbb{R}^{1x6}$ is the output matrix, and $B_d \in \mathbb{R}^{6x3}$ is the disturbance input matrix. We define:

$$x = [v_y\ Y\ \dot{\psi}\ \psi\ \dot{\phi}\ \phi\ ]^T,\ u = [\delta_f\ ],\ w_d = [F_{wy}\ \theta\ \dot{P}_b\ ]^T,\ y = [LTR] \quad (6.8)$$

We seek to estimate the wind pressure on the vehicle and road bank by using the method of the state-space disturbance observer. The disturbance input w_d, consisting of linear waveform description, can be interpreted as:

$$\dot{x}_w = A_w x_w\ , \qquad w_d = C_w x_w \quad (6.9)$$

where $x_w \in \mathbb{R}^{xw}$ is the disturbance states vector, and $w_d \in \mathbb{R}^{wd}$ is the disturbance vector. Next, w_d can be considered one of the state variables which can be estimated by the following equation, which is combined with Equations (6.7) and (6.9):

$$\begin{bmatrix}\dot{x}\\ \dot{x}_w\end{bmatrix} = \begin{bmatrix}A & B_d\\ 0 & A_w\end{bmatrix}\begin{bmatrix}x\\ x_w\end{bmatrix} + \begin{bmatrix}B_1\\ 0\end{bmatrix}u\,, \qquad Y = \begin{bmatrix}C & 0\end{bmatrix}\begin{bmatrix}x\\ x_w\end{bmatrix} \quad (6.10)$$

Using the model developed in Equation (6.10), we obtain the estimated state $\hat{x}$ and estimated disturbance input $\hat{w}_d$. An augmenting equation is given by:

$$\begin{bmatrix}\dot{\hat{x}}\\ \dot{\hat{x}}_w\end{bmatrix} = \begin{bmatrix}A & B_d\\ 0 & A_w\end{bmatrix}\begin{bmatrix}\hat{x}\\ \hat{x}_w\end{bmatrix} + \begin{bmatrix}B_1\\ 0\end{bmatrix}u + M(\dot{\hat{Y}} - \hat{Y})\,, \qquad \hat{Y} = \begin{bmatrix}C & 0\end{bmatrix}\begin{bmatrix}\hat{x}\\ \hat{x}_w\end{bmatrix} \quad (6.11)$$

We can express the error $e = \hat{x} - x$ with respect to the parameters of the system from the differential of Equations (6.10) and (6.11), which yields:

$$\dot{e}(t) = (A + MC)\,e(t) \quad (6.12)$$

This type of observer is called an asymptotic state observer. The observer gain M is designed by the pole assignment. We can ensure that the error converge is

towards zero, while setting all eigenvalues of $A + MC$ with a negative real part with respect to M.

As the LTR cannot be estimated directly in real time, an indirect estimate method which depends on the roll motion is proposed. The roll rate can be estimated directly using a GPS attitude system in combination with an automotive grade gyroscope oriented to measure the roll rate. As a consequence, the roll angle is calculated from the measured roll rate. The yaw rate can be easily measured by a gyroscope or a virtual sensor, or can be synthesized from accelerometers. GPS measurements contain high levels of noise compared to traditional inertial sensors, so white noise is added to the measured state. The noise also greatly impacts the estimated disturbance input as the main reason of the disturbance estimation error.

The block diagram of the MPC is illustrated in Figure 6.1. Since the MPC is designed in discrete-time, we discretize the vehicle dynamics in Equation (6.7) without unmeasured disturbances to obtain:

$$x(k+1) = Ax(k)+B_1 u(k), \qquad y(k) = Cx(k)+Du(k) \tag{6.13}$$

where $x(k)$ is the state vector at time step k, and $x(k+1)$ is the state vector at time step $k+1$. $u(k)$ is defined as the optimal input calculated by the MPC optimizer; the front steer angle $\delta_f(k)$ with the compensation for disturbance rejection can be described as:

$$\delta_f(k) = u(k) - O_w(s)\hat{F}_w - O_b(s)\hat{\theta} - O_p(s)\hat{\dot{P}}_b \tag{6.14}$$

The aim of the MPC optimizer is to find the optimal control input vector $\Delta\bar{u}(k+i)$, so that the error between the predicted output $\bar{y}(k+i)$ and the reference signal $r(k+i)$ can be minimized.

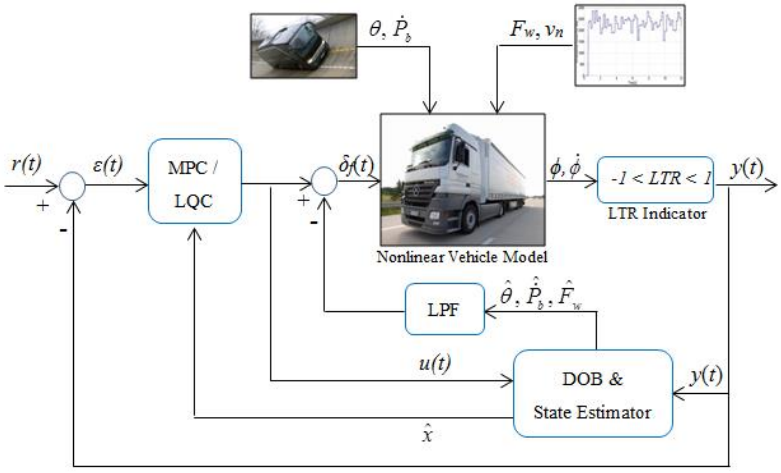

Figure 6.1: Block diagram of MPC and LQC with DOB for truck vehicle.

The optimization of the predictive control system is solved by minimizing the cost function:

$$Minimize: J_{mpc}(k)=\sum_{i=1}^{H_p}\left\|\bar{y}(k+i)-r(k+i)\right\|^2_{S_q(i)}+\sum_{i=0}^{H_c-1}\left\|\Delta\bar{u}(k+i)\right\|^2_{S_r(i)} \tag{6.15}$$

The weight matrices $S_q(i)$ and $S_r(i)$ are diagonal matrices which can be adjusted for the desired closed-loop performance. The variation of the front steer angle $\Delta\bar{u}(k+i)$ can be obtained when the cost function is made to be as small as possible. The prediction and control horizon are described as H_p and H_c, and it is usually assumed $H_p \geq H_c$. We formulate the optimization of the predictive control system which takes the constraints of steering actuators into consideration, such as the operating range of the front tires. At every time step, the controller solves an optimization problem that can be written as:

$$\begin{aligned}
&\min: J_{mpc}(x(k),\Delta u(k))\\
&subject\ \ to:\\
&\quad \bar{x}(k+1)=Ax(k)+B_1u(k)\\
&\quad \bar{x}(k+2)=A\bar{x}(k+1)+B_1\bar{u}(k+1)\\
&\quad\quad\vdots\\
&\quad \bar{x}(k+i)=A\bar{x}(k+i-1)+B_1\bar{u}(k+i-1)\\
&\quad \left|\bar{u}(k+i)\right|\leq\delta_f\\
&\quad \left|\Delta\bar{u}(k+i)\right|\leq\Delta\delta_f\\
&\quad \left|\bar{y}(k+i)\right|\leq LTR\quad (i=1,\cdots H_p)
\end{aligned} \tag{6.16}$$

In the concept of the MPC, only the first input sample of the complete optimal sequence is applied to the process. New samples are taken to determine the new current state of the system, and the entire procedure is repeated.

With the aim of limiting the compensation to a preselected low frequency range, a LPF called Q-filter [171] is essentially utilized in the feedback signals of DOB. Filter $M_i(s)$ is designed for LQC, while filter $O_i(s)$ is added in MPC. The transfer functions of the two filters are expressed as follows:

$$M_i(s)=\frac{F_i}{\eta_i s+1},\qquad O_i(s)=\frac{G_i}{\xi_i s+1} \tag{6.17}$$

where, η_i and ξ_i are the filter time constants F_i and G_i are the filter pass-band gain, while the subscript i is nominated to be w, b and p to constitute three cancellation signals. The cut-off frequency of the filter is the reciprocal of its filter time constant. The cut-off frequency designed for wind is 50Hz, while for the road bank is 100Hz, considering the unstructured external disturbances and observation

noise. The tuning of F_i and G_i for each filter is conducted through the process of trial and error.

The LPF plays a significant role in determining the robustness and disturbance suppression performance of the system. It is considered that, for a disturbance signal in which maximum frequency is lower than the cut-off frequency of the LPF, the disturbance signal is effectively rejected, and the real plant behaves as a nominal plant.

Note that white noise v_n is added to the observed roll rate and roll angle. The mean and power spectral density of white noise is set to $[0.1, 3.5 \times 10^{-5}]$.

In the first scenario, we aim to mitigate roll motion while running the heavy vehicle without a driver's operation with strong winds and road bank disturbance. We assume that the vehicle is moving in a straight path on the wide open ground with a speed of v_x = 55km/h. The autonomous steering control is simulated in two different environmental conditions: (i) step wind of a typhoon, and (ii) combination of sinusoidal wind of a typhoon with a random road bank angle.

It is important to highlight that the weighting matrices for the input and outputs of the MPC and LQC are selected based on the process of trial and error from the best output responses through repetitive implementation, concentrating on the output weighting gain rather than on the input weighting gain. Furthermore, the reference value is set to zero, which means the LTR and roll angle are in turn mitigated to zero.

Vehicle behavior is strongly influenced by the wind in real life. We refer to the typhoon level as defined by the Japan Meteorological Agency. Here, the step wind speed that is considered a strong typhoon is set to v_w = 220km/h, while the attack angle is given as β_w = 75.96deg.

In order to obtain better convergence to the estimated wind force, we set the eigenvalues of $A + MC$ far from real part. For the LQC design, the cut-off frequency and filter pass-band gain are set at 50Hz and 1.5Hz respectively.

Figure 6.2 shows the simulation result of the estimated wind force using the proposed disturbance observer. The estimation fluctuates by the effect of white noise. The estimated wind force is verified with its real value from the estimation error. The wind estimation is within the accuracy of the wind measurement and rollover prevention system, suggesting that dynamic separation works well.

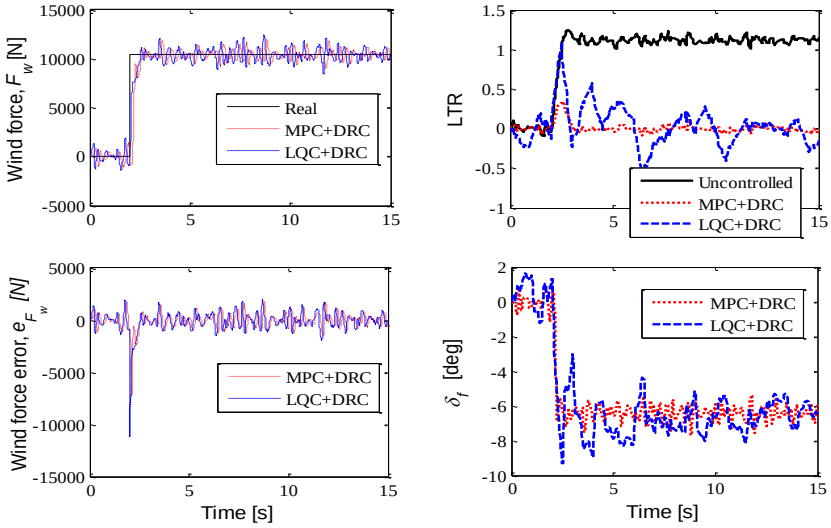

Figure 6.2: Autonomous control under the step wind.

In Figure 6.2, the LTR response without control exceeds by 1 in the average of 1.25. This means the left side of the tires loses touch with the ground under the influence of strong winds acting on the left side of the vehicle body. Therefore, we consider that the vehicle is at risk of fatal rollover accidents. Although steady-state error in both controllers to the reference signal are kept at zero, the settling time with the MPC controller is faster than in the case controlled by the LQC. It is also clear that the overshoot with the MPC controller mitigates more compared to the case controlled by LQC. Furthermore, the undershoot in LQC is revised by DRC based on DOB.

It is considered to be the worst condition when the vehicle is moving on a bumpy road through strong winds. The roll motion is unexpected under the influence of random disturbances combined with random road banks and sinusoidal winds.

The real bank angle is simulated as “Gaussian noise”, of which the variance, mean, and frequency are designed as 2, 2, and 2 respectively. Here, the bank angle is assumed to be estimated accurately using the DOB. Our aim is to assess the behavior of the vehicle and suppress the vibration around the roll motion in the sine-wave disturbance response. The average speed of the wind sine-wave is considered a small typhoon set at v_w = 165km/h, and its frequency set at 0.25Hz. The attack angle is calculated as β_w = 71.56deg. The wind disturbance is set as the sine-wave strong wind described in Figure 6.3.

The results of the road bank angle estimation can be found in Figure 6.3, and $\dot{P}_b$ can be computed by the estimation result of the road bank angle. Similar to the result of wind force estimation, the road bank angle is also successfully estimated.

In Figure 6.3, the LTR of the uncontrolled case increases significantly under the impact of both sinusoidal wind and road bank, compared to the results of previous simulations, which only took into consideration step wind, as seen in Figure 6.2. The abrupt increase and variation of the LTR is generated when the positive value of two disturbances are combined together. A positive value of both disturbances combined around their peach value can even enable LTR to exceed the limit.

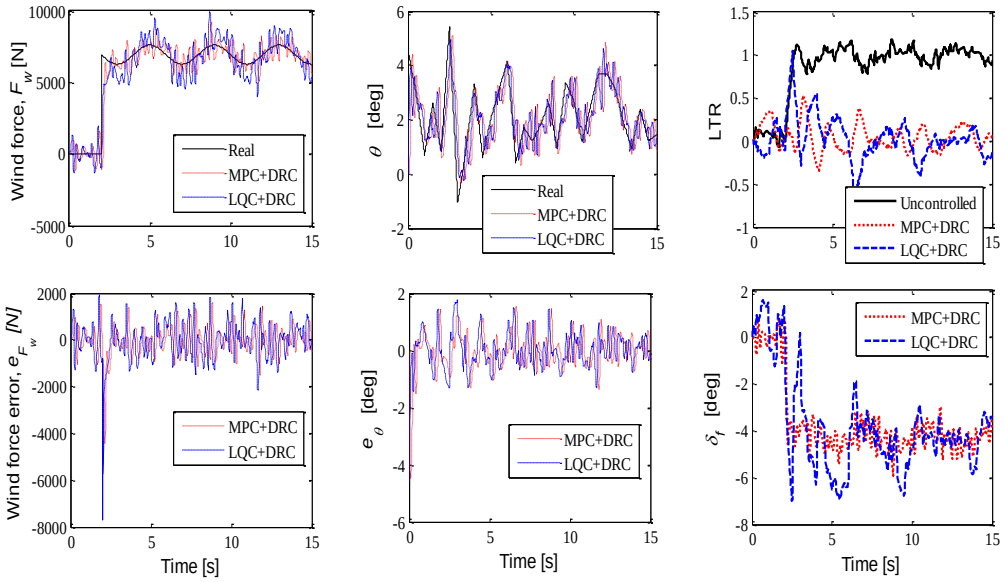

Figure 6.3: Autonomous control on the bumpy road under the sinusoidal wind.

Bibliography

1. E. Ackerman, Why you shouldn't worry about self-driving car accidents. May 12, (2015), IEEE Spectrum, Cars that think, http://spectrum.ieee.org/cars-that-think/transportation/self-driving/why-you-shouldnt-worry-about-googles-selfdriving-car-accidents/?utm_source=carsthatthink&utm_medium=email&utm_campaign=051315
2. 2013 traffic safety facts FARS/GES annual report, NHTSA, No. 812139, (2015).
3. R. V. Dukkipati, J. Pang, M. S. Qatu, G. Sheng, and Z. Shuguang. *Road Vehicle Dynamics*. SAE International, USA, (2008).
4. International Road *Traffic* and *Accident Database*. Japan Traffic Accidents Databases (J-TAD), (2013). : http://www.itarda.or.jp/
5. National Highway Traffic Safety Administration. (2013). http://www.nhtsa.gov/
6. B. A. Guvenc, L. Guvenc, and S. Karaman. Robust yaw stability controller design and hardware-in-the-loop testing for a road vehicle. *IEEE Trans. Veh. Tech.*, Vol. 58, No. 2, pp. 555-571, (2009).
7. M. Krid and F. Benamar. Design and control of an active anti-roll system for a fast rover. *Intelligent Robots and Systems 2011 IEEE/RSJ Int. Conf.*, pp. 274-279, (2011).
8. J. Ackermann and D. Odenthal. Damping of vehicle roll dynamics by gain scheduled active steering. *European Control Conf.*, Germany, pp. 1-6, (1999).
9. Y. Yoon, J. Shin, H. Kim, Y. Park, and S. Sastry. Model predictive active steering and obstacle avoidance for autonomous ground vehicles. *Control Eng. Practice*, Vol. 17, No. 7, pp. 741–750, (2009).
10. J. Ackermann and W. Sienel. Robust yaw damping of cars with front and rear wheel steering. *IEEE Trans. on Control Systems Tech.*, Vol. 1, No. 1, pp. 15–20, (1993).
11. T. Hiraoka, O. Nishihara, and H. Kumamoto. Automatic path-tracking controller of a four-wheel steering vehicle. *Vehicle System Dynamics*, Vol. 47, No. 10, pp. 1205-1227, (2009).
12. J. Song. Integrated control of brake pressure and rear-wheel steering to improve lateral stability with fuzzy logic. *Int. J. Automotive Tech.*, Vol. 13, No. 4, pp. 563-570, (2012).
13. H. Lv and S. Liu. Closed-loop handling stability of 4WS vehicle with yaw rate control. *J. of Mechanical Eng.*, Vol. 59, pp. 595-603, (2013).
14. B. Chen and H. Peng. Differential-braking-based rollover prevention for sport utility vehicles with human-in-the-loop evaluations. *Vehicle System Dynamics*, Vol. 36, No. 4–5, pp. 359–389, (2001).
15. O. Barbarisi, G. Palmieri, S. Scala, and L. Glielmo. LTV-MPC for yaw rate control and side slip control with dynamically constrained differential braking. *European J. of Control*, Vol. 15, No. 3-4, pp. 468-479, (2009).
16. H. Yonezawa, H. Hirata, and H. Sasai. Positioning table with high accuracy and speed. *Annal CIRP*. Vol. 39, pp. 433-436, (1990).
17. F. Yakub, A. A. Wijaya, and M. Al-Ani. Practical control for two-mass positioning systems in presence of saturation. *Telkomnika*, Vol. 10, No. 1, pp. 91-102, (2012).

18. E. F. Camacho and C. Bordons. *Model Predictive Control*. 2nd edn. Springer Verlag, London, (2007).
19. J. M. Maciejowski. *Predictive Control with Constraints*. Prentice Hall, England, (2002).
20. C. E. Garcia, D. M. Prett, and M. Morari. Model predictive control: theory and practice. *Automatica*, Vol. 3, No. 25, pp. 335–348, (1989).
21. A. Lie, C. Tingvall, M. Krafft, and A. Kullgren. The effectiveness of ESC in reducing real life crashes and injuries. *Traffic Injury Prevention*, Vol.7, No. 1, pp. 38-43, (2006).
22. J. Lu, D. Messih, A. Salib, and D. Harmison. An enhancement to an electronic stability control system to include a rollover control function. *SAE Trans.*, Vol. 116, pp. 303–313, (2007).
23. S. A. Ferguson. The effectiveness of electronic stability control in reducing real-world crashes: a literature review. *Traffic Injury Prevention*, Vol. 8, pp. 329–338, (2007).
24. A. Hoye. The effects of electronic stability control (ESC) on crashes—an update. *Accident Analysis Prevention*, Vol. 43, No. 3, pp. 1148-1159, (2011).
25. E. Ono, Y. Hattori, Y. Muragishi, and K. Koibuchi. Vehicle dynamic integrated control for four-wheel-distributed steering and four-wheel-distributed traction/ braking systems. *Vehicle System Dynamics*, Vol. 44, pp. 139–151, (2006).
26. J. Wang and R. G. Longoria. Coordinated vehicle dynamics control with control distribution. *Proc. American Control Conf.*, Minneapolis, pp. 5348–5353, (2006).
27. H. E. Seng, B. Ashrafi, D. Madau, T. A. Brown, and D. Recker. The development of vehicle stability control at Ford. *IEEE/ASME Trans. on Mechatronics*, Vol. 4, No. 3, pp. 223-234, (1999).
28. P. Raksincharoensak, M. Nagai, and M. Shino. Lane keeping control strategy with direct yaw moment control input by considering dynamics of electric vehicle. *Vehicle System Dynamics*, Vol. 44, Supplement, pp. 192-201, (2006).
29. J. Ackermann, T. Bunte, and D. Odenthal. Advantage of active steering for vehicle dynamics control. *Proceeding of 32nd ISATA*, (1999).
30. M. Abe. *Vehicle Handling Dynamics: Theory and Application*. Elsevier, UK, (2009).
31. S. Horiuchi, K. Okada, and S. Nohtomi. Analysis of accelerating and braking stability using constrained bifurcation and continuation methods. *Vehicle System Dynamics*, Vol. 46, Supplement, pp. 585-597, (2008)
32. K. Zboinski and M. Dusza. Development of the method and analysis for nonlinear lateral stability of railway vehicles in a curved track. *Vehicle System Dynamics*, Vol. 44, Supplement, pp. 147-157, (2006).
33. D. B. Marghitu, D. G. Beale, and S. C. Sinha. Dynamic Stability of vehicle system via Poincare maps. *Vehicle System Dynamics*, Vol. 28, pp. 41-55, (1997).
34. S. C. Peters and K. Iagnemma. Stability measurement of high-speed vehicles. *Vehicle System Dynamics*, Vol. 47, No. 6, pp. 701-720, (2009).
35. B. P. Minaker and R. J. Rieveley. Automatic generation of the non-holonomic equations of motion for vehicle stability analysis. *Vehicle System Dynamics*, Vol. 48, No. 9, pp. 1043-1063, (2010).
36. S. Shen, J. Wang, P. Shi, and G. Premeir. Nonlinear dynamics and stability analysis of vehicle plane motions. *Vehicle System Dynamics*, Vol. 45, No. 1, pp. 15-35, (2007).

37. M. Borner and R. Isermann. The characteristic velocity stability indicator for passenger car. V*ehicle System Dynamics*, Vol. 43, No. 8, pp. 601-612, (2005).
38. S. Anwar. Yaw stability control of an automotive vehicle via generalized predictive algorithm. *Proc. American Control Conf.*, pp. 435– 440, (2005).
39. R. Karbalaei, A. Ghaffari, R. Kazemi, and S. H. Tabatabaei. Design of an integrated AFS/DYC based on fuzzy logic control. *Proc. ICVES Vehicular Electronics and Safety IEEE Int. Conf.*, pp. 1–6, (2007).
40. S. Zhao, Y. Li, L. Zheng, and S. Lu. Vehicle lateral stability control based on sliding mode control. *Proc. IEEE Int. Conf., on Automation and Logistics*, pp. 638–642, (2007).
41. A. Nishio, K. Tozu, H. Yamaguchi, K. Asano, and Y. Amano. Development of vehicle stability control system based on vehicle sideslip angle estimation. *Vehicle Dynamics and Simulation*, Vol. SP-1602, pp. 1–10, (2001).
42. E. K. Liebemann, K. Meder, J. Schuh, and G. Nenninger. Safety and performance enhancement: The Bosch electronic stability control. *Robert Bosch GmbH, Tech. Rep*. 05-0471, (2004).
43. J. S. Putney. Reactive navigation of an autonomous ground vehicle using dynamic expanding zones. *Master's thesis*, Virginia Polytechnic Institute and State University, (2006).
44. D. Odenthal, T. Bunte, and J. Ackermann. Nonlinear steering and braking control for vehicle rollover avoidance. *Proc. in European Control Conf.*, Karlsruhe, pp. 598-603, (1999).
45. R. Whitehead, B. Clark, M. Breland, K. Lambert, D. Bevly, and G. Flowers. Scaled vehicle electronic stability control. *ESV Int. Collegiate Student Safety Technology Design Competition*, North American Regional Review, (2005).
46. K. Lambert. A study of vehicle properties that influence rollover and their effect on electronic stability controllers. *Master's thesis*, Auburn University, (2007).
47. E. Papadopoulos and D. A. Rey. The force-angle measure of tip over stability margin for mobile manipulators. *Vehicle System Dynamics*, Vol. 33, pp. 29–48, (2000).
48. S. C. Peters and K. Iagnemma. An analysis of rollover stability measurement for high-speed mobile robots. *Proc. IEEE Int. Conf. on Robotics and Automation*, pp. 3711–3716, (2006).
49. B. C. Chen and H. Peng. Rollover warning for articulated heavy vehicles based on a time-to-rollover metric. *ASME J. of Dynamic Systems, Measurement, and Control*, Vol. 127, pp. 406–414, (2005).
50. H. Yu, L. Guvenc, and U. Ozguner. Heavy duty vehicle rollover detection and active roll control. *Vehicle System Dynamics*, Vol. 46, pp. 451–470, (2008).
51. E. Dahlberg. A method for determining the rollover threshold of commercial vehicles. *SAE, Tech. Rep*. 2000-01-3492, (2000).
52. P. Hingwe and M. Tomizuka. Experimental evaluation of a chatter free sliding mode control for lateral control in AHS. *Proc. of the American Control Conf.*, Albuquerque, New Maxico, pp. 3365-3369, (1997).
53. R. Y. Hindiyeh, K. L. R. Talvala, and J. C. Gerdes. Lane keeping at the handling limits. *Int. Symp. on Advanced Vehicle Control*, Kobe, Japan, (2008).
54. J. Hsu, S. M. Laws, and J. C. Gerdes. Estimation of tire slip angle and friction limits using steering torque. *IEEE Trans. of Control Systems Tech.*, Vol. 18, No. 4, pp. 896-907, (2010).
55. K. Kritayakirana and J. C. Gerdes. Autonomous cornering at the limits:

Maximizing a “g-g" diagram by using feedforward trail-braking and throttle-on-exit. *IFAC Symp. Advances in Automotive Control*, (2010).
56. *C. Z. Pan, X .Z. Lai, S. X. Yang, and M. Wu. An efficient neural network approach to tracking control of an autonomous surface vehicle with unknown dynamics. Expert Syst. Appl. Vol. 40, No. 5, pp. 1629–1635, (2013).*
57. M. Kothari and I. Postlethwaite. A probabilistically robust path planning algorithm for UAVs using rapidly-exploring random trees. *J. Intell. Robot. Syst*., Vol. 71, No. 2, pp. 231-253, (2013).
58. A. Sidhu, D. Mikesell, D. Guenther, R. Bixel, and G. Heydinger. Development and Implementation of a path-following algorithm for an autonomous vehicle. SAE Paper No. 2007-01-0815, Detroit, MI, (2007).
59. H. E. Tseng, J. Asgari, D. Hrovat, P. van der Jagt, A. Cherry, and S. Neads. Evasive manoeuvres with a steering robot. *Vehicle System Dynamics*, Vol. 43, No. 3, pp. 199-216, (2005).
60. A. Bemporad and M. Morari. Robust model predictive control: a survey. *Lecture Notes in Control and Information Sciences*, Vol. 245, pp. 207–226, (1999).
61. S. J. Qin and T. A. Badgewell. An overview of industrial model predictive control technology. *Chemical Process Control* – V, Vol. 93, No. 316. pp. 232-256, (1997).
62. S. J. Qin and T. A. Badgwell. A survey of industrial model predictive control technology. *Control Engineering Practice*, Vol. 11, pp. 733–764, (2003).
63. J. Richalet. Industrial applications of model based predictive control. *Automatica*, Vol. 29, No. 5, pp. 1251-1274, (1993).
64. J. Richalet, A. Rault, J. L. Testud, and J. Papon. Model predictive heuristic control: Applications to industrial processes. *Automatica*, Vol. 14, pp. 413-428, (1978).
65. J. Rossiter, L. Wang, and G. P. Valencia. Efficient algorithms for trading off feasibility and performance in predictive control. *Int. Journal of Control*, Vol. 83, No. 4, pp. 789–797, (2010).
66. L. Wang. *Model Predictive Control System Design and Implementation Using MATLAB*. Springer Verlag, London, (2009).
67. B. Wahlberg. System identification using Laguerre models. *IEEE Trans. on Automatic Control*, Vo1.36, pp. 551-562, (1991).
68. B. Wahlberg. System identification using Kautz models. *IEEE Trans. on Automatic Control*, Vol. 39, No. 6, pp. 1276-1282, (1994).
69. A. Leva and L. Bascetta. Designing the feedforward part of 2-d.o.f.industrial controllers for optimal tracking. *Control Eng. Practice*, Vol. 15, No. 8, pp. 909–921, (2007).
70. O. T. C. Matthew and W. Theeraphong. Optimal LQ feedforward tracking with preview: Practical design for rigid body motion control. *Control Eng. Practice*, Vol. 26, pp. 41–50, (2014).
71. Q. Zou. Optimal preview-based stable inversion for output tracking of nonminimum-phase systems. *Automatica*, Vol. 45, No. 1, pp. 230–237, (2009).
72. R. R. Fletcher. *Practical Methods of Optimization*. Wiley, 2nd edition, (1987).
73. J. E. Neserov and A. S. Nemirovsky. Interior point polynomial methods in convex programming- Theory and applications. *SIAM*, Philadelphia, (1994).
74. S. Chang and T. J. Gordon. A flexible hierarchical model-based control methodology for vehicle active safety systems. *Vehicle System Dynamics*, Vol.

46, Supplement, pp. 63-75, (2008).
75. M. Kamal, M. Mukai, J. Murata, and T. Kawabe. Ecological vehicle control on roads with up-down slopes. *IEEE Trans. on Intelligent Transportation Systems*, Vol. 12, No. 3, pp. 783–794, (2011).
76. M. Nagai, M. Shino, and F. Gao. Study on integrated control of active front steer angle and direct yaw moment. *JSAE Review*, Vol. 23, No. 3, pp. 309–315, (2002).
77. P. Falcone, H. E. Tseng, F. Borrelli, J. Asgari, and D. Hrovat. MPC-based yaw and lateral stabilisation via active front steering and braking. *Vehicle System Dynamics*, Vol. 46, No. 1, pp. 611–628, (2008).
78. S. D. Keen and D. J. Cole. Steering control using model predictive control and multiple internal models. *Proc. Advanced Vehicle Control*, Taipei, Taiwan, pp. 1-6, (2006).
79. P. Manfred and E. Johannes. Driver models in automobile dynamics application. *Vehicle System Dynamics*, Vol. 45, No. 7/8, pp. 699–741, (2007).
80. G. Adireddy and T. Shim. MPC based integrated chassis control to enhance vehicle handling considering roll stability. *Proc. ASME 2011 Dynamic Systems and Control Conf. and Bath/ASME Symp. on Fluid Power and Motion Control*, Vol. 2, pp. 877–884, (2011).
81. S. Anwar. Yaw stability control of an automotive vehicle via generalized predictive algorithm. *Proc. 2006 American Control Conf.*, Portland, Oregon, pp. 435–440, (2005).
82. C. March and T. Shim. Integrated control of suspension and front steering to enhance vehicle handling. *J. of Automobile Eng.*, Vol. 221, No. 4, pp. 377–391, (2007).
83. M. Tanelli, C. Vecchio, M. Corno, A. Ferrara, and S. Savaresi. Traction control for ride-by-wire sport motorcycles: a second order sliding mode approach. *IEEE Trans. on Industrial Electronics*, Vol. 56, No. 9, pp. 3347–3356, (2009).
84. M. Canale, L. Fagiano, M. Milanese, and P. Borodani. Robust vehicle yaw control using active differential and internal model control techniques. *Proc. 2006 American Control Conf.*, Minnesota, pp. 1–6, (2006).
85. E. C. Conde, F. B. Carbajal, A. V. González, and R. C. Bracamontes. Robust control of active vehicle suspension systems using sliding modes and differential flatness with MATLAB. In Perutka, K. (Ed.) *MATLAB for engineers—applications in control, electrical engineering, IT and robotics*. InTech, (2011).
86. J. Wang, D. A. Wilson, W. Xu, and D. A. Crolla. Integrated vehicle ride and steady-state handling control via active suspensions. *Int. J. of Vehicle Design*, Vol. 2, No. 3, pp. 306–327, (2006).
87. W. J. Manning and D. A. Crolla. A review of yaw rate and sideslip controllers for passenger vehicles. *Trans. of the Institute of Measurement and Control*, Vol. 29, pp. 117- 135, (2007).
88. K. Nam, S. Oh, H. Fujimoto, and Y. Hori. Robust yaw stability control for electric vehicles based on active front steering control through a steer-by-wire system. *Int. J. of Automotive Tech.*, Vol. 13, No. 7, pp. 1169–1176, (2012).
89. D. Bianchi, A. Borri, M. D. Di Benedetto, S. Di Gennaro, and G. Burgio. Adaptive integrated vehicle control using active front steering and rear torque vectoring. *Int. J. of Vehicle Autonomous Systems*, Vol. 8, No. 2/3/4, pp. 85–105, (2010).

90. H. Yoshida, S. Shinohara, and M. Nagai. Lane change steering manoeuvre using model predictive control theory. *Vehicle System Dynamics*, Vol. 46, Supplement, pp. 669–681, (2008).
91. M. Abe, N. Ohkubo, and Y. Kano. A direct yaw moment control for improving limit performance of vehicle handling - comparison and cooperation with 4ws. *Vehicle System Dynamics*, Vol. 25, Supplement 1, pp. 3–23, (1996).
92. S. Arabi and M. Behroozi. Design of an integrated active front steering and active rear differential controller using fuzzy logic control. *Proc. World Congress on Eng.*, London, U. K, Vol II, pp. 1-6, (2010).
93. W. Kim, D. Kim, K. Yi, and H. J. Kim. Development of a path-tracking control system based on model predictive control using infrastructure sensors. *Vehicle System Dynamics*, Vol. 50, No. 6, pp. 1001–102, (2012).
94. F. Borrelli, P. Falcone, T. Keviczky, J. Asgari, and D. Hrovat. MPC-based approach to active steering for autonomous vehicle systems. *Int. J. Vehicle Autonomous Systems*, Vol. 3, No. 2/3/4, pp. 265–291, (2005).
95. P. Falcone, F. Borrelli, J. Asgari, H. E. Tseng, and D. Hrovat. A real-time model predictive control approach for autonomous active steering. *Nonlinear Model Predictive Control for Fast Systems*, Grenoble, France, (2006).
96. J. Nilsson and J. Sjöberg, Strategic decision making for automated driving on two-lane, one way roads using model predictive control. *Proc. IEEE Intelligent Vehicles Symp.*, Gold Coast, pp. 1253-125, (2013).
97. D. J. Cole, A. J. Pick, and A. M. C. Odhams. Predictive and linear quadratic methods for modelling driver steering control. *Vehicle System Dynamics*, Vol. 44, No. 3, pp. 259-284, (2006).
98. S. D. Keen and D. J. Cole. Application of time-variant predictive control to modelling driver steering skill. *Int. J. of Vehicle Mechanics and Mobility*, Vol. 49, No. 4, pp. 527-559, (2011).
99. P. Falcone, F. Borrelli, J. Asgariy, H. E. Tsengy, and D. Hrovat. A model predictive control approach for combined braking and steering in autonomous vehicles. *Mediterranean Control and Automation*, (2007).
100. M. Ali, P. Falcone, and J. Sjöberg. A predictive approach to roadway departure prevention. *Int. Symp. on Dynamics of Vehicles on Roads and Tracks*, Stockholm, pp. 1-12, (2009).
101. D. Di. Bernardini, S. Cairanoz, A. Bemporad, and H. E. Tseng. Drive-by-wire vehicle stabilization and yaw regulation: a hybrid Model Predictive Control design. *IEEE Decision and Control*, pp.7621-7626, (2009).
102. S. Di Cairano, H. Tseng, D. Bernardini, and A. Bemporad. Steering vehicle control by switched model predictive control. *IFAC Symposium on Advances in Automotive Control*, Munich, Germany, (2010).
103. C. E. Beal. Applications of model predictive control to vehicle dynamics for active safety and stability. A Dissertation for the degree of doctor of philosophy, (2011).
104. A. Gray, Y. Gao, T. Lin, J. K. Hedrick, H. E. Tseng, and F. Borrelli. Predictive control for agile semi-autonomous ground vehicles using motion primitives. *American Control Conf.*, (2012).
105. P. Tøndel and T. Johansen. Control allocation for yaw stabilization in automotive vehicles using multiparametric nonlinear programming. *American Control Conf.*, (2005).
106. M. Canale and L. Fagiano. Vehicle yaw control using a fast NMPC approach.

IEEE Conf. on Decision and Control, pp. 5360-5365, (2008).
107. H. L. Zhou and Z. Y. Liu. Design of vehicle yaw stability controller based on model predictive control. *IEEE Intelligent Vehicles Symp.*, pp. 66-71, (2009).
108. L. Gang, Z. C. Fu, Z. Hong-Yu, and H. Wei. Vehicle active front steering and yaw moment integrated control. *IEEE on Transportation, Mechanical, and Electrical Eng.*, Changchun, China, pp. 787-790, (2011).
109. G. Palmieri, P. Falcone, H. E. Tseng, and L. Glielmo. A preliminary study on the effect of roll dynamics in predictive vehicle stability control. *IEEE Conf. on Decision and Control*, Cancun, Mexico, pp. 5354-5359, (2008).
110. C. E. Beal and J. C. Gerdes. Rollover event prediction through predictive control of coordinated actuators. *Int. Symp. on Dynamics of Vehicles on Roads and Tracks*, Stockholm, Sweden, (2009).
111. C. E. Beal and J. C. Gerdes. Predictive control of vehicle roll dynamics with rear wheel steering. *IEEE American Control Conf.*, MD, USA, pp. 1489-1494, (2010).
112. R. Mehra, J. Amin, K. Hedrick, C. Osorio, and S. Gopalasamy. Active suspension using preview information and model predictive control. *IEEE Int. Conf. on Control Applications*, pp. 860-865, (1997).
113. B. K. Cho, G. Ryu, and S. J. Song. Control strategy of an active suspension for a half car model with preview information. *Int. J. of Automotive Tech.*, Vol. 6, pp. 243–249, (2005).
114. O. A. Dahunsi, J. O. Pedro, and O. T. Nyandoro. Neural network based model predictive control of a servo-hydraulic vehicle suspension system. *IEEE AFRICON*, Nairobi, Kenya, pp.1-6, (2009).
115. J. Xu and J. Fei. Neural network predictive control of vehicle suspension. *IEEE ICISE*, Changzhou, China, pp. 1319-1322, (2010).
116. C. Gohrle, A. Wagner, A. Schindler, and O. Sawodny. Active suspension controller using MPC based on full-car model with preview information. *American Control Conf.*, Montreal, Canada, pp. 497-502, (2012).
117. M. Canale, M. Milanese, and C. Novara. Semi-active suspension control using "fast" model predictive control techniques. *IEEE Trans. on Control Systems Tech.*, Vol. 14, pp. 1034-1046, (2006).
118. K. S. Narendra and K. Parthasarathy. Identification and control of dynamical system using neural networks. *IEEE Trans. on Neural Networks*, Vol. 3, No. 1, (1990).
119. R. N. Jazar. *Vehicle Dynamics Theory and Application*. 3rd edition. NY USA, Springer, (2009).
120. K. Berntorp. Derivation of a six degrees-of-freedom g round-vehicle model for automotive applications. *Technical Report ISRN LUTFD2/TFRT*--7627--SE, Department of Automatic Control, Lund University, Sweden, (2013).
121. E. J. Bedner and W. G. Chester. Methods, systems, and computer program products for tire slip angle limiting in a steering control system. *U.S. Patent No. 7,756,620*, (2010).
122. J. Svendenius and B. Wittenmark. Brush tire model with increased flexibility. *Proc. European Control Conf.*, Cambridge, UK, pp. 1863-1868, (2003).
123. P. Tsiotras, E. Velenis, and M. Sorine. A LuGre tire friction model with exact aggregate dynamics. *Vehicle System Dynamics*, Vol. 42, No. 3, pp. 195–210, (2004).
124. N. Ding and S. Taheri. A modified dugoff tyre model for combined-slip forces.

Tyre Science & Tech., Vol. 38, No. 3, pp.17-27, (2010).
125. E. Bakker, H. B. Pacejka, and L. Lidner. A new tire model with an application in vehicle dynamics studies. *SAE Paper 890087*, (1989).
126. H. B. Pacejka and E. Bakker. Magic Formula Tyre Model. *Vehicle System Dynamics*, Vol. 21, Supplement, pp. 1–18, (1993).
127. H. Pacejka. *Tire and vehicle dynamics*. 3rd edn. Elsevier Ltd, Oxford, (2012).
128. S. Glaser, S. Mammar, and D. Dakhlallah. Lateral wind force and torque estimation for a driving assistance. *17th World Congress*, Vol. 17, Part.1, Seoul, Korea, pp. 5688-5693, (2008).
129. C. J. Baker. Measures to control vehicle movement at exposed sites during windy periods. *J. of Wind Eng. and Industrial Aerodynamics*, Vol. 25, No. 2, pp. 151-161, (1987).
130. T. Keviczky, P. Falcone, F. Borrelli, J. Asgari, and D. Hrovat. Predictive control approach to autonomous vehicle steering. *Proc. Amer. Cont. Conf.*, MN, US, pp. 4670-4675, (2006).
131. H. E. Tseng. Dynamic estimation of road bank angle, *Int. J. of Vehicle Mechanics and Mobility*, Vol. 36, No. 4-5, pp. 307-328, (2001).
132. J. Ryu and J. C. Gerdes. Estimation of vehicle roll and road bank angle. *Proc. Amer. Contr. Conf*., pp. 2110–2115, (2004).
133. C. Ahn, B. Kim, and M. Lee. Modeling and control of anti-lock brake and steering system for cooperative control on split-mu surfaces. *Int. J. of Auto. Tech*., Vol. 13, No. 4, pp. 571-581, (2012).
134. R. G. Hebden, C. Edwards, and S. K. Spurgeon. An application of sliding mode control to vehicle steering in a split-mu manoeuvre. *Proc. of the American Control Conf.*, Vol. 5, pp. 4359–4364, (2003).
135. M. C. Walz. Trends in the static stability factor of passenger cars, light trucks and vans. *NHTSA Technical Report*, DOT HS 809 868, (2005).
136. S. Solmaz, M. Corless, and R. Shorten. A methodology for the design of robust rollover prevention controllers for automotive vehicles with active steering. *Int. J. of Control*, Vol. 80, No. 11, pp. 1763-1779, (2007).
137. D. C. Viano and C. Parenteau. Case study of vehicle maneuvers leading to rollovers: Need for a vehicle test simulating off road excursions, recovery and handling. *SAE Trans.*, no. 2003-01-0169, (2003).
138. N. Elmi, A. Ohadis, and B. Samadi. Active front-steering control of a sport utility vehicle using a robust linear quadratic regulator method, with emphasis on the roll dynamics. *J. of Automobile Eng.*, Vol.227, No.12, pp. 1636-1649, (2013).
139. L. Shihao, F. Yakub, M. Kasahara, and Y. Mori. Rollover prevention with predictive control of differential braking and rear wheel steering. *Proc. Conf. Robotics, Automation and Mechatronics*, Manila, Philippines, pp. 144-149, (2013).
140. M. J. L. Boada, B. L. Boada, and V. Diaz. Integrated control of front-wheel steering and front braking forces on the basis of fuzzy logic. *J. of Automobile Eng.*, Vol. 220, No. 2, pp. 253-267, (2006).
141. A. Balluchi, et al. Path-following with a bounded-curvature vehicle: a hybrid control approach. *Int. J. of Control*, Vol. 78, No. 15, pp. 1228-1247, (2005).
142. K. Moriwaki. Autonomous steering control for electric vehicles using nonlinear state feedback H-infinity control. *Nonlinear Analysis*, Vol.63, No.5-7, pp. 2257-2268, (2005).

143. B. Mashadi, P. Ahmadizadeh, and M. Majidi. Integrated controller design for path following in autonomous vehicles. *SAE Technical Paper*, pp. 1-10, (2011).
144. J. M. Park, D. W. Kim, Y. S. Yoon, H. J. Kim, and K. S. Yi. Obstacles avoidance of autonomous vehicle based on model predictive control. *J. of Automobile Eng.*, Vol. 223, No. 12, pp. 1499-1516, (2009).
145. P. Falcone, F. Borrelli, J. Asgari, H. E. Tseng, and D. Hrovat. Predictive active steering control for autonomous vehicle systems. *IEEE Trans. on Control System Tech.*, Vol. 15, No. 3, pp. 566–580, (2007).
146. M. Doumiati, O. Sename, L. Dugard, J. M. Martinez-Molina, P. Gaspar, and Z. Szabo. Integrated vehicle dynamics control via coordination of active front steering and rear braking. *European J. of Control*, Vol. 19, pp. 121-143, (2013).
147. W. Cho, J. Yoon, J. Kim, J. Hur, and K. Yi. An investigation into unified chassis control scheme for optimized vehicle stability and manoeuvrability. *Vehicle System Dynamics*, Vol. 46, pp. 87−105, (2008).
148. J. H. Lee and W. S. Yoo. Predictive control of a vehicle trajectory using a coupled vector with vehicle velocity and sideslip angle. *Int. J. of Automotive Tech.*, Vol. 10, No. 2, pp. 211-217, (2009).
149. A. Katriniok and D. Abel. LTV-MPC approach for lateral vehicle guidance by front steering at limits of vehicle dynamics. *Proc. CDC-ECC Conf.*, Orlando, FL, pp. 6828-6833, (2011).
150. D. Q. Mayne, J. B. Rawlings, C. V. Rao, and P. O. M. Scokaert. Constrained model predictive control: Stability and optimality. *Automatica*, Vol. 36, No, 6, pp. 789–814, (2000).
151. K. P. Groves, D. O Sigthorsson, A. Serrani, S. Yurkovich, M. A. Bolender, and D. B. Doman. Reference command tracking for a linearized model of an air-breathing hypersonic vehicle. *Proc. AIAA Guidance, Navigation, and Control Conf. and Exhibit*, AIAA-2005-6144, (2005).
152. G. Hammar and V. Ovtchinnikov. Structural intelligent platooning by a systematic LQR algorithm. *Master's thesis*, Royal Institute of Technology, KTH, (2010).
153. R. S. Sharp and V. Valtetsiotis. Optimal preview car steering control. *Vehicle System Dynamics*, Vol. 35, Supplement, pp. 101–117, (2001).
154. C. MacAdam. Application of an optimal preview control for simulation of closed-loop automobile driving. *IEEE Trans. on Systems, Man and Cybernetics*, Vol. 11, No. 6, pp. 393-399, (1981).
155. R. Rajamani. *Vehicle dynamics and control*. 2nd edition, Springer Science, New York, (2012).
156. M. Doumiati, A. Victorino, A. Charara, and D. Lechner, Onboard real-time estimation of vehicle lateral tire-forces and sideslip angle. *IEEE Trans. on Mechatronics*, Vol. 16, No. 4, pp. 601-614, (2011).
157. C. R. Carlson and J. C. Gerdes. Optimal rollover prevention with steer by wire and differential braking. *ASME Dynamic systems and Control*, Vol. 1-2, pp. 345-354, (2003).
158. S. F. van der Westhuizen and P. S. Els. Slow active suspension control for rollover prevention. *J. of Terramechanics*, Vol. 50, No. 1, pp. 29-36, (2013).
159. B. Schofield, T. Hägglund, and A. Rantzer. Vehicle dynamics control and controller allocation for rollover prevention. *IEEE Conf. on Control Applications*, Munich, pp. 149-154, (2006).
160. J. Yoon, W. Cho, J. Kang, B. Koo, and K. Yi. Design and evaluation of a unified

chassis control system for rollover prevention and vehicle stability improvement on a virtual test track. *Control Eng., Practice*, Vol. 18, pp. 585-597, (2010).
161. L. Boyuan. Modelling, dynamic stability analysis and control of an omni-directional road vehicle. University of Wallongkong, Australia, *Ms. Thesis* (2012).
162. N. S. Edgar, J. R. Luis, L. Reza, and S. Danial. Rollover prediction and control in heavy vehicles via recurrent high order neural networks. *Intelligent Automation & Soft Computing*, Vol. 17, No. 1, pp. 95-107, (2011).
163. S. Kharazzi, J. Fredriksson, and M. Lidberg. Lateral stability control of long heavy vehicle combination by active steering of the towed units. *IEEE Ann. Conf. on Intelligent Trans. Systems*, Medeira Island, Portugal, pp. 168-173, (2010).
164. Z. Petres, S. Nagy, P. Gaspar, and P. Baranyi. Hinf gain-scheduling based control of the heavy vehicle model, a TP model transformation based control. *IEEE Int. Conf., on World Congress on Computational Intelligence*, Hong Kong, pp. 1542-1547, (2008).
165. D. Oberoi. Enhancing roll stability and directional performance of articulated heavy vehicles based on anti-roll control and design optimization. *Ms. Thesis*, University of Ontario Institute of Technology, Oshawa, Ontario-Canada, (2011).
166. E. Gilbert and K. Tan. Linear systems with state and control constraints: The theory and application of maximal output admissible sets. *IEEE Trans. on Automatic Control*, Vol. 36, No. 9, pp. 1008-1020, (1991).
167. Y. Sebsadji, S. Glaser, S. Mammar, and M. Netto. Vehicle roll and road rank angles estimation. *17th World Congress*, Seoul, Korea 17, Vol. 1, pp. 7091-7097, (2008).
168. G. Yu, D. Wang, Q. Li, P. Wang, and Y. Wang. Road bank estimation for bus rollover prediction. *Appl. Math. Inf. Sci*., Vol. 7, No. 5, pp. 2027-2034, (2013).
169. Y. D. Yoon, E. Jung, and S. K. Sul. Application of a disturbance observer for relative position control system. *IEEE Trans. Ind. Appl*., Vol. 46, No. 2, pp. 849-856, (2010).
170. J. Yang, S. H. Li, X. S. Chen, and Q. Li. Disturbance rejection of dead-time processes using disturbance observer and model predictive control. *Chem. Eng. Res. Des.*, Vol. 89, No. 2, pp. 125-135, (2011).
171. B. A. Guvenc, T. Bunte, D. Odenthal, and L. Guvenc. Robust two degree-of-freedom vehicle steering controller design. *IEEE Control Syst. Technol.*, Vol. 12, No. 4, pp. 627-636, (2004).
172. http://www.subaru-global.com/tec_vdc.html
173. M. Ahmadi and A. M. Jafari. Is nonlinear model predictive control with fuzzy predictive model propoer for managing the blood glucose level in typeI diabetes?. J. of Biomedical Science and Engineering, Vol. 5, No. 5, pp. 1-12, (2012).

Publication

Indexed Journal

1. Fitri Yakub and Yasuchika Mori. Heavy vehicle stability and rollover prevention via switching model predictive control. *International Journal of Innovative Computing, Information & Control (IJICIC)*. Vol. 11, No. 5, pp. (2015. 10).
2. Fitri Yakub and Yasuchika Mori. Minimizing tracking error in path following control of autonomous ground vehicle. *ICIC Express Letters,* Vol. 9, No. 6, pp. 1609-1615. (2015. 6).
3. Fitri Yakub and Yasuchika Mori. Comparative study of autonomous path-following vehicle control via model predictive control and linear quadratic control. *Journal of Automobile Engineering, Part D,* doi: 10.1177/0954407014566031. (2015. 1).
4. Fitri Yakub and Yasuchika Mori. Enhancing path following control performance of autonomous ground vehicle through coordinated approach under disturbance effect. *IEEJ Transactions on Electronics, Information and Systems (C)*. Vol. 135, No. 1, pp. 102-110. (2015. 1).
5. Fitri Yakub and Yasuchika Mori. Enhancing rollover prevention and vehicle stability of heavy vehicle under disturbance effect. *Applied Mechanics and Materials*. Vol. 695, pp. 596-600. (2014. 11).

International Conference

1. Fitri Yakub and Yasuchika Mori. Heavy vehicle stability and rollover prevention through switching model predictive control. *Asian Control Conference,* 31 May-3 June, Sabah, Malaysia. (2015. 6).
2. Fitri Yakub and Yasuchika Mori. Autonomous ground vehicle of path following control through model predictive control with feed forward controller. *Proc. of 12th Int. Symp. on Advanced Vehicle Control (AVEC)*, 22-26 September, Tokyo, Japan, pp. 603-610. (2014. 9).
3. Fitri Yakub and Yasuchika Mori. Model predictive control based on kautz function for autonomous ground vehicle path following control application. *Proc. of SICE Annual Conf. (SICE),* 9-12 September, Hokkaido, Japan, pp. 1035-1040. (2014. 9).
4. Lee Shihao, Fitri Yakub, Misawa Kasahara, and Yasuchika Mori. Rollover prevention with predictive control of differential braking and rear wheel steering. *Proc. of 6th IEEE Int. Conf. Robotics, Automation and Mechatronics (RAM),* 12-15 November, Manila, Philippines, pp. 144-149. (2013. 11).
5. Fitri Yakub and Yasuchika Mori. Autonomous car in path following control under side wind effect by laguerre function. *Proc. of 6th IEEE Int. Conf. Robotics,*

Automation and Mechatronics (RAM), 12-15 November, Manila, Philippines, pp. 61-66. (2013. 11).

6. Fitri Yakub and Yasuchika Mori. Model predictive control for car vehicle dynamics system - Comparative study. *Proc. of 3th IEEE Conf. on Information Science and Technology,* 23-25 March, Yangzhou, China, pp. 172-177. (2013. 3).